DuneFront

Deliverable 12.3

September 2026



Cover figure © DuneFront

Legal notice

Flanders Hydraulics is of the opinion that the information and positions in this report are substantiated by the available data and knowledge at the time of writing.
The positions taken in this report are those of Flanders Hydraulics and do not reflect necessarily the opinion of the Government of Flanders or any of its institutions.
Flanders Hydraulics nor any person or company acting on behalf of Flanders Hydraulics is responsible for any loss or damage arising from the use of the information in this report.

Copyright and citation

© The Government of Flanders, Department of Mobility and Public Works, Flanders Hydraulics 2026
D/2026/3241/243

This publication should be cited as follows:

Gruwez, V.; Adeli, A.; Willems, M.; Aertsens, T.; Sevindik, C.; Hofland, B.; Troch, P.; Reniers, A.; Lojek, O.; Tissier, M.; Verwaest, T. (2026). Physical modelling of the Belgian Demonstrator(s): dune-dike interactions - the DUKEx-dataset. DuneFront report D12.3, Version 4.0. FH Reports, 23_031_1. Flanders Hydraulics: Antwerp

Reproduction of and reference to this publication is authorised provided the source is acknowledged correctly.

Document identification

Customer:	European Commission	Ref.:	WL2026R23_031_1
Keywords (3-5):	Physical modelling; Coastal protection; Wave overtopping; Erosion; Dune; Dike		
Knowledge domains:	Coastal protection > Coastal safety against extreme storms > Sea dikes > Physical modelling Coastal protection > Coastal safety against extreme storms > Soft coastal defences > Physical modelling Coastal protection > Coastal protection against erosion > Dunes > Physical modelling Hydraulics and sediment > Hydrodynamics > Waves > Physical modelling Hydraulics and sediment > Hydrodynamics > Current velocities and patterns > Physical modelling Hydraulics and sediment > Sediment > Non-cohesive sediment > Physical modelling Hydraulics and sediment > Sediment > Sediment transport > Physical modelling Hydraulics and sediment > Morphology > Erosion / sedimentation > Physical modelling		
Text (p.):	92	Appendices (p.):	5
Confidential:	☒ No	☒ Available online	

Author(s):	Gruwez, V.; Adeli, A.; Willems, M.; Aertsens, T.; Sevindik, C.; Hofland, B.; Troch, P.; Reniers, A.; Lojek, O.; Tissier, M.; Verwaest, T.

Control

	Name	Signature
Reviser(s):	Verwaest, T.	Signed by:Verwaest Toon Signed at:2026-10-19 17:55:11 +02:00 Reason:Ik keur dit document goed Verwaest Toon Vlaamse overheid
Project leader:	Gruwez, V.	Signed by:Gruwez Vincent Signed at:2026-10-19 07:54:30 +02:00 Reason:I approve this document Vincent Gruwez Vlaamse overheid

Approval

Head of Division:	Bellafkih, K.	Signed by:Bellafkih Abdelkarim Signed at:2026-10-16 10:46:34 +02:00 Reason:Ik keur dit document goed Bellafkih Abdelkarim Vlaamse overheid

Physical modelling of the Belgian Demonstrator(s), focus: dune-dike interactions - the DUKEx-dataset

Deliverable 12.3 – D12.3

Deliverable information

Title	Physical modelling of the Belgian Demonstrator(s), focus: dune-dike interactions - the DUKEx-dataset
Deliverable number	D12.3
WP number	12
Author(s)	Vincent Gruwez, Marc Willems, Tim Aertsens, Toon Verwaest (FH), Afshar Adeli, Peter Troch (UGent-E), Cem Sevindik, Bas Hofland, Ad Reniers, Marion Tissier (TU Delft), Oliver Lojek (TUB-E)
Lead beneficiary	Flanders Hydraulics (FH)
Contributors	See authors (UGent-E, TU Delft, TUB-E), and Dries Bonte.
Type	Report
Dissemination level	Public
How to cite	Gruwez, V., Adeli, A., Willems, M., Aertsens, T., Sevindik, C. , Hofland, B., Troch, P., Reniers, A., Lojek, O., Tissier, M., Verwaest, T. (2026) Physical modelling of the Belgian Demonstrator(s), focus: dune-dike interactions - the DUKEx-dataset. DuneFront report D12.3, Version 4.0. FH Reports, 23_031_1. Flanders Hydraulics: Antwerp
Copyright license*	© Authors and DuneFront consortium, 2024-2027. *This work is openly licensed via* CC-BY-4.0.

Versioning and contribution history

Version	Date	Authors (Institution)	Notes
Version 0.1	31/08/2026	Vincent Gruwez, Marc Willems, Tim Aertsens (FH), Afshar Adeli (UGent-E)	Draft created by FH and UGent-E
Version 0.2	25/09/2026	Vincent Gruwez, Toon Verwaest (FH), Afshar Adeli, Peter Troch (UGent-E), Bas Hofland, Cem Sevindik (TU Delft)	Reviewed and revised version
Version 1.0	30/09/2026	All	Final version approved by all Beneficiaries

Funded by the European Union. Views and opinions expressed are however those of the author(s) only and do not necessarily reflect those of the European Union. Neither the European Union nor the granting authority can be held responsible for them.

Funded by the European Union

DuneFront

Cover page

Coastal communities need protection systems that remain reliable under extreme storms while retaining the capacity of sandy coasts to adapt. Dune-dike hybrid Nature-based Solutions (DD-Hybrid NbS) combine a hard dike with a dynamic dune. These can therefore contribute to both flood safety and nature-inclusive coastal management. Their design requires a quantitative understanding of how storm waves erode the dune, expose and load the dike, generate overwash and overtopping, and transport sediment. This report is DuneFront Deliverable D12.3 and presents the wave flume scale modelling experiments done in the DuneFront project to increase this understanding. The report includes: the experimental modelling setup, the test program and the experimental DUKEx-dataset (DUne diKE Experiments). The test program includes the Belgian Physical Twin to demonstrate the performance of Belgian demonstrators under design storm conditions.

The experiments were conducted from March to June 2026 in the 84 m long Large Wave Flume at Flanders Hydraulics. A 1:12.5 Froude-scaled mobile-bed model combined a 1/40 sandy foreshore slope and an erodible dune with a fixed, smooth and impermeable 1/2 dike slope. The test program comprised 15 (re)shaped dune geometry cases and in total 156 wave tests based on nine principal physical dune geometries. The tested dune geometries were roughly derived (or schematized) from the demonstrators at Raversijde (BE), Middelkerke (BE), Katwijk (NL) and Dunkerque (FR). The test program was focused on varying dune volume (and dune crest width), keeping dune volume constant but varying the dune crest level and the distance between the dune and dike. Test conditions covered swash, collision, overwash and transition-to-inundation conditions. The HybridDune field configuration at the Sand Engine in the Netherlands was also reproduced at model scale.

Most tests used the same design-storm conditions to allow direct comparison between geometries. Additional tests examined experimental repeatability, a lower incident wave height, a changing tide and storm-surge level, and the influence of added free infragravity waves at the wave paddle. The HybridDune tests reproduced wave conditions measured during a field storm and provide a basis for evaluating the transferability of laboratory results to prototype scale.

An integrated measurement system captured water-surface elevations, near-bed horizontal velocities and suspended-sediment response over the foreshore, pore-water pressures in the dune, dune and foreshore evolution, water temperature, and overtopping and overwash. An innovative robust measurement system was developed for the overtopping and overwash: an instrumented collection tank (overtopping tank) combined load-cell and acoustic measurements to separate and determine the overtopped water volume and the dry mass of overwashed sediment. Dedicated Python workflows were developed for signal filtering, LiDAR data-processing and bed-profile reconstruction. The report also derives the

procedure for calculating mean overtopping discharge and overwashed sediment mass. Data gaps and faulty records are documented so that appropriate tests can be selected for subsequent analyses.

This campaign provides the experimental foundation for future validation of XBeach-SB, XBeach-NH (or SWASH) and for numerically extending the experimental database beyond the tested conditions to demonstrate the efficiency of the hybrid system compared to standalone dune and dike coastal defense systems (D12.5). For coastal authorities, the acquired DUKEx-dataset can support transparent comparison of adaptation options before field implementation. It can also contribute to designs that combine a dependable hard safety line with the adaptive and ecological value of dunes. The present report does not yet identify an optimal geometry. Design and policy decisions should therefore use the subsequent validated-model analyses, accounting explicitly for scale effects, long-crested flume waves and measurement limitations, and remain tailored to local storm climate, bathymetry, sediment characteristics and maintenance requirements (D14.5).

The DUKEx-dataset presented here will also be used further in other work packages in the DuneFront project: in the development of the Predictive Digital Twin (WP13) and consequently the development of the Decision Support System (WP14).

DuneFront

Table of Content

1. Introduction 12
   1.1 General background 12
   1.2 Overview of Work Package 12 12
      1.2.1 Work Package description 12
      1.2.2 Work Package sub-tasks and deliverables 13
   1.3 Aims of D12.3 13
   1.4 Outline of this report 13
2. Schematisation of the demonstrators for the laboratory experiment 14
   2.1 Overview schematisation parameter ranges 14
   2.2 Model geometries 15
   2.3 Model hydrodynamics 17
   2.4 Field case HybridDune 19
3. Experimental setup 22
   3.1 Experimental facilities 22
   3.2 Wave flume coordinate system 23
   3.3 Model setup 23
   3.4 Instrumentation 26
      3.4.1 Wave hydrodynamics 26
      3.4.2 Beach/dune morphodynamics and sediment transport 33
      3.4.3 Wave overtopping and overwash 38
4. Test program 42
   4.1 Overview 42
   4.2 DUNE00 44
   4.3 DUNE01 45
   4.4 DUNE02, DUNE02cor and DUNE02loH 47
   4.5 DUNE03 49
   4.6 DUNE04 50

4.7 DUNE05, DUNE05rep, DUNE05loH, DUNE05var and DUNE05fig 52
4.8 DUNE06 56
4.9 DUNE07 58
4.10 DUNE12 59
5. Data processing and first visualizations 60
5.1 Overview 60
5.2 Bed profiles 63
5.2.1 Distance laser bed profiles 63
5.2.1 LIDAR 66
5.3 Hydrodynamics 68
5.3.1 Acoustic wave gauges (AWG_01-AWG_11) 68
5.3.2 Resistive wave gauges (RWG) 69
5.3.3 Pressure transducer gauges (PTG) 70
5.3.4 Electromagnetic current meters (ECM) 71
5.4 Overtopping and -wash 75
5.4.1 Load cells 75
5.4.2 Acoustic wave gauges (AWG_12-AWG_16) 75
5.4.3 Overtopping/-wash calculation 80
5.5 Sediment transport 82
5.5.1 Optical backscatter sensors (OBS) 82
6. Dataset structure, archiving and availability 86
7. Conclusion 88
8. Acknowledgements 90
9. References 91
Annex 1: Sallenger storm impact regimes 93
Annex 2: OBS sensor calibration 95

List of abbreviations

Parameter	Explanation
α_{beach}	Angle of the (uneroded) beach (degrees)
α_{dike}	Slope angle of seaward dike slope (degrees)
α_{dune}	Slope angle of seaward dune slope (degrees)
AWG	Acoustic wave gauges
ECM	Electromagnetic current meters
cot α_{fore}	Cotangent of the foreshore slope angle
cot α_{dune}	Cotangent of the dune-face slope angle
cot α_{dike}	Cotangent of the dune-face slope angle
D_{50}	Sand diameter (micron)
D_{dune}	Distance between dike and dune (m)
f	Frequency
$h_{dunefoot}$	Elevation of transition dune/beach w.r.t. design water level (m)
h_{deep} / h_p	Depth at which the offshore wave boundary conditions are specified (m)
h_{toe}	Depth at toe of the dike at maximum eroded dune (m)
H_{m0}	(Spectral) significant wave height
$H_{s,IG}$	Offshore significant wave height (H_{m0}) for free infragravity waves (m)
$H_{m0,fig}$	Offshore significant wave height for free infragravity waves (m)
$H_{s,ss}$	Offshore significant wave height (H_{m0}) for sea/swell waves (m)
$H_{m0,,ss}$	Offshore significant wave height for sea-swell waves (m)
JSON	JavaScript Object Notation (Data type)
LDM	Laser distance meters
LIDAR	Light Detection and Ranging
N.A.P	Normaal Amsterdams Peil (Amsterdam Ordnance Datum)
OBS	Optical backscatter sensors
OTT	Overtopping Tank
PCAP	Packet Capture
PTG	Pressure transducer gauge
RWG	Resistive wave gauges
Rc_{dike}	Crest freeboard of dike relative to extreme/design water level (m)
Rc_{dune}	Crest freeboard of dune relative to extreme/design water level (m)
SSC	Suspended sediment concentration
TEMP / TMP	Water temperature
$T_{m-1,0,ss}$	Spectral wave period for sea swell wave part of the spectrum (s)
$T_{m-1,0,IG}$	Spectral wave period for (total) infragravity wave part of the spectrum (s)
$T_{m-1,0,FIG}$	Spectral wave period for free infragravity waves (s)
T_{m02}	Mean spectral wave period
$T_{p,ss}$	Peak wave period for the sea-swell waves (s)

$T_{p,FIG}$	Peak period for the free infragravity waves (s)
V_{dune}	Dune volume
$V_{dune,Kat}$	Dune volume of Katwijk
$V_{dune,Mi}$	Dune volume of Middelkerke
$V_{dune,Mid1ong}$	Dune volume of Middelkerke (lengthened)
$V_{dune,Rav}$	Dune volume of Raversijde
W_{dike}	Crest width of dike (m)
W_{dune}	Crest width of dune (m)
W_{wall}	Width of wall at top of dike slope (m)

1. Introduction

1.1 General background

The primary objective of the DuneFront project is to optimize dune-dike hybrid Nature-based Solutions (DD-Hybrid NbS) as a new generation of sustainable, nature-inclusive coastal protection. Such coastal protection measures, that combine a hard safety line (dike) and biodiverse and resilient dune systems, have the potential to adapt to sea-level rise provided that the physical and biological conditions are met. In this context, a key challenge of DuneFront is to identify the biological, physical, and socio-economic boundary conditions and their interactions to enhance the protection provided by these hybrid approaches. The DuneFront concept is summarized in Figure 1.

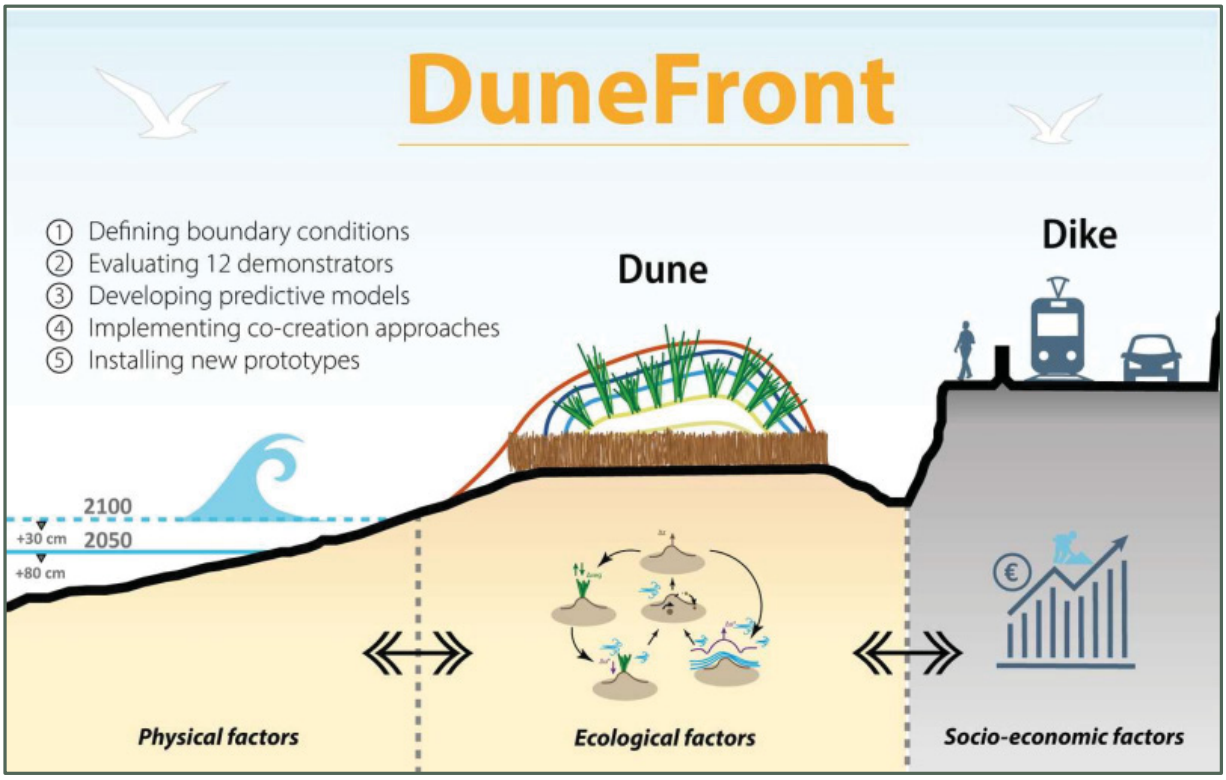


Figure 1 - DuneFront concept in one graphical abstract

1.2 Overview of Work Package 12

1.2.1 Work Package description

The primary objective of Work Package (WP) 12 is to evaluate the coastal protection functioning of DD-hybrid NbS during extreme storms. This requires gaining new insights into the physical processes specific to storm wave interactions with DD-hybrid NbS, such as dune erosion in the presence of a hard structure, the effect of the eroding dune on dike loading,

wave overtopping, and wave impacts, but also dune strengthening by vegetation. To obtain those, currently unavailable data on the functioning of DD-Hybrid NbS under extreme storm conditions will be collected using dedicated physical experiments of a selection of the DuneFront demonstrators, using the input from WP7. These so-called Physical Twins will also be used to communicate with stakeholders (WP17). The physical modeling data will be used to validate and improve the process-based numerical models and subsequently expand the physical model dataset for a wider range of conditions and geometries of the DD-Hybrid NbS. Ultimately, this will be used to demonstrate the efficiency of the DD-Hybrid NbS coastal protection system as an adaptive defense against climate change impacts.

1.2.2 Work Package sub-tasks and deliverables

WP12 consists of 5 tasks listed below, each of them associated with a deliverable:

Task 12.1. Physical modeling of the Dutch Demonstrator(s), focus: wave-dike interactions (Deliverable D12.1, available)

Task 12.2. Physical modeling of the German Demonstrator(s), focus: vegetation influence on dune erosion (Deliverable D12.2, available)

Task 12.3. Physical modeling of the Belgian Demonstrator(s), focus: dune-dike interactions (Deliverable D12.3, **this report**)

Task 12.4. Validation of the numerical models XBeach-SB, XBeach-NH, and SWASH using the experimental data (Deliverable D12.4, available)

Task 12.5. Demonstration of the DD-hybrid NbS coastal protection efficiency using the validated models (Deliverable D12.5, June 2027)

1.3 Aims of D12.3

In the scope of D12.3 (this report), EVFH realized the physical model for the Belgian Demonstrator in the large wave flume of Flanders Hydraulics in close collaboration with UGENT-E, TU Delft and TUB-E. The main objective of this task is to provide a database of dune morphodynamics, wave hydrodynamics, overwash and wave overtopping on the dike during dune erosion by focusing measurements on both the morpho- and hydrodynamics. The resulting database is called the DUKEx-dataset (DUne diKE Experiments).

1.4 Outline of this report

This report is structured as follows: Chapter 2 describes the schematization process of the demonstrators for the laboratory experiments, building on the work performed in WP7. Chapter 3 presents the experimental setup. The test program followed during the experiments is presented in Chapter 4. Then, in Chapter 5, data processing is discussed and some first visualizations of the gathered data are provided. Finally, the dataset structure, archiving and availability are discussed in Chapter 6. Conclusions are provided in Chapter 7.

2. Schematisation of the demonstrators for the laboratory experiment

2.1 Overview schematisation parameter ranges

The Belgian laboratory experiments focus on the combined morpho- and hydrodynamic processes for the hybrid functioning of the dune-dike system during design storm conditions. The focus of these experiments was on the morpho- and hydrodynamics at the peak of the design storm, where the dune is eroding and interacting with the dike. The dune interaction with the dike (the dune overwash and ultimately the overtopping over the dike) depends on the initial dune geometry and its relative position to the dike. A mobile bed was used to represent the sandy parts of the foreshore and dune while a fixed bed was used to represent the hard dike part of the hybrid system. All geometries considered in the experiments were designed according to the geometric schematization presented in DuneFront deliverable D7.2. (Figure 2).

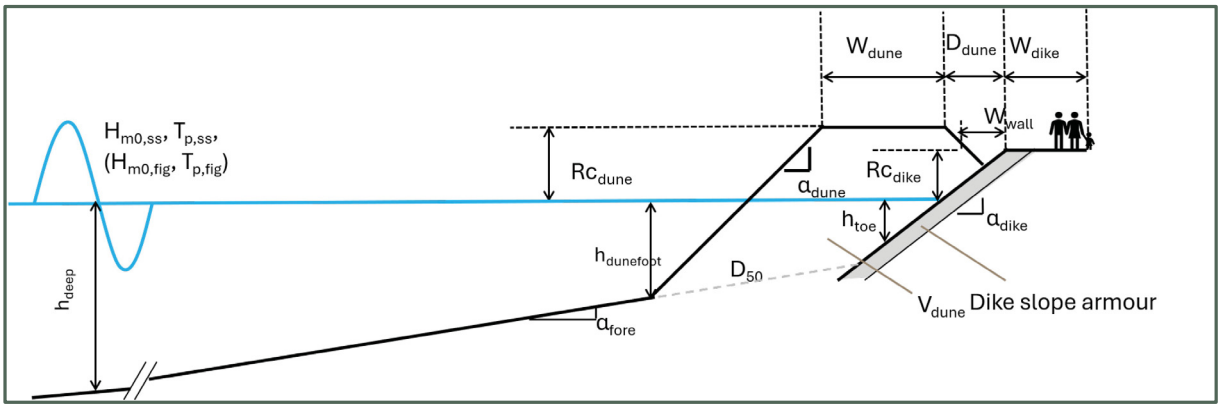


Figure 2 - General setup for the physical model test series on dune-dike processes. These tests focus on the dune-dike interactions during design storm conditions. Adapted from Sevindik et al. (2024).

The model geometry is primarily derived schematically from the Belgian demonstrators Raversijde (BE) and Middelkerke (BE), but representation of the other selected demonstrators in D7.1 (Adeli *et al.*, 2024) and D7.2 (Sevindik *et al.*, 2024) (i.e., Katwijk (NL), Sankt Peter-Ording (DE), Dunkerque (FR)) is also investigated. All considered demonstrators are in a meso-tidal area of the North Sea. The bed geometry and hydraulic conditions were chosen to resemble as much as possible the conditions expected at these demonstrators around the peak of the design storm while accounting for practical constraints. These considerations resulted in the test ranges presented in Table 1 (last column, at prototype scale). In this table, these actual test ranges are compared to the expected conditions at the demonstrators previously mentioned. The main schematization choices and compromises are discussed below for the model geometries and hydrodynamics.

Table 1 - Prototype scale test ranges considered in the Belgian physical model test on dune-dike processes compared to the ranges defined in the framework D7.2 (Sevindik et al.*, 2024) and in D7.1 for the demonstrator at Dunkerque (Adeli* et al.*, 2024).*

Hydraulic parameters	Raversijde (BE)	Middelkerke (BE)	Katwijk (NL)	Sankt Peter Ording (DE)	Dunkerque (FR)	Prototype scale test ranges for dune-dike experiments
$H_{m0,ss}$ [m]	4.66	4.95	7.99	6.60	2.00-3.00	2.00-4.25
$T_{p,ss}$ [s]	10.9	11.0	15.3	11.9-12.9	N/A	12.0
$H_{m0,fig}$ [m]	N/A	N/A	N/A	N/A	N/A	0.75
$T_{p,fig}$ [s]	N/A	N/A	N/A	N/A	N/A	66.0
h_{deep} [m]	12.37	12.44	25.30	25.70	N/A	17.25
Foreshore parameters						
cot α_{fore} [-]	30-60	50	35-41	1000	100	40
Dune parameters						
cot α_{dune} [-]	4.8-17	18	3	3	3	3
D_{dune} [m]	18	0	-15	750-1000	35	0-45
W_{dune} [m]	21	8	70	12	25	10-60
$R_{c,dune}$ [m]	0.10-1.60	1.60-3.10	2.55-2.75	0.57	(-1.00)-0.00	1.35-4.35
$h_{dunefoot}$ [m]	0.0-1.5	0.0-1.5	1.9	0.7	2.1-3.0	0.9-2.6
Dike parameters						
cot α_{dike} [-]	2	2	3	10	4	2
$R_{c,dike}$ [m]	1.35-2.85	1.60-3.10	1.30-2.00	0.70	1.00-2.00	2.85
Sand parameters						
D_{50} [µm]	271	300	211	245	260	271

2.2 Model geometries

The analysis carried out in WP7 revealed that the beach or foreshore slope at the selected demonstrators (cot(α_{fore})) is most similar for the Belgian and Dutch demonstrators (Table 1). The foreshore slope is therefore chosen as a constant 1/40, which is consistent with the choice made for the foreshore slope (no erosion berm) in the first test series at TU Delft (Sevindik *et al.*, 2025). The foreshore slope is kept constant (cot α_{fore} = 40) throughout the

test series and different dune geometries, since reprofiling/reshaping the sandy foreshore slope is very labour intensive. Furthermore, one constant dike geometry design was considered for all experiments and represents the Belgian demonstrators best: a smooth impermeable dike slope (cot α_{dike} = 2) with a vertical sheet pile of length 2.7 m (prototype) at the dike toe to correctly represent the physics in case of scouring.

On the foreshore in front of the dike, the dune geometry was varied to investigate its effect on the dune-dike interactions (dune erosion behaviour and its effect on overwash and wave overtopping). For all geometries the dune slope (connecting the dune crest with the foreshore, front and – when relevant – back dune slope) was fixed to cot(α_{dune}) = 3. The variation of the dune geometries was done in three ways (Figure 3):

1. Variation of dune volume V_{dune} [m³] and width W_{dune} [m], for a constant $R_{c,dune}$ (= $R_{c,dike}$ = 2.85 m) and a dune connected to the dike (D_{dune} = 0 m):
    a. Representation of Katwijk (lowered):
    W_{dune} = 60 m ($V_{dune,Kat}$ = 287 m³/m)
    b. Representation of Middelkerke (lengthened): **BASE CASE**
    W_{dune} = 32 m ($V_{dune,Mid1ong}$ = $V_{dune,Kat}$/2 = 143 m³/m)
    c. Representation of Middelkerke:
    W_{dune} = 10 m ($V_{dune,Mid}$ = $V_{dune,\ Mid1ong}$/3 = 48 m³/m)
2. Variation of the gap width between dune and dike D_{dune} [m], for a constant dune volume ($V_{dune,Rav}$ = 143 m³/m) and constant $R_{c,dune}$ (= $R_{c,dike}$ = 2.85 m):
    a. Representation of Dunkerque:
    D_{dune} = 45.5 m (W_{dune} = 14.5 m)
    b. Representation of Raversijde (heightened):
    D_{dune} = 20 m (W_{dune} = 20 m)
    c. Representation of Middelkerke (lengthened): **BASE CASE**
    D_{dune} = 0 m (W_{dune} = 32 m)
3. Variation of the dune crest freeboard $R_{c,dune}$ [m] for a constant dune volume ($V_{dune,Rav}$ = 143 m³/m) and a fixed dike crest freeboard ($R_{c,dike}$ = 2.85 m):
    a. Representation of Katwijk (shortened):
    $R_{c,dune}$ = 1.35 m (W_{dune} = 16 m)
    b. Representation of Middelkerke (lengthened): **BASE CASE**
    $R_{c,dune}$ = $R_{c,dike}$ = 2.85 m (W_{dune} = 20 m)
    c. Representation of Raversijde (connected):
    $R_{c,dune}$ = 4.35 m (W_{dune} = 32 m)

All three variations share one same dune geometry (BASE CASE) to reduce the amount of dune geometries to be modelled. The first variation provides design insights into the required dune volume V_{dune} (defined as the volume of sand on top of the 1/40 foreshore virtually extended until the dike, see dashed gray line in Figure 2) to sufficiently protect against a given storm condition. From the point of view of coastal managers/designers it is

also interesting to know which dune geometry is best in terms of coastal safety for a given volume of sand (V_{dune} = constant) to shape a new dune on an existing beach/foreshore slope.

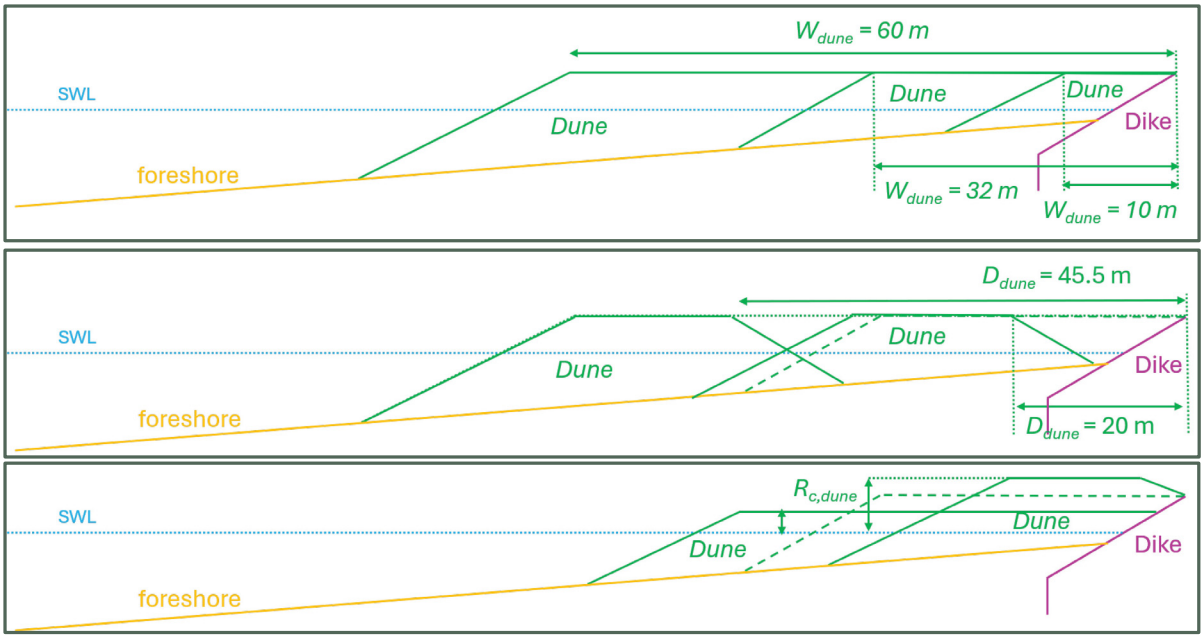


Figure 3 – Variations in dune geometry. Top: variation of dune volume (over width). Middle: variation of the gap width between dune and dike. Bottom: variation of the dune crest freeboard.

2.3 Model hydrodynamics

Due to practical constraints (e.g., sand scaling and wave paddle capabilities), the maximum sea-swell significant wave height $H_{m0,ss}$ considered was 4.25 m (prototype), which allows for a representative range for the design storm wave height of the Belgian and French demonstrators. This wave height is also similar to the maximum wave height used in the first test series at TU Delft (Sevindik *et al.*, 2025). A lower $H_{m0,ss}$ (= 2.0 m, prototype) was also considered in the experiment as a way to (partly) compensate for the overestimation of the bound IG wave energy by the long-crested waves that are generated in the wave flumes (compared to the bound IG of short-crested waves in the field).

When the Demonstrators were designed, the presence of offshore generated free infragravity (FIG) waves was not taken into account. It has been found recently that significant amounts of FIG waves can also be present in the North Sea (Akrish *et al.*, 2025; Reniers *et al.*, 2021; Rijnsdorp *et al.*, 2021). Like in the first test series (Sevindik *et al.*, 2025), the potential effect of these FIG was examined, now also on the dune morphodynamics instead of only on the wave hydrodynamics. While most tests were performed without these additional FIG, one dune geometry was repeated with the addition of very large offshore free IG waves ($H_{m0,FIG}/H_{m0,ss} \approx 0.18$) on top of the already present bound IG waves.

For all dune geometries the same still water level (corresponding to $R_{c,dike}$ = 2.85 m, prototype) is used. This assumes the most important processes are occurring at the peak of the storm (when the water level is more or less constant during high tide). To test this assumption also a variable water level was considered for the BASE CASE dune geometry, to model the tide and storm surge evolution over the storm duration of 45h (prototype, Figure 4). For modelling a variable water level in the flume, a discretized stepwise approach with an interval of 1h was used. Because of practical limitations (e.g., instrument range), the number of tests was reduced to the water levels at or exceeding the limit between the swash and collision regimes (Sallenger, 2000) (see red dashed line in Figure 4a). The criteria for the Sallenger storm impact regimes are provided in Annex 1.

Other variations in the hydrodynamic boundary conditions were not considered, since the main focus of this experimental campaign is comparing the performance of different dune geometries for the same (prototype) hydrodynamic conditions (**BASE CONDITIONS**):

- $H_{m0,ss}$ = 4.25 m;
- T_p = 12.0 s;
- $R_{c,dike}$ = 2.85 m.

The BASE CASE dune geometry (and for all other cases with $R_{c,dune} = R_{c,dike}$) with these BASE CONDITIONS is in the transition zone between the collision and overwash regimes according to the dune storm impact classification by Sallenger (2000). The variations in de dune geometry and wave conditions make sure the test matrix includes clear collision and overwash regimes and a transition zone overwash/inundation regime as well.

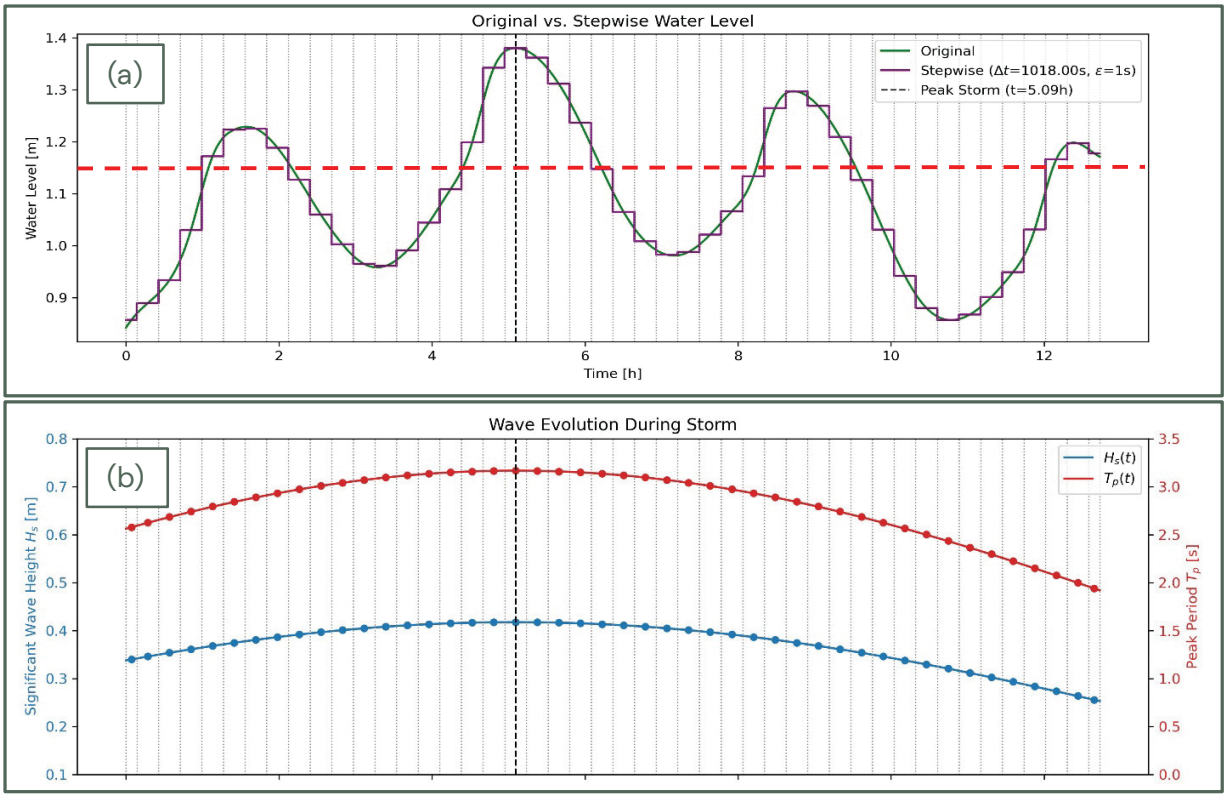


Figure 4 – Hydrodynamic conditions for the Belgian prototype 45h design storm (Sevindik et al.*, 2024). All values in model scale (1:12.5). (a) Tide and storm surge evolution over time including a discretized stepwise approach with an interval of 1h (prototype) for modelling the tidal/surge variation in the wave flume. The vertical dashed line indicates the peak of the storm. The horizontal red dashed line indicates the water level threshold between the swash (lower) and collision (higher) regimes (Sallenger, 2000). (b) Design storm wave conditions over the same prototype 45h storm (shares x-axis with top figure).*

2.4 Field case HybridDune

Within the NWO (Dutch scientific research fund) funded programme called the "Future Flood Risk Management Technologies (Future FRM Tech) programme", a field measurement setup called "HybridDune" of a hybrid dune-dike coastal protection system was constructed end of 2024 at the Sand Engine site in The Netherlands (Poppema *et al.*, 2026). The dune geometry, sand grain size and hydrodynamic conditions of the measured storms were compatible with the DuneFront model scale and setup in the Large Wave Flume of Flanders Hydraulics (present setup). This presented an opportunity to include the field setup of the hybrid dune-dike section in the flume experiments, and reproduce the storm conditions as measured in the field, so that a model scale effects analysis can be done. The results of this test series allow to investigate how well the (absolute) flume experiment results are transferable to prototype scale.

The cross-shore bed profile of the field setup is shown in Figure 5. One of the main challenges was to reproduce the storm conditions in the flume as accurately as possible:

- The directional spreading of the short-crested waves in the field is not reproduced in a wave flume (only long-crested waves possible).
- The foreshore slope of the flume model (1/40) is not the same as in the field (1/18, 1/147 and 1/90 (Figure 5)).

The measured offshore wave conditions could therefore not be used as input for the wave conditions at the wave paddle in the flume. The wave conditions measured during the storm near the dune foot were used instead, by de-shoaling the incident wave spectrum near the dune foot to the water depth at the wave paddle with a foreshore slope of 1/40.

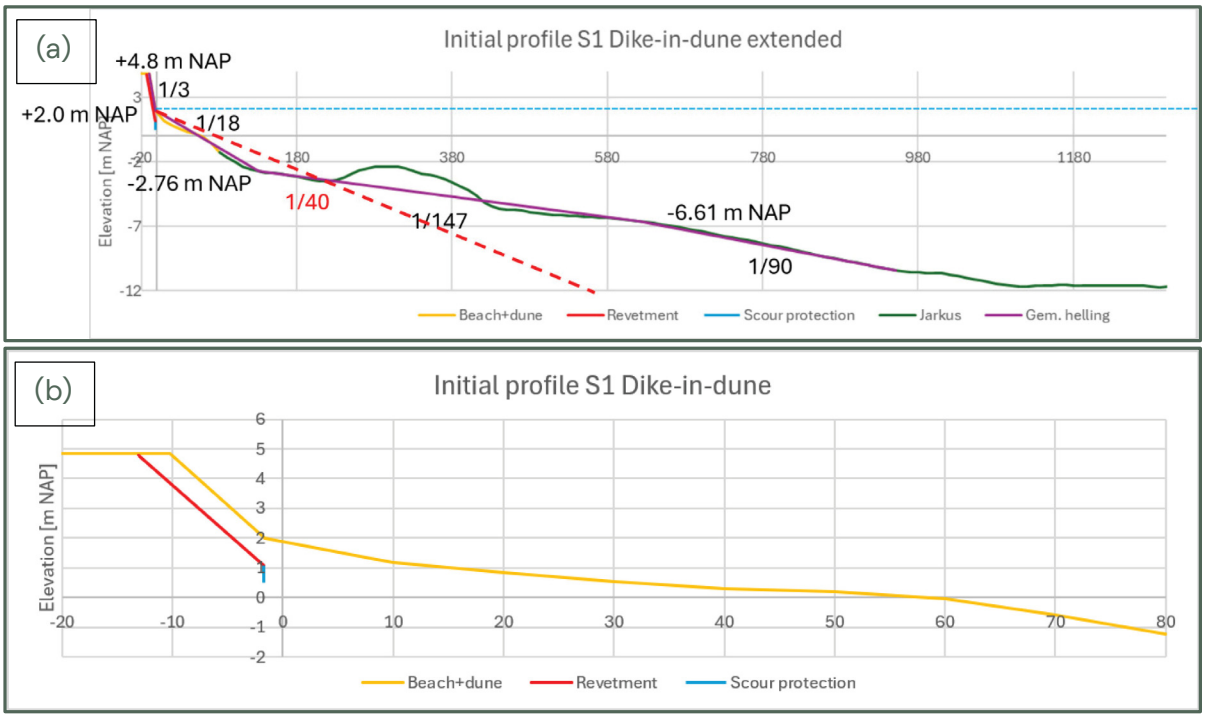


Figure 5 – Cross-shore bed profile of the HybridDune field setup (red line: dike slope; yellow line: beach survey; green line: foreshore survey (March 2024); purple line: simplified linear beach and foreshore slopes; red dashed line: the 1/40 foreshore slope available in the DuneFront flume experiment). (a) Overview from dike to deep water. (b) Close-up on the hybrid dune-dike cross-section and the beach in front of it.

During the first measured storm (Storm 1, 19/12/2024), most of the initial dune erosion occurred and exposed the dike slope. The most severe dune erosion happened in the first 104 min (prototype) of the second high tide during Storm 1 (Figure 6). The incident hydrodynamic conditions at +0.00 m NAP near the dune foot were:

1. First 52 min (prototype): SWL = 1.95 m NAP; H_{m0} = 1.67 m; Tp = 7.1 s;
2. Second 52 min (prototype): SWL = 2.02 m NAP; H_{m0} = 1.67 m; Tp = 8.0 s.

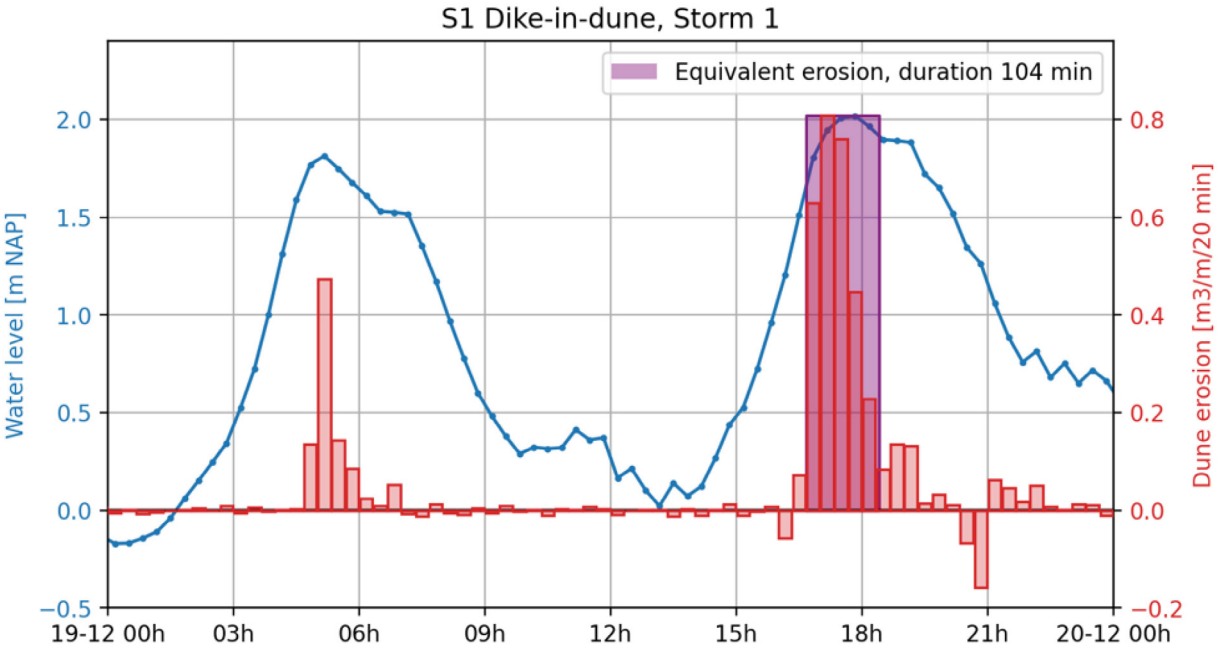


Figure 6 – Measured water level (left Y-axis) and dune erosion rates (right Y-axis) at the HybridDune field setup during the first measured storm.

3. Experimental setup

3.1 Experimental facilities

The experiments were conducted in the large wave flume of Flanders Hydraulics (Antwerp, Belgium) from March to June 2026. The flume is 84 m long, 2 m wide and 2.5 m deep (Figure 7). This flume is equipped with a piston type wave paddle actuated by electromotors and the steering software Merlin (HR Wallingford, 2024). The system is capable of generating regular waves with a wave height of up to 0.80 m and irregular waves with a significant wave height of up to 0.40 m for a water depth of up to 1.50 m. Irregular waves can be generated using 2nd order sub- and super-harmonic corrections, and compensation for reflected waves is done using active wave absorption (for wave frequencies f in the flume: 0.1 Hz < f < 1.5 Hz).



Figure 7 – The large wave flume of Flanders Hydraulics with the DuneFront model setup.

3.2 Wave flume coordinate system

The origin of the wave flume coordinate system is located at the home (zero) wave paddle position, in the middle over the width of the flume and for flume water depth h = 0.00 m (= zero of the temposonic water level instrument reference). The coordinate system axes are defined as:

- X-axis: origin at home (zero) wave paddle position, aligned along the length of the flume, and positive in the incident wave propagation direction.
- Y-axis: origin at centre of wave flume, aligned along the width of the flume, and positive towards the left side of the flume (looking along the positive X-axis).
- Z-axis: origin at flume water depth h = 0.00 m (= zero of temposonic water level reference), directed vertically, and positive upwards.

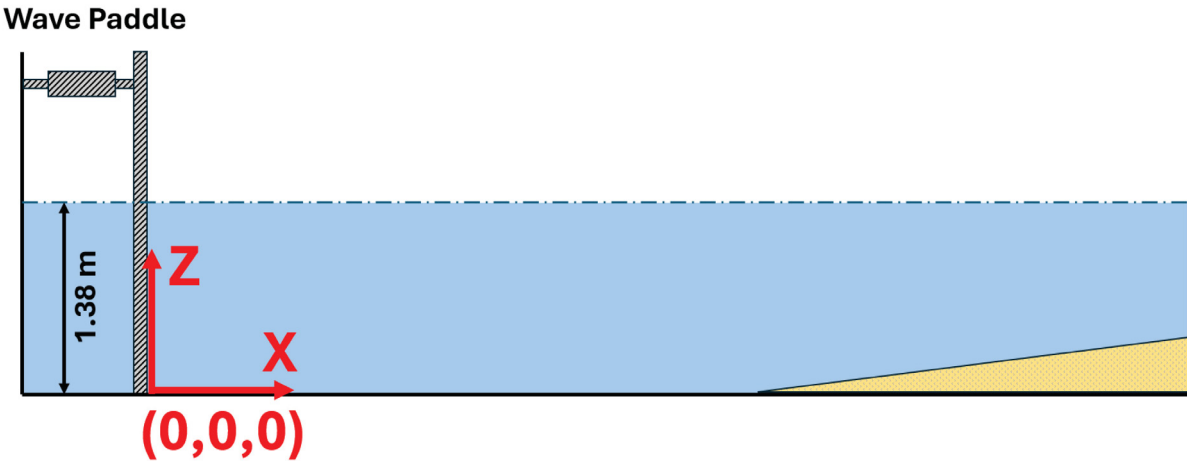


Figure 8 - Origin of the reference system in the wave flume

3.3 Model setup

The experiments were caried out using a 1:12.5 Froude-scaled model. In the model setup, the foreshore and dune consisted of 74 m³ of well-sorted silica sand (properties in Table 2) with a grain size of D_{50} = 126 µm, compacted to medium to dense sand using a vibration tool and a few days of wave action in the flume before profiling the first dune geometry.
Reproduction of prototype wave run-up, overwash and overtopping requires (Vellinga, 1986):

- Undistorted scaling (length and depth model scales are the same);
- An accurate reproduction of prototype dune erosion, which can be achieved by Froude scaling of the hydraulic conditions (wave height $H = H_{m0,ss}$ and wave period $T = T_p$) and the fall velocity w_s of the model sand. This means that Dean's parameter (= $H/(Tw_s)$) remains constant (approximately: Vellinga demonstrated that a difference of 30% is acceptable) between prototype and model scale.

When acquiring the sand, an empirical formula for calculating the fall velocity (Ahrens, 2000) was used (w_s = 0.011 m/s, Table 2). Afterwards the fall velocity was measured in a laboratory leading to a higher value (w_s = 0.018 m/s, Table 2). For the BASE CONDITIONS, based on the calculated w_s, Dean's parameter is 30% lower than that of prototype, but still acceptable according to Vellinga (1986). Based on the measured w_s, Dean's parameter is 57% lower than that of prototype. Further study is needed to determine the impact of a higher than 30% deviation on the accuracy of reproduction of prototype dune and beach morphodynamics.

The main properties of the sand used for the model are provided in Table 2.

Table 2 – Properties of the sand used in the experiments.

Parameter	Value
Median grain size D_{50} [µm]	126
10th percentile grain size D_{10} [µm]	87
90th percentile grain size D_{90} [µm]	170
Solid grain density [kg/m³]	2701
Fall velocity [m/s]	0.011 (calculated using (Ahrens, 2000)) 0.018 (measured)

The general model setup in the large wave flume is shown in Figure 9, and includes a 1/40 foreshore slope for all dune geometries. The wave instrumentation is partly shown in Figure 9 as well, but more detailed in Section 3.4.1. The different dune geometries and dune geometry case dependent positions of AWG_10 – AWG_11 are provided in Chapter 4.

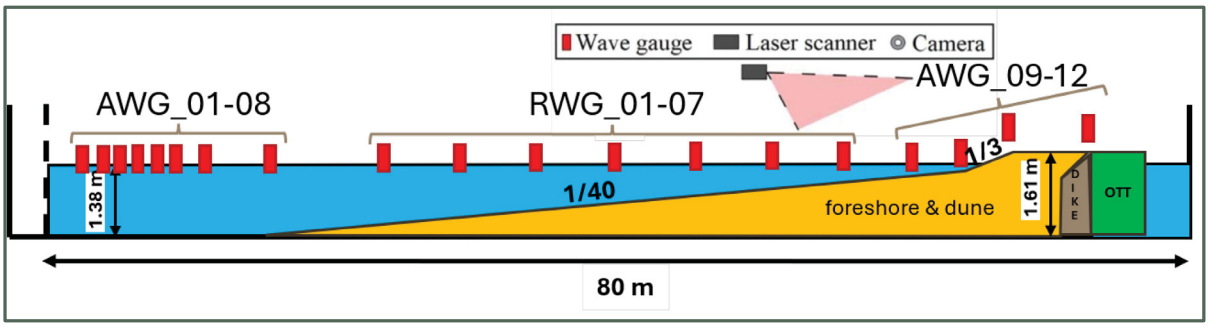


Figure 9 – Model setup in the LWF, with indication of the instrumentation (partially: acoustic wave gauge (AWG), resistive wave gauge (RWG) and overtopping tank (OTT)).

Figure 10 provides a frontal and top view on the dike slope, overtopping chute, recirculation platforms, and the laser reference beam and blocks.



Figure 10 –Views on dike. (a) Frontal view on dike slope, overtopping chute (in the middle), overtopping recirculation platforms (left and right from chute), and overtopping event detector AWG_12 fixed through the LIDAR reference beam. (b) Top view of dike after fitting the four laser distance meter reference (wooden) blocks on the LIDAR reference beam. The four laser reference blocks were available from DUNE02 onwards.

3.4 Instrumentation

3.4.1 Wave hydrodynamics

Resistive wave gauges

Resistive wave gauges (RWG) measure water surface elevation based on the electrical current between two parallel stainless steel wires. The current is proportional to the water depth and converted into a voltage signal. The sensors are designed to minimize interference with the wave field.



Figure 11 - Resistive Wave Gauge (RWG)

RWG data were recorded using a sampling frequency of 40 Hz in seven location along the length of the flume (along the X axis). These wave gauges had fixed position during all the dune geometries and tests conducted during the campaign. The X-coordinates of these resistive wave gauges are reported in Table 3. Every RWG was equipped with an automatic 5-point vertical calibration system. RWG calibration (for conversion of voltage to meters) was done on a daily basis.

Table 3 – X-coordinates of the resistive wave gauges (RWG).

Sensor	X [m]
RWG_01	38.738
RWG_02	42.732
RWG_03	46.748
RWG_04	50.744
RWG_05	54.734
RWG_06	58.739
RWG_07	62.738

Acoustic wave gauges

Acoustic wave gauges (AWGs) are non-contact instruments used to measure the instantaneous water-surface elevation in laboratory wave experiments. They operate by transmitting ultrasonic pulses toward the water surface and determining the distance between the sensor and the free surface from the travel time of the reflected acoustic signal. Continuous measurements of this distance provide time series of free-surface elevation that can be used to characterize wave height, period, and other wave-related fluctuations. Because AWGs are mounted above the water surface, they do not physically interfere with the flow and are therefore particularly useful in regions with rapidly varying water levels. Their measurements can, however, be affected by factors such as steep or highly disturbed free surfaces, aeration, spray, and variations in the strength of the reflected acoustic signal (Sener *et al.*, 2023). For this reason, the AWG's were only used in the non-breaking or swash zone areas, using RWGs in the surf zone instead (Figure 9).

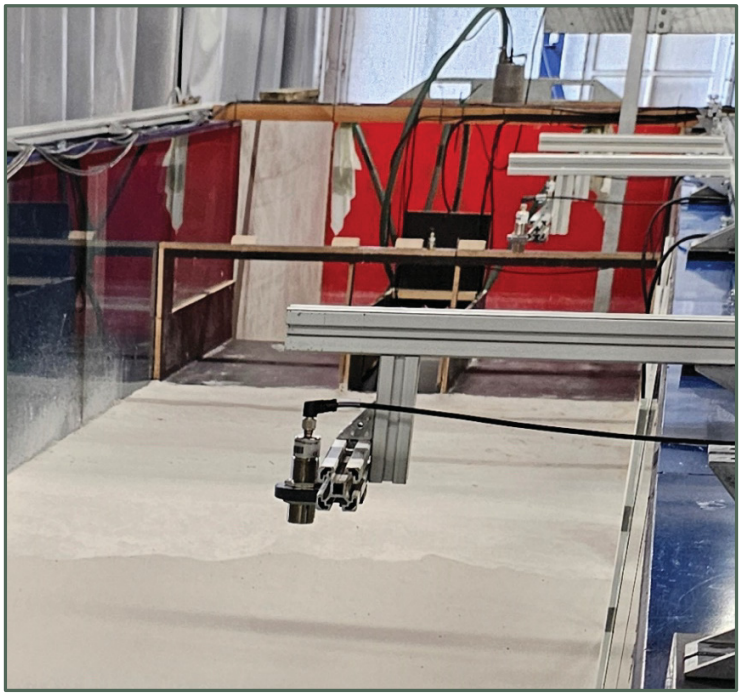


Figure 12 - Acoustic wave gauge (AWG), from General Acoustics.

AWGs from (and calibration by) General Acoustics were used. The AWG data in this campaign were recorded using a sampling frequency of 50 Hz. The location of AWGs are presented in Table 4. AWGs from 01 to 08 were located in offshore area at the paddle for analysis of incident and reflected waves. AWGs 10 and 11 are dune geometry dependent, usually collocated with pressure transducer gauges (PTG) and their exact locations are described in Chapter 4. AWG 12 is located at the entrance of the overtopping (OTT) chute to identify individual overtopping events. AWGs 13 to 16 are located in the four corners at the top of the OTT to measure the water surface level (Section 3.4.3).

Table 4 – X-coordinates of the acoustic wave gauges (AWG), corresponding to the middle of the instrument.

Sensor	X [m]
AWG_01	11.470
AWG_02	12.620
AWG_03	13.350
AWG_04	13.991
AWG_05	14.661
AWG_06	15.032
AWG_07	16.062
AWG_08	27.562
AWG_09	68.032
AWG_10	Test case-dependent

AWG_11	Test case-dependent
AWG_12	Entrance of OTT chute
AWG_13	In OTT
AWG_14	In OTT
AWG_15	In OTT
AWG_16	In OTT

Electromagnetic current meters

Electromagnetic current meters (ECMs) are used to measure the local water-flow velocity by applying Faraday's principle of electromagnetic induction. When electrically conductive water moves through the magnetic field generated by the sensor, an electrical voltage is induced between a pair of electrodes, with its magnitude proportional to the velocity component perpendicular to the magnetic field (Chen *et al.*, 2023).



Figure 13 - Electromagnetic current meter (ECM), Deltares E30 probe (water velocity measurement in two perpendicular directions in the plane parallel to and below the black ellipsoid (11x33 mm) at the end of the instrument).

During this campaign, four electromagnetic current meters (ECM) were installed collocated with AWG/RWG so that they can be used to separate incoming and reflected wave components (Buckley *et al.*, 2015; Guza *et al.*, 1984):

- ECM_01 was collocated with AWG_04;
- ECM_02 was collocated with RWG_01;
- ECM_03 was collocated with RWG_07;
- ECM_04 was collocated with AWG_09.

Calibration of the four ECMs was checked in a current flume for known flow velocities.

Table 5 – X, Z-coordinates of the electromagnetic current meters (ECM), middle of the undersize of the black ECM ellipsoid.

Sensor	X [m]	Z [m]
ECM_01	14.0015	0.8884
ECM_02	38.7616	0.9133
ECM_03	62.7585	1.0617
ECM_04	68.0465	1.2914

Pressure transducer gauges

Four DRUCK UNIK 5000 pressure transducer gauges (PTGs; Figure 14) were installed to measure pore-water pressure within the sand bed. The locations of the PTGs depended on the tested dune geometry. Some were installed beneath the shallow-water zone seaward of the dune, for example near the dune toe. Others were placed beneath the dune to monitor pore-water pressure and associated wave-induced fluctuations in the groundwater level. For configurations in which the dune was disconnected from the dike, PTGs were also installed beneath the shallow-water zone between the dune and the dike. To prevent sand intrusion into the sensitive pressure membrane in the PTGs, the sensors were wrapped in a nylon filter cloth before being buried in the sand (Figure 14). To prevent air pockets from forming around the sensing elements, the PTGs were installed with a slight upward inclination, allowing trapped air to escape naturally as the flume was filled and the instruments became submerged. The PTG measurements were recorded at a sampling frequency of 40 Hz.



Figure 14 – Pressure sensor used for pore pressure measurement in the sand. Top: pressure sensor and cable. Bottom left: close-up of pressure sensor and black guard to diaphragm (+/- 1 cm recessed). Bottom right: PTG01 in the flume (exposed after dike toe scouring).

The PTGs were positioned beneath the foreshore to monitor free-surface elevations and beneath the dune to monitor the groundwater table and its response to wave action. If the overlying dune material was eroded during a test and a free water surface developed above a PTG, the instrument could subsequently be used to determine the local free-surface elevation. The individual gauges were aligned with key features of the tested geometries: PTG_01 was positioned in line with the upper edge of the seaward slope of DUNE01 and DUNE05, while PTG_02 was aligned with the upper edge of the landward slope of DUNE05. PTG_03 was aligned with the centre of the DUNE04 crest, and PTG_04 was installed as close as practically possible to the dike toe.

Table 6 – Coordinates of the Pressure Transducer Gauges (PTG).

Sensor	X [m]	Y [m]	Z [m]
PTG_01	70.223	-0.796	1.075
PTG _02	71.376	-0.797	1.097
PTG _03	72.617	-0.795	1.135
PTG _04	73.920	-0.802	1.169

3.4.2 Beach/dune morphodynamics and sediment transport

Mobile distance laser bed profile system

A high resolution sub-aerial and sub-aqueous laser based laboratory beach profile measurement system was developed based on Atkinson and Baldock (2016) and validated in Gruwez et al. (2026). The system consists of a trolley (Figure 15) equipped with four laser distance meters (LDM) (SICK DT80, Figure 16 left) pointing downwards (negative Z-direction) with a slight inclination of 3.2° to avoid detecting any beam portion reflected off the water surface. The four lasers are fixed next to each other (over the width of the flume) on the trolley (Figure 15), programmed to drive autonomously along the length of the flume (positive X-direction). The Y and Z-coordinates of the four LDM sensors are provided in Table 7. The X-coordinate is registered when the trolley is driving along the length of the flume by the step motor (Figure 17 top) and by a wheel distance meter (except for the first tested dune geometry DUNE01) fixed to the trolley and rolling on the flume side wall (Figure 17 bottom).

Table 7 – Y and Z-coordinates of the laser distance meters (SICK DT80) (LDM).

Sensor	Y [m]	Z [m]
LDM_01	0.635	2.285
LDM_02	0.239	2.282
LDM_03	-0.017	2.283
LDM_04	-0.260	2.278

The trolley could be started from five reference home positions (Table 8).

Table 8 – X-coordinates of the laser distance meters for the five home positions.

Trolley home	X [m]
Home 1	23.58
Home 2	40.70
Home 3	60.00
Home 4	64.60
Home 5	66.86

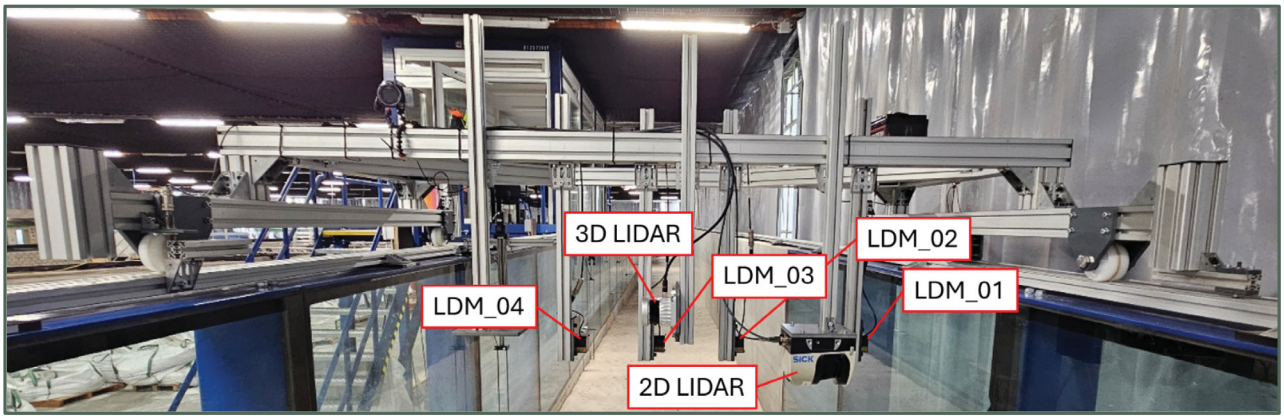


Figure 15 – Trolley equipped with four laser distance meters, a 2D and 3D LIDAR.

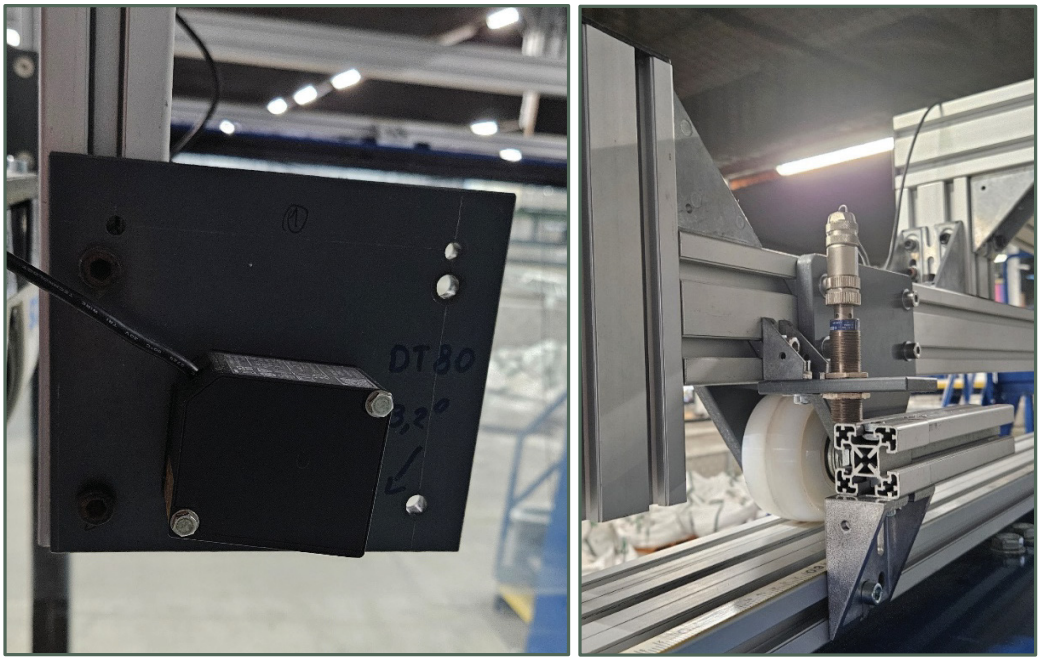


Figure 16 – Left: close-up of one of the laser distance meters on the trolley. Right: close-up of the magnet sensor for accurate homing to one of the fixed home positions (Table 8).

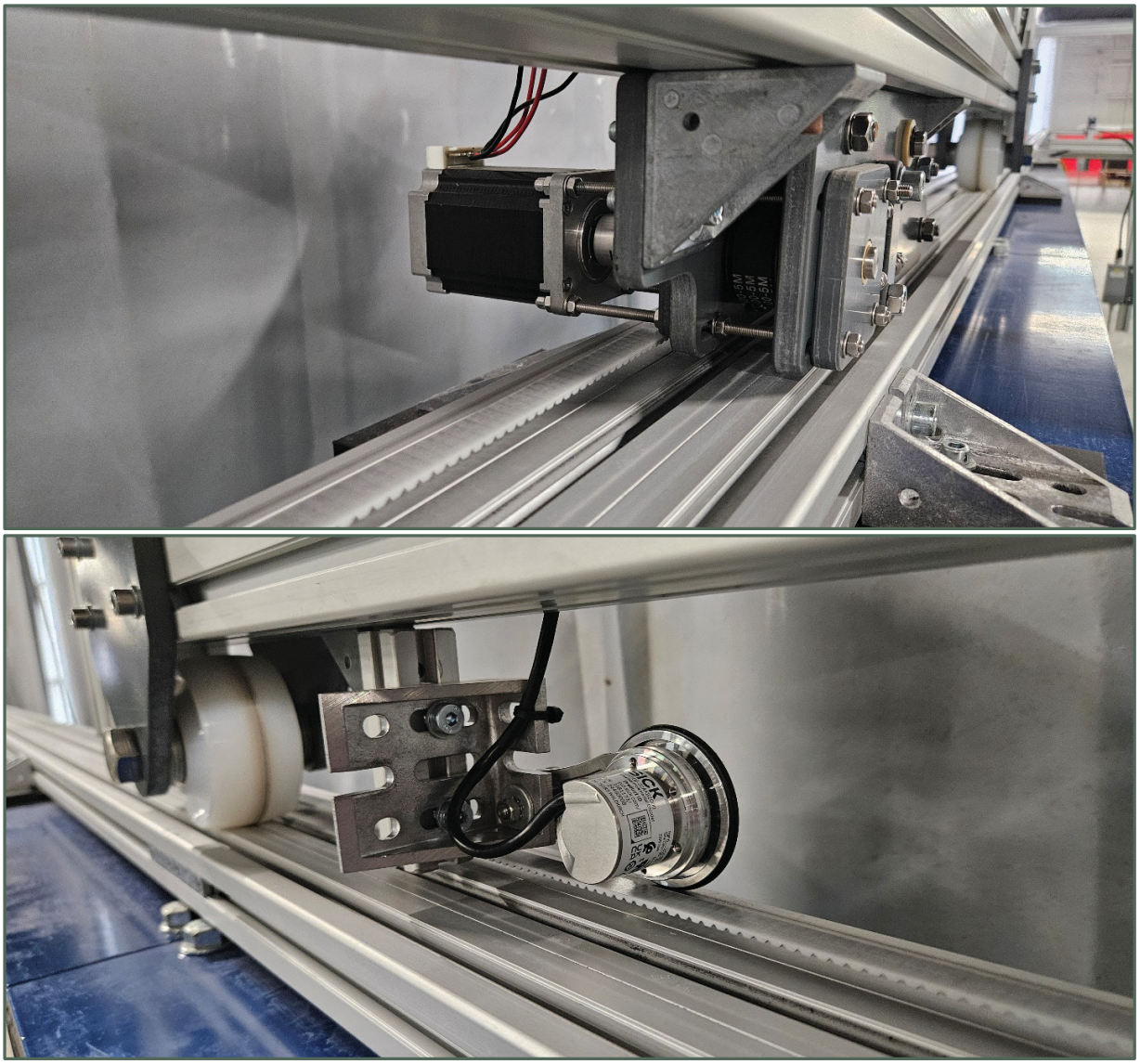


Figure 17 – Top: trolley step motor to move the trolley along the length of the flume. Steps are counted to determine the distance travelled by the trolley. Bottom: A wheel distance meter attached to the trolley for a second registration of travelled distance along the length of the flume.

2D and 3D LIDARs

The laser trolley serves three functions:

1. Mobile bed profiling in between tests for still water conditions;
2. 2D and 3D LIDAR measurements during wave tests capturing the dune erosion processes during the test. The 3D LIDAR potentially also captured the wave surface and runup process (to be investigated further);

3. Using the 3D LIDAR, snapshots were taken at all Home positions of the dry beach/dune bed profile before and after each test series and of the dry part of the dune profile in between tests.

Both LIDARs were fixed on the trolley (Figure 18), with Y and Z coordinates provided in Table 9. The trolley was positioned at one of two fixed locations during most of the tests: either at Home 4 or 5 (Table 8), depending on the dune geometry and progression of the dune erosion. Close enough to achieve good accuracy, but also far and low enough to capture dune erosion overhangs (Mehrtens *et al.*, 2025) that occur in collision regime (Sallenger, 2000). A reference beam was constructed above the dike crest (Figure 10a), which was always in view of both LIDARs. This reference beam (among other available fixed reference points: e.g. floor, window beams,...) is used to reference all LIDAR measurements to in the post-processing of the data.

Table 9 – Y and Z-coordinates of the 2D LIDAR (SICK LMS511-20100) and 3D LIDAR (Ouster Lidar OSO 128 SR).

Sensor	Y [m]	Z [m]
2D LIDAR	0.52	To be related to reference points.
3D LIDAR	0.00	To be related to reference points.

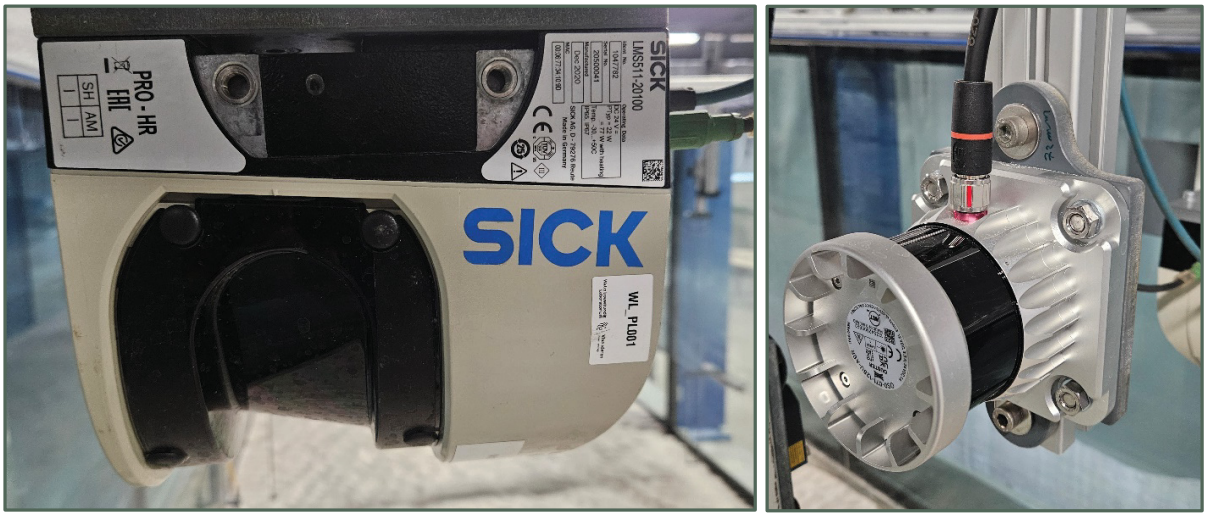


Figure 18 – Left: 2D LIDAR on the trolley. Right: 3D LIDAR on the trolley.

Optical backscatter sensors

Optical backscatter sensors (OBS) are commonly used to measure suspended sediment concentration (SSC) in laboratory and field studies of sediment transport. The sensor emits infrared light into the water, and suspended sediment particles scatter part of this light

back toward a photodetector, producing an electrical signal related to the amount of sediment in suspension (Downing, 2006).

In this campaign two OBSs were installed to measure SSC and water temperature (TEMP) collocated with the two shallow water ECMs (Figure 19/section) and RWG/AWG:

- OBS01 was collocated with ECM03 and RWG07;
- OBS02 was collocated with ECM04 and AWG09.

OBS data were recorded using a sampling frequency of 40 Hz and their coordinates are provided in Table 5.

The calibration of both OBS instruments was done after the wave flume experiments and is included in Annex 2.



Figure 19 –OBS collocated with ECM during the campaign. Left: overview of mount, right: close-up of sensors (ECM ellipsoid sensor on the left and OBS on the right).

Table 10 – X, Z-coordinates of the optical backscatter sensors (OBS), middle of the sensor.

Sensor	X [m]	Z [m]
OBS_01	62.7429	1.0510
OBS_02	68.0505	1.2800

Thermometer

The water temperature is needed to be able to calculate the fall velocity of the sand in the water of the flume. Therefore, a thermometer was installed in zone 3 of the flume (recirculation zone of overtopped water). This sensor was installed later in the test campaign, and available temperature data are indicated inTable *28*.

Temperature data were recorded using a sampling frequency of 40 Hz.

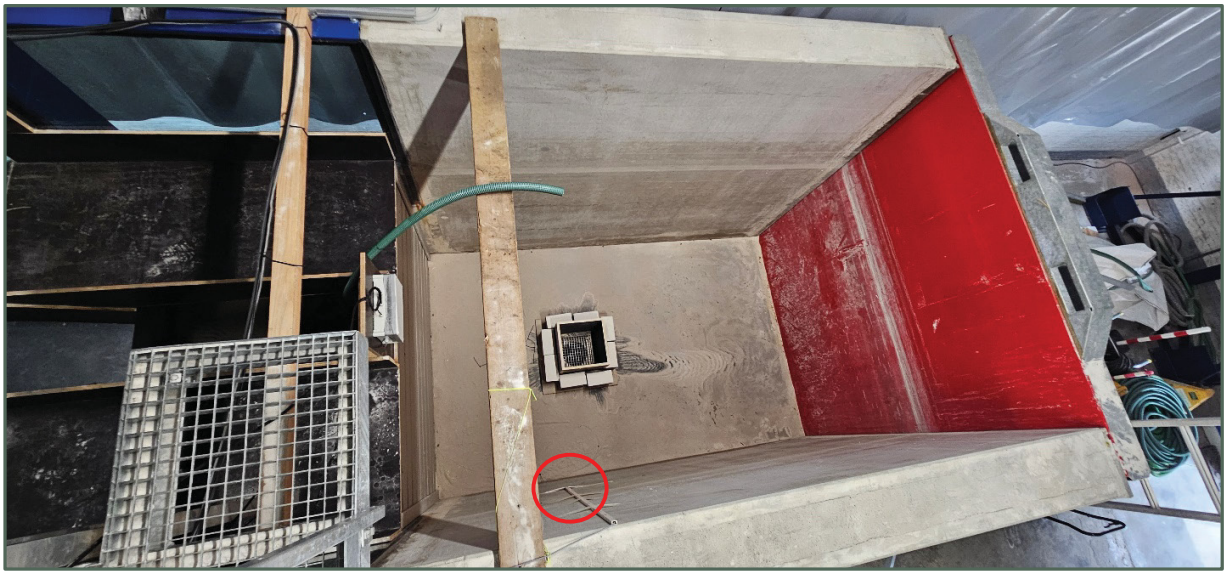


Figure 20 - Temperature sensor (red circle) in the recirculation area of the flume (behind the OTT).

3.4.3 Wave overtopping and overwash

The wave overtopping and overwash measurement system consists of a rigid bottom frame (Figure 21, a) and a collection or overtopping tank (OTT) with a rectangular base measuring 1.25 m × 1.50 m (with a height of +/- 0.70 m) and a usable internal volume of approximately 1 m³. The OTT is supported by three load cells (Figure 21, b), which continuously measure the forces transmitted from the tank to its supports. The total instantaneous weight of the OTT

and its contents is obtained by summing the measurements from the three load cells. Changes in this total weight during a test therefore provide a continuous measurement of the mass entering the overtopping tank. To isolate the rigid frame, overtopping tank and the load cells and remove the effect of buoyancy the overtopping section is separated from the end of the flume by using impermeable aluminium water retaining walls as shown in Figure 22.

Overtopping flow is conveyed into the tank through a 0.40 m-wide chute, Figure 10a and b (chute width at different levels is presented in

Table 11). Since the total flume width is 2.0 m, only a portion of the overtopping discharge is collected, while the flow over the remaining 1.60 m width bypasses the collection system and returns to the flume behind the tank (Figure 22). This arrangement serves two purposes. First, allowing part of the overtopping discharge to return to the flume helps maintain the offshore water level and limits artificial set-down during the experiments. Second, restricting the collection width reduces the volume accumulated in the tank, thereby maintaining sufficient sensitivity and accuracy of the load-cell measurements.

Four ultrasonic sensors (from AWG 13 to AWG 16) are installed above the tank, one near each corner, to continuously monitor the water surface elevation within the tank. The ultrasonic measurements, together with the total mass obtained from the load cells, provide complementary information on the material collected during overtopping. By combining these measurements, the volume of overtopping water and the amount of entrained sediment deposited in the tank can be estimated. The detailed procedure used for this separation is described in Section 5.4.3.

Table 11 – Coordinates of the dike crest at the overtopping chute wide..

	Value
X [m]	75.030
Z [m]	1.610
Chute Width (for Z = 1.610) [m]	0.403
Chute Width (for Z = 1.660) [m]	0.405
Chute Width (for Z = 1.879 m) [m]	0.405



Figure 21 - Overtopping tank (OTT) set-up: (a) frame and (b) installed load cells.



Figure 22 – Separation of overtopping tank and the load cells from back of the flume (dry dock for OTT). Left: view on overtopping tank (OTT) on three load cells without the back retaining wall for dry dock of OTT. Right: with back retaining wall dry dock OTT.

4. Test program

4.1 Overview

Based on Chapter 2, the experimental test programme (summarized in Table 12) included a range of dune-dike configurations representing the selected DuneFront demonstrators (Section 2.2), covering different hydrodynamic conditions and storm impact regimes according to Sallenger (2000) (Section 2.3), and including the field case HybridDune (Section 2.4). In addition to variations in dune geometry, selected configurations were repeated, including an exact repetition (i.e. , DUNE05 and DUNE05rep) to demonstrate repeatability of the experiments. Other repeated geometries focussed on modified hydrodynamic conditions to investigate specific effects, such as a lower wave height, variable water level and the presence of offshore free IG waves (Section 2.3).

For all dune geometries (except DUNE05var) the same hydrodynamic wave conditions were repeated for at least six tests, where in the first three tests progressively increasing test durations were applied to allow intermediate measurements of the evolving bed profile using the mobile trolley equipped with laser distance meters, following the approach of van Gent et al. (2008). The following tests each represented approximately 2.5 h of prototype high water and storm surge conditions. When possible, the tests were continued until exposure of the dike slope.

In the following sections the test matrix and specific instrumentation positions for each dune geometry are provided.

Table 12 – Test program overview of the tested DUNE geometries and associated Sallenger regime of the dune erosion behaviour (Sallenger, 2000).

Order [-]	Dune ID [-]	V_{dune} [m³/m]	W_{dune} [m]	D_{dune} [m]	$R_{c,dune}$ [m]	$R_{c,dike}$ [m]	Sallenger regime [-]	Representing demonstrator [-]
15	DUNE00	0.000	0.000	0.000	N/A	0.228	SWASH	Raversijde (no dune)
1	DUNE01	1.836	4.800	0.000	0.228	0.228	COLLISION/OVERWASH	Katwijk (lowered)
2	DUNE02	0.915	1.158	3.642	0.228	0.228	COLLISION/OVERWASH	Dunkerque ($H_{m0,ss}$ too high)
9	DUNE02loH	0.915	1.158	3.642	0.228	0.228	COLLISION/OVERWASH	Dunkerque, lower $H_{m0,ss}$
10	DUNE02cor	0.915	1.158	3.642	0.228	0.228	COLLISION/OVERWASH	Dunkerque (corrected $H_{m0,ss}$)
6	DUNE03	0.915	3.805	0.000	0.348	0.228	OVERWASH/INUNDATION	Raversijde (connected)
3	DUNE04	0.915	1.600	1.600	0.228	0.228	COLLISION/OVERWASH	Raversijde (heightened)
4	DUNE05	0.915	2.542	0.000	0.228	0.228	COLLISION/OVERWASH	Middelkerke (lengthened)
7	DUNE05rep	0.915	2.542	0.000	0.228	0.228	COLLISION/OVERWASH	Middelkerke (lengthened), repeated
8	DUNE05loH	0.915	2.542	0.000	0.228	0.228	COLLISION/OVERWASH	Middelkerke (lengthened), lower $H_{m0,ss}$
11	DUNE05var	0.915	2.542	0.000	0.228	0.228	COLLISION/OVERWASH	Middelkerke (lengthened), variable water level
12	DUNE05fig	0.915	2.542	0.000	0.228	0.228	COLLISION/OVERWASH	Middelkerke (lengthened), added free IG waves
5	DUNE06	0.915	1.292	0.357	0.108	0.228	COLLISION	Katwijk (shortened)
13	DUNE07	0.307	0.820	0.000	0.228	0.228	COLLISION/OVERWASH	Middelkerke
14	DUNE12	0.276	0.251	0.000	0.220	0.220	COLLISION	HybridDune (field case)

4.2 DUNE00

The DUNE00 case represents the geometry without a dune in the flume, consisting only of a shallow foreshore with a 1:40 slope and the exposed dike slope. In this configuration, AWG 10 is co-located with PTG 02 at X= 71.378 m, while AWG 11 is located at the dike toe location (X = 74.420 m). The test program corresponding to the DUNE00 geometry is presented in Table 13 (and also includes the spectral or mean wave period T_{m02}).

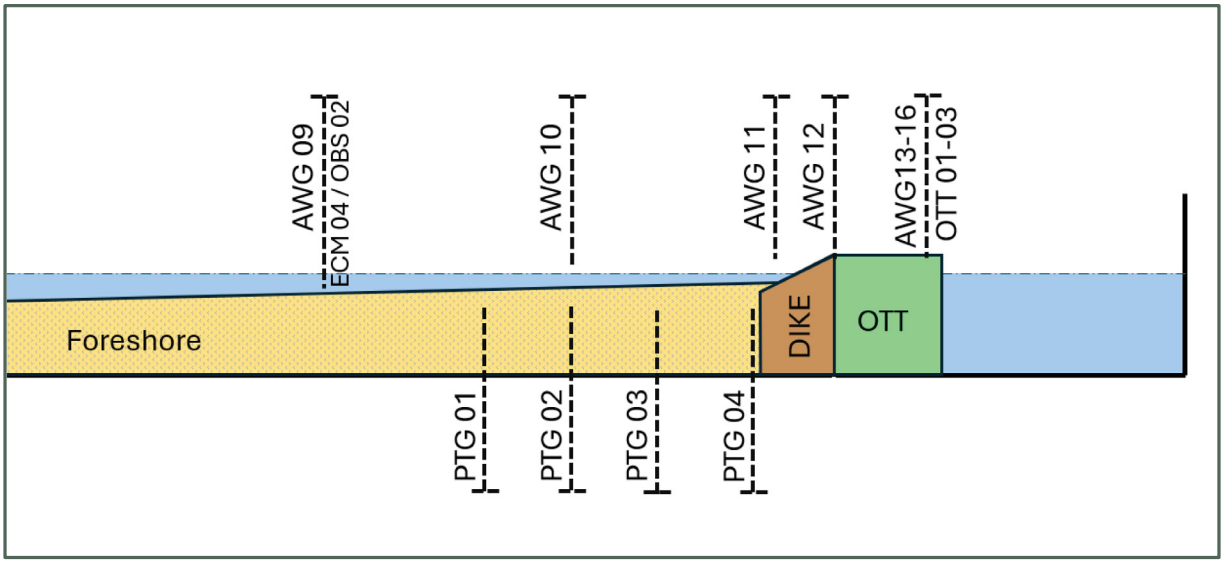


Figure 23 - Close-up view of the dune–dike geometry and instrumentation layout for test DUNE00. The PTGs were located in the sand (at the top end of the dashed lines).

Table 13 – Test program for dune geometry DUNE00.

Test or profile ID [-]	h_p [m]	$H_{m0,ss}$ [m]	$T_{p,ss}$ [s]	T_{m02} [s]	$H_{m0,fig}$ [m]	$T_{p,fig}$ [s]	Duration [s]	#waves [-]
DUNE00_P00_dry_rep0_H1	0.00	–	–	–	–	–	–	–
DUNE00_P00_wet_rep0_H5	1.38	–	–	–	–	–	–	–
DUNE00T001	1.38	0.34	3.4	2.83	0.00	n/a	283	100
DUNE00_P01_wet_rep0_H3	1.38	–	–	–	–	–	–	–
DUNE00T002	1.38	0.34	3.4	2.83	0.00	n/a	600	212
DUNE00_P02_wet_rep0_H1	1.38	–	–	–	–	–	–	–
DUNE00T003	1.38	0.34	3.4	2.83	0.00	n/a	1131	400
DUNE00_P03_wet_rep0_H3	1.38	–	–	–	–	–	–	–
DUNE00T004	1.38	0.34	3.4	2.83	0.00	n/a	2546	900
DUNE00_P04_wet_rep0_H3	1.38	–	–	–	–	–	–	–
DUNE00T005	1.38	0.34	3.4	2.83	0.06	18.7	2546	900
DUNE00_P05_dry_rep0_H1	0.00	–	–	–	–	–	–	–

4.3 DUNE01

The DUNE01 case represents the dune geometry at Katwijk with lowered dune crest and a foreshore of 1:40 slope. In this configuration, AWG 10 is co-located with PTG 01 at X= 70.220 m, while AWG 11 is located at X= 73.922 m. The test program corresponding to the DUNE01 geometry is presented in Table 13. The duration of running this test is longer than a normal test to let the dune erosion being fully developed and reach the dike location.

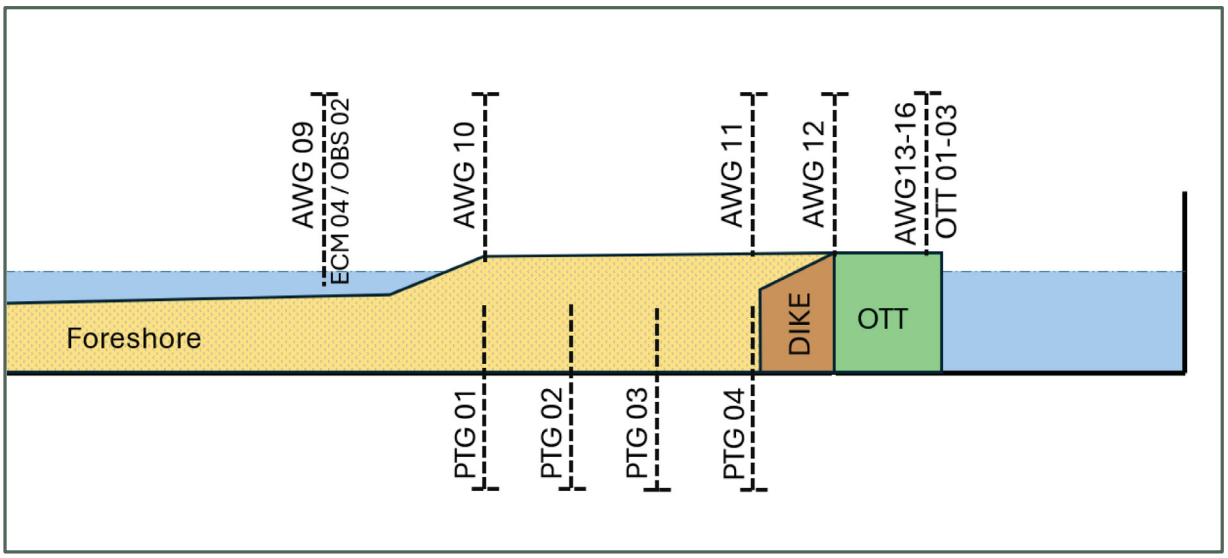


Figure 24 - Close-up view of the dune–dike geometry and instrumentation layout for test DUNE01. The PTGs were located in the sand (at the top end of the dashed lines).

Table 14 - Test program for dune geometry DUNE01.

Test or profile ID [-]	h_p [m]	$H_{m0,ss}$ [m]	$T_{p,ss}$ [s]	T_{m02} [s]	$H_{m0,fig}$ [m]	$T_{p,fig}$ [s]	Duration [s]	#waves [-]
DUNE01_P00_dry_rep0_H1	0.00	–	–	–	–	–	–	–
DUNE01_P00_wet_rep0_H1	1.38	–	–	–	–	–	–	–
DUNE01T001	1.38	0.34	3.4	2.83	0.00	n/a	283	100
DUNE01_P01_wet_rep0_H1	1.38	–	–	–	–	–	–	–
DUNE01T002	1.38	0.34	3.4	2.83	0.00	n/a	600	212
DUNE01_P02_wet_rep0_H1	1.38	–	–	–	–	–	–	–
DUNE01T003	1.38	0.34	3.4	2.83	0.00	n/a	1131	400
DUNE01_P03_wet_rep1_H1	1.38	–	–	–	–	–	–	–
DUNE01T004	1.38	0.34	3.4	2.83	0.00	n/a	2546	900
DUNE01_P04_wet_rep0_H1	1.38	–	–	–	–	–	–	–

DUNE01T005	1.38	0.34	3.4	2.83	0.00	n/a	1660	586
DUNE01_P05_dry_rep0_H1	0.00	–	–	–	–	–	–	–
DUNE01_P05_wet_rep1_H1	1.38	–	–	–	–	–	–	–
DUNE01T006	1.38	0.34	3.4	2.83	0.00	n/a	2546	900
DUNE01T007	1.38	0.34	3.4	2.83	0.00	n/a	2546	900
DUNE01_P06_wet_rep0_H1	1.38	–	–	–	–	–	–	–
DUNE01T008	1.38	0.34	3.4	2.83	0.00	n/a	2546	900
DUNE01_P07_wet_rep0_H1	1.38	–	–	–	–	–	–	–
DUNE01T009	1.38	0.34	3.4	2.83	0.00	n/a	1660	586
DUNE01T010	1.38	0.34	3.4	2.83	0.00	n/a	2546	900
DUNE01T011	1.38	0.34	3.4	2.83	0.00	n/a	2546	900
DUNE01_P08_wet_rep0_H1	1.38	–	–	–	–	–	–	–
DUNE01T012	1.38	0.34	3.4	2.83	0.00	n/a	2546	900
DUNE01T013	1.38	0.34	3.4	2.83	0.00	n/a	2546	900
DUNE01T014	1.38	0.34	3.4	2.83	0.00	n/a	2546	900
DUNE01T015	1.38	0.34	3.4	2.83	0.00	n/a	2546	900
DUNE01T016	1.38	0.34	3.4	2.83	0.00	n/a	2260	798
DUNE01_P09_wet_rep0_H1	1.38	–	–	–	–	–	–	–
DUNE01_P09_wet_rep1_H1	1.38	–	–	–	–	–	–	–
DUNE01T017	1.38	0.34	3.4	2.83	0.00	n/a	1273	450
DUNE01T018	1.38	0.34	3.4	2.83	0.00	n/a	1273	450
DUNE01T019	1.38	0.34	3.4	2.83	0.00	n/a	1273	450
DUNE01T020	1.38	0.34	3.4	2.83	0.00	n/a	1273	450
DUNE01T021	1.38	0.34	3.4	2.83	0.00	n/a	2546	900
DUNE01T022	1.38	0.34	3.4	2.83	0.00	n/a	2546	900
DUNE01_P10_wet_rep0_H1	1.38	–	–	–	–	–	–	–
DUNE01T023	1.38	0.34	3.4	2.83	0.00	n/a	2546	900
DUNE01T024	1.38	0.34	3.4	2.83	0.00	n/a	2546	900
DUNE01T025	1.38	0.34	3.4	2.83	0.00	n/a	2546	900
DUNE01T026	1.38	0.34	3.4	2.83	0.00	n/a	2546	900
DUNE01T027	1.38	0.34	3.4	2.83	0.00	n/a	1800	636
DUNE01T028	1.38	0.34	3.4	2.83	0.00	n/a	2546	900
DUNE01_P11_wet_rep0_H1	1.38	–	–	–	–	–	–	–
DUNE01T029	1.38	0.34	3.4	2.83	0.00	n/a	2546	900
DUNE01T030	1.38	0.34	3.4	2.83	0.00	n/a	2546	900
DUNE01T031	1.38	0.34	3.4	2.83	0.00	n/a	2546	900
DUNE01T032	1.38	0.34	3.4	2.83	0.00	n/a	2546	900
DUNE01T033	1.38	0.34	3.4	2.83	0.00	n/a	2546	900
DUNE01T034	1.38	0.34	3.4	2.83	0.00	n/a	2546	900
DUNE01_P12_wet_rep0_H1	1.38	–	–	–	–	–	–	–
DUNE01T035	1.38	0.34	3.4	2.83	0.00	n/a	2546	900
DUNE01T036	1.38	0.34	3.4	2.83	0.00	n/a	2546	900

DUNE01T037	1.38	0.34	3.4	2.83	0.00	n/a	2546	900
DUNE01T038	1.38	0.34	3.4	2.83	0.00	n/a	2546	900
DUNE01T039	1.38	0.34	3.4	2.83	0.00	n/a	2546	900
DUNE01T040	1.38	0.34	3.4	2.83	0.00	n/a	2546	900
DUNE01T041	1.38	0.34	3.4	2.83	0.00	n/a	2546	900
DUNE01T042	1.38	0.34	3.4	2.83	0.00	n/a	2546	900
DUNE01_P13_dry_rep0_H1	1.38	-	-	-	-	-	-	-

4.4 DUNE02, DUNE02cor and DUNE02loH

The DUNE02 case represents the dune geometry at Dunkerque with a gap between dune and dike on a foreshore with 1:40 slope. In this configuration, AWG 10 is co-located with PTG 01 at X= 70.220 m, while AWG 11 is co-located with PTG 02 at X= 71.378 m. DUNE02cor and DUNE02loH are using the same geometry as DUNE02, but with different incident wave $H_{m0,ss}$. The DUNE02 experiments were started using a 9% too high $H_{m0,ss}$ compared to the other dune geometries. These experiments were therefore repeated, using the correct $H_{m0,ss}$ (DUNE02cor), and these results should be used for comparison to the other dune geometries, based on the same $H_{m0,ss}$. The test program corresponding to these tests are presented in Table 15 to Table 17.

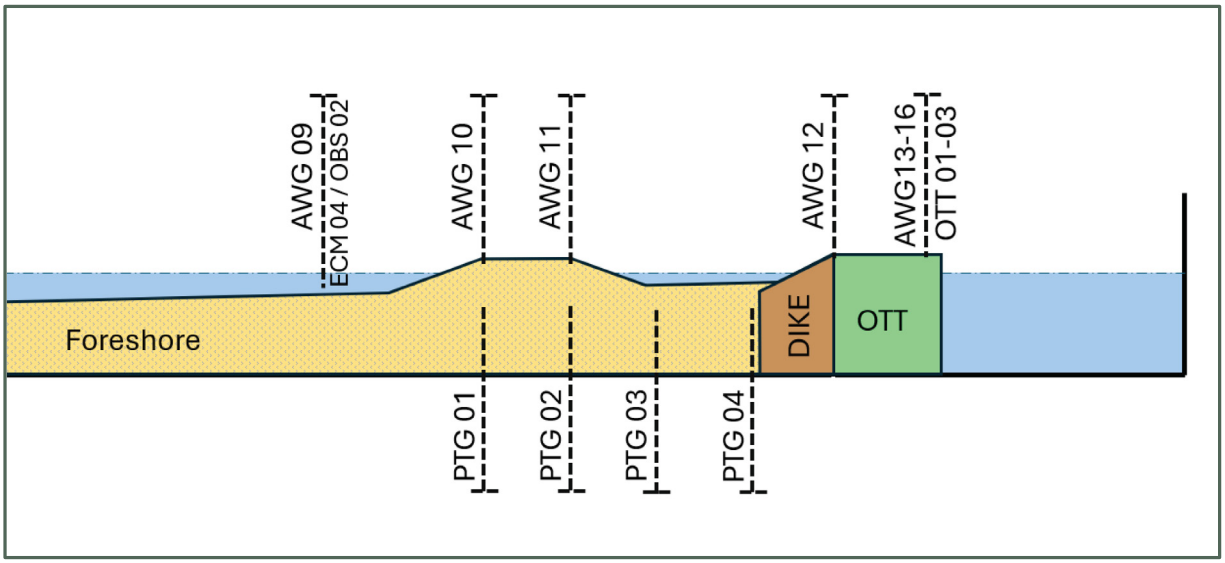


Figure 25 - Close-up view of the dune–dike geometry and instrumentation layout for test DUNE02, DUNE02cor and DUNE02loH. The PTGs were located in the sand (at the top end of the dashed lines).

Table 15 - Test program for dune geometry DUNE02.

Test or profile ID [-]	h_p [m]	$H_{m0,ss}$ [m]	$T_{p,ss}$ [s]	T_{m02} [s]	$H_{m0,fig}$ [m]	$T_{p,fig}$ [s]	Duration [s]	#waves [-]
DUNE02_P00_dry_rep0_H1	0.00	-	-	-	-	-	-	-
DUNE02_P00_dry_rep1_H1	0.00	-	-	-	-	-	-	-
DUNE02_P00_wet_rep0_H1	1.38	-	-	-	-	-	-	-
DUNE02T001	1.38	0.37	3.4	2.83	0.00	n/a	283	100
DUNE02_P01_wet_rep0_H2	1.38	-	-	-	-	-	-	-
DUNE02_P01_wet_rep1_H6	1.38	-	-	-	-	-	-	-
DUNE02T002	1.38	0.37	3.4	2.83	0.00	n/a	600	212
DUNE02_P02_wet_rep0_H1	1.38	-	-	-	-	-	-	-
DUNE02T003	1.38	0.37	3.4	2.83	0.00	n/a	1131	400
DUNE02_P03_wet_rep0_H2	1.38	-	-	-	-	-	-	-
DUNE02T004	1.38	0.37	3.4	2.83	0.00	n/a	2546	900
DUNE02_P04_wet_rep0_H2	1.38	-	-	-	-	-	-	-
DUNE02T005	1.38	0.37	3.4	2.83	0.00	n/a	2546	900
DUNE02T006	1.38	0.37	3.4	2.83	0.00	n/a	2546	900
DUNE02_P05_wet_rep0_H2	1.38	-	-	-	-	-	-	-
DUNE02T007	1.38	0.34	3.4	2.83	0.00	n/a	2546	900
DUNE02T008	1.38	0.35	3.4	2.83	0.00	n/a	2546	900
DUNE02_P06_dry_rep0_H1	0.00	-	-	-	-	-	-	-

Table 16 - Test program for dune geometry DUNE02cor.

Test or profile ID [-]	h_p [m]	$H_{m0,ss}$ [m]	$T_{p,ss}$ [s]	T_{m02} [s]	$H_{m0,fig}$ [m]	$T_{p,fig}$ [s]	Duration [s]	#waves [-]
DUNE02cor_P00_dry_rep0_H2	0.00	-	-	-	-	-	-	-
DUNE02cor_P00_wet_rep0_H4	1.38	-	-	-	-	-	-	-
DUNE02corT001	1.38	0.34	3.4	2.83	0.00	n/a	283	100
DUNE02cor_P01_wet_rep0_H2	1.38	-	-	-	-	-	-	-
DUNE02corT002	1.38	0.34	3.4	2.83	0.00	n/a	600	212
DUNE02cor_P02_wet_rep0_H2	1.38	-	-	-	-	-	-	-
DUNE02corT003	1.38	0.34	3.4	2.83	0.00	n/a	1131	400
DUNE02cor_P03_wet_rep0_H1	1.38	-	-	-	-	-	-	-
DUNE02cor_P03_wet_rep0_H4	1.38	-	-	-	-	-	-	-
DUNE02corT004	1.38	0.34	3.4	2.83	0.00	n/a	2546	900
DUNE02cor_P04_wet_rep0_H2	1.38	-	-	-	-	-	-	-
DUNE02corT005	1.38	0.34	3.4	2.83	0.00	n/a	2546	900
DUNE02corT006	1.38	0.34	3.4	2.83	0.00	n/a	2546	900
DUNE02cor_P05_dry_rep0_H2	1.38	-	-	-	-	-	-	-

Table 17 - Test program for dune geometry DUNE02loH

Test or profile ID [-]	h_p [m]	$H_{m0,ss}$ [m]	$T_{p,ss}$ [s]	T_{m02} [s]	$H_{m0,fig}$ [m]	$T_{p,fig}$ [s]	Duration [s]	#waves [-]
DUNE02loH_P00_dry_rep0_H1	0.00	-	-	-	-	-	-	-
DUNE02loHT001	1.38	0.165	3.4	2.83	0.00	n/a	283	100
DUNE02loH_P01_wet_rep0_H2	1.38	-	-	-	-	-	-	-
DUNE02loHT002	1.38	0.165	3.4	2.83	0.00	n/a	600	212
DUNE02loH _P02_wet_rep0_H2	1.38	-	-	-	-	-	-	-
DUNE02loHT003	1.38	0.165	3.4	2.83	0.00	n/a	1131	400
DUNE02loH_P03_wet_rep0_H1	1.38	-	-	-	-	-	-	-
DUNE02loHT004	1.38	0.165	3.4	2.83	0.00	n/a	2546	900
DUNE02loH_P04_wet_rep0_H2	1.38	-	-	-	-	-	-	-
DUNE02loHT005	1.38	0.165	3.4	2.83	0.00	n/a	2546	900
DUNE02loHT006	1.38	0.165	3.4	2.83	0.00	n/a	2546	900
DUNE02loH_P05_wet_rep0_H1	1.38	-	-	-	-	-	-	-
DUNE02loHT007	1.38	0.165	3.4	2.83	0.00	n/a	2546	900
DUNE02loHT008	1.38	0.165	3.4	2.83	0.00	n/a	2546	900
DUNE02loHT009	1.38	0.165	3.4	2.83	0.00	n/a	2546	900
DUNE02loH_P06_dry_rep0_H1	1.38	-	-	-	-	-	-	-

4.5 DUNE03

The DUNE03 case represents the dune geometry at Raversijde with connected dune and dike. The dune crest height in lower than the typical level ($R_{c,dune}$ = 0.348 m), consequently the designed regime for this case would be overwash/inundation regime. In this configuration, AWG 10 is co-located with PTG 02 at X= 71.378 m, while AWG 11 is co-located with PTG 04 at X= 73.922 m. The test program corresponding to the DUNE03 geometry is presented in Table 18.

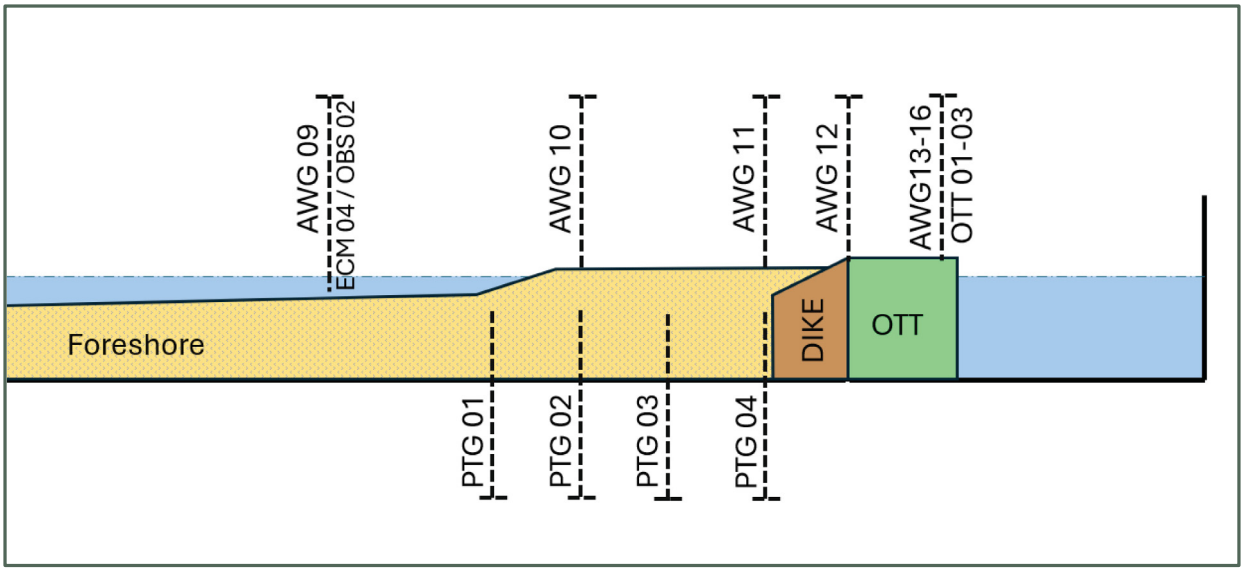


Figure 26 - Close-up view of the dune–dike geometry and instrumentation layout for test DUNE03. The PTGs were located in the sand (at the top end of the dashed lines).

Table 18 - Test program for dune geometry DUNE03.

Test or profile ID [-]	h_p [m]	$H_{m0,ss}$ [m]	$T_{p,ss}$ [s]	T_{m02} [s]	$H_{m0,fig}$ [m]	$T_{p,fig}$ [s]	Duration [s]	#waves [-]
DUNE03_P00_dry_rep0_H1	0.00	-	-	-	-	-	-	-
DUNE03 _P00_wet_rep0_H4	1.38	-	-	-	-	-	-	-
DUNE03T001	1.38	0.34	3.4	2.83	0.00	n/a	283	100
DUNE03 _P01_wet_rep0_H2	1.38	-	-	-	-	-	-	-
DUNE03T002	1.38	0.34	3.4	2.83	0.00	n/a	600	212
DUNE03 _P02_wet_rep0_H2	1.38	-	-	-	-	-	-	-
DUNE03 T003	1.38	0.34	3.4	2.83	0.00	n/a	1131	400
DUNE03_P03_wet_rep0_H1	1.38	-	-	-	-	-	-	-
DUNE03T004	1.38	0.34	3.4	2.83	0.00	n/a	2546	900
DUNE03_P04_wet_rep0_H2	1.38	-	-	-	-	-	-	-
DUNE03T005	1.38	0.34	3.4	2.83	0.00	n/a	2546	900
DUNE03T006	1.38	0.34	3.4	2.83	0.00	n/a	2546	900
DUNE03_P05_dry_rep0_H1	1.38	-	-	-	-	-	-	-
DUNE03_P05_dry_rep0_H2	1.38	-	-	-	-	-	-	-

4.6 DUNE04

The DUNE04 case represents the dune geometry at Raversijde with a gap between dune and dike. The dune crest height in at the standard level ($R_{c,dune}$ = 0.228 m), consequently the

designed regime for this case would be collision/overwash regime. In this configuration, AWG 10 is co-located with PTG 03 at X= 72.620 m, while AWG 11 is co-located with PTG 04 at X= 73.922 m. The test program corresponding to the DUNE04 geometry is presented in Table 19.

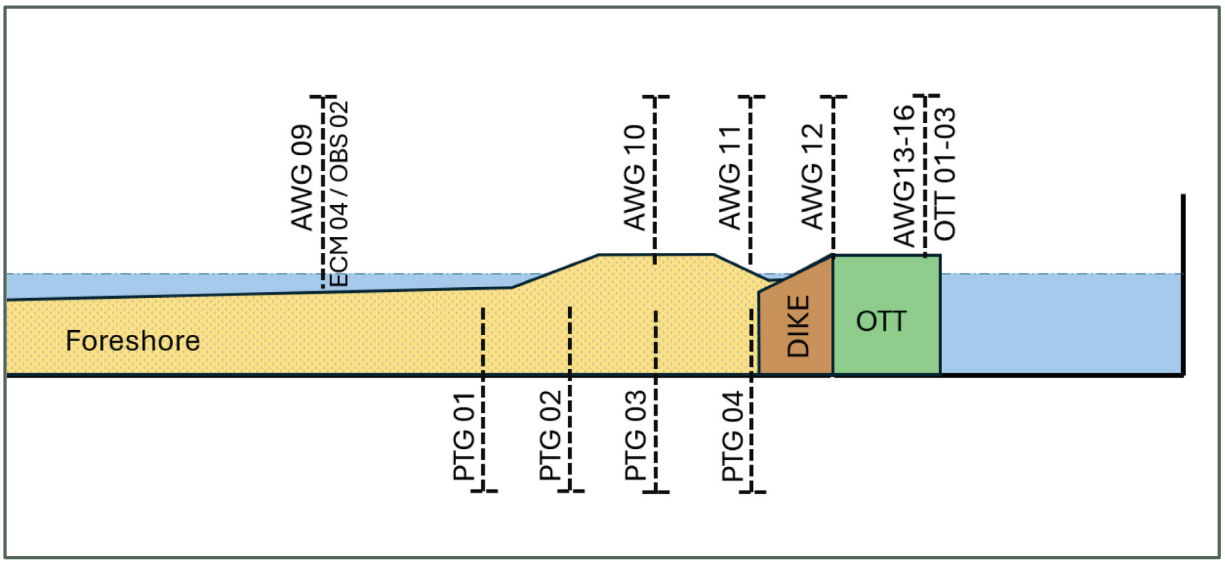


Figure 27 - Close-up view of the dune–dike geometry and instrumentation layout for test DUNE04. The PTGs were located in the sand (at the top end of the dashed lines).

Table 19 - Test program for dune geometry DUNE04.

Test or profile ID [-]	h_p [m]	$H_{m0,ss}$ [m]	$T_{p,ss}$ [s]	T_{m02} [s]	$H_{m0,fig}$ [m]	$T_{p,fig}$ [s]	Duration [s]	#waves [-]
DUNE04_P00_dry_rep0_H2	0.00	-	-	-	-	-	-	-
DUNE04_P00_dry_rep1_H5	0.00	-	-	-	-	-	-	-
DUNE04_P00_dry_rep2_H5	0.00	-	-	-	-	-	-	-
DUNE04 _P00_wet_rep0_H1	1.38	-	-	-	-	-	-	-
DUNE04T001	1.38	0.34	3.4	2.83	0.00	n/a	283	100
DUNE04 _P01_wet_rep0_H2	1.38	-	-	-	-	-	-	-
DUNE04T002	1.38	0.34	3.4	2.83	0.00	n/a	600	212
DUNE04 _P02_wet_rep0_H2	1.38	-	-	-	-	-	-	-
DUNE04T003	1.38	0.34	3.4	2.83	0.00	n/a	1131	400
DUNE04_P03_wet_rep0_H2	1.38	-	-	-	-	-	-	-
DUNE04T004	1.38	0.34	3.4	2.83	0.00	n/a	2546	900
DUNE04_P04_wet_rep0_H2	1.38	-	-	-	-	-	-	-
DUNE04T005	1.38	0.34	3.4	2.83	0.00	n/a	2546	900
DUNE04T006	1.38	0.34	3.4	2.83	0.00	n/a	1660	586
DUNE04_P05_wet_rep0_H2	1.38	-	-	-	-	-	-	-
DUNE04T007	1.38	0.34	3.4	2.83	0.00	n/a	1660	586
DUNE04_P06_dry_rep0_H1	1.38	-	-	-	-	-	-	-

4.7 DUNE05, DUNE05rep, DUNE05loH, DUNE05var and DUNE05fig

The DUNE05 case represents the Mariakerke (lengthened) dune geometry with a connected wider dune. The dune crest height is set at the standard level, $R_{c,dune}$=0.228 m; consequently, the expected response regime for this case is the collision/overwash regime. In this configuration, AWG 10 is co-located with PTG 02 at X=71.378 m, while AWG 11 is co-located with PTG 03 at X=72.620 m. Several additional scenarios were tested using the same dune and dike geometry. These include a repeat of the reference case to assess the repeatability of the flume experiments (DUNE05rep), a case with a lower incident wave height, H_{m0}=0.165 m (DUNE05loH), cases with varying water levels representing high and low tide conditions (DUNE05var), and a case including free IG waves under storm conditions (DUNE05fig). The custom spectrum used to add FIG to this case is illustrated in Figure 29. The test program corresponding these test presented in Table 20 to Table 24.

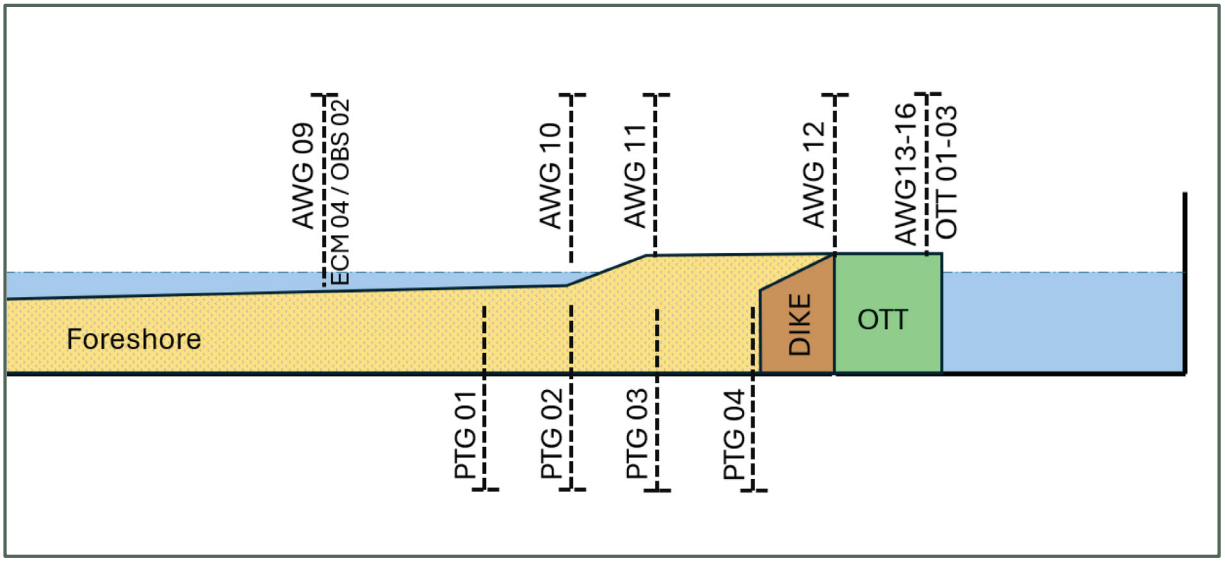


Figure 28 - Close-up view of the dune–dike geometry and instrumentation layout for test DUNE05, DUNE05rep, DUNE05loH, DUNE05var and DUNE05fig. The PTGs were located in the sand (at the top end of the dashed lines).

Table 20 - Test program for dune geometry DUNE05.

Test or profile ID [-]	h_p [m]	$H_{m0,ss}$[m]	$T_{p,ss}$ [s]	T_{m02} [s]	$H_{m0,fig}$ [m]	$T_{p,fig}$ [s]	Duration [s]	#waves [-]
DUNE05_P00_dry_rep0_H2	0.00	-	-	-	-	-	-	-
DUNE05_P00_dry_rep1_H4	0.00	-	-	-	-	-	-	-
DUNE05_P00_dry_rep2_H6	0.00	-	-	-	-	-	-	-
DUNE05 _P00_wet_rep0_H1	1.38	-	-	-	-	-	-	-
DUNE05T001	1.38	0.34	3.4	2.83	0.00	n/a	283	100
DUNE05_P01_wet_rep0_H2	1.38	-	-	-	-	-	-	-

DUNE05T002	1.38	0.34	3.4	2.83	0.00	n/a	600	212
DUNE05_P02_wet_rep0_H1	1.38	–	–	–	–	–	–	–
DUNE05_P02_wet_rep0_H2	1.38	–	–	–	–	–	–	–
DUNE05T003	1.38	0.34	3.4	2.83	0.00	n/a	1131	400
DUNE05_P03_wet_rep0_H2	1.38	–	–	–	–	–	–	–
DUNE05T004	1.38	0.34	3.4	2.83	0.00	n/a	2546	900
DUNE05_P04_wet_rep0_H2	1.38	–	–	–	–	–	–	–
DUNE05T005	1.38	0.34	3.4	2.83	0.00	n/a	2546	900
DUNE05T006	1.38	0.34	3.4	2.83	0.00	n/a	2546	900
DUNE05_P05_wet_rep0_H2	1.38	–	–	–	–	–	–	–
DUNE05T007	1.38	0.34	3.4	2.83	0.00	n/a	1660	586
DUNE05_P06_wet _rep0_H2	1.38	–	–	–	–	–	–	–
DUNE05_P06_wet_rep1_H1	1.38	–	–	–	–	–	–	–
DUNE05_P07_dry_rep0_H1	0.00	–	–	–	–	–	–	–

Table 21 - Test program for the repeated dune geometry DUNE05rep.

Test or profile ID [-]	h_p [m]	$H_{m0,ss}$ [m]	$T_{p,ss}$ [s]	T_{m02} [s]	$H_{m0,fig}$ [m]	$T_{p,fig}$ [s]	Duration [s]	#waves [-]
DUNE05rep_P00_dry_rep0_H1	0.00	–	–	–	–	–	–	–
DUNE05rep _P00_wet_rep0_H4	1.38	–	–	–	–	–	–	–
DUNE05repT001	1.38	0.34	3.4	2.83	0.00	n/a	283	100
DUNE05rep _P01_wet_rep0_H2	1.38	–	–	–	–	–	–	–
DUNE05repT002	1.38	0.34	3.4	2.83	0.00	n/a	600	212
DUNE05rep_P02_wet_rep0_H2	1.38	–	–	–	–	–	–	–
DUNE05repT003	1.38	0.34	3.4	2.83	0.00	n/a	1131	400
DUNE05rep_P03_wet_rep0_H1	1.38	–	–	–	–	–	–	–
DUNE05repT004	1.38	0.34	3.4	2.83	0.00	n/a	2546	900
DUNE05rep_P04_wet_rep0_H2	1.38	–	–	–	–	–	–	–
DUNE05repT005	1.38	0.34	3.4	2.83	0.00	n/a	2546	900
DUNE05repT006	1.38	0.34	3.4	2.83	0.00	n/a	2546	900
DUNE05rep_P05_wet_rep0_H1	1.38	–	–	–	–	–	–	–
DUNE05repT007	1.38	0.34	3.4	2.83	0.00	n/a	2546	900
DUNE05repT008	1.38	0.34	3.4	2.83	0.00	n/a	2546	900
DUNE05repT009	1.38	0.34	3.4	2.83	0.00	n/a	2546	900
DUNE05rep_P06_dry_rep0_H2	0.00	–	–	–	–	–	–	–

Table 22 - Test program for dune geometry DUNE05loH.

Test or profile ID [-]	h_p [m]	$H_{m0,ss}$ [m]	$T_{p,ss}$ [s]	T_{m02} [s]	$H_{m0,fig}$ [m]	$T_{p,fig}$ [s]	Duration [s]	#waves [-]

DUNE05loH_P00_dry_rep0_H1	0.00	–	–	–	–	–	–	–
DUNE05loH_P00_wet_rep0_H4	1.38	–	–	–	–	–	–	–
DUNE05loHT001	1.38	0.165	3.4	2.83	0.00	n/a	283	100
DUNE05loH_P01_wet_rep0_H2	1.38	–	–	–	–	–	–	–
DUNE05TloH002	1.38	0.165	3.4	2.83	0.00	n/a	600	212
DUNE05loH_P02_wet_rep0_H2	1.38	–	–	–	–	–	–	–
DUNE05loHT003	1.38	0.165	3.4	2.83	0.00	n/a	1131	400
DUNE05loH_P03_wet_rep0_H1	1.38	–	–	–	–	–	–	–
DUNE05loHT004	1.38	0.165	3.4	2.83	0.00	n/a	2546	900
DUNE05loH_P04_wet_rep0_H2	1.38	–	–	–	–	–	–	–
DUNE05loHT005	1.38	0.165	3.4	2.83	0.00	n/a	2546	900
DUNE05loHT006	1.38	0.165	3.4	2.83	0.00	n/a	2546	900
DUNE05loH_P05_wet_rep0_H1	1.38	–	–	–	–	–	–	–
DUNE05loHT007	1.38	0.165	3.4	2.83	0.00	n/a	2546	900
DUNE05loHT008	1.38	0.165	3.4	2.83	0.00	n/a	2546	900
DUNE05loHT009	1.38	0.165	3.4	2.83	0.00	n/a	2546	900
DUNE05loH_P06_wet _rep0_H2	1.38	–	–	–	–	–	–	–
DUNE05loHT010	1.38	0.165	3.4	2.83	0.00	n/a	2546	900
DUNE05loHT011	1.38	0.165	3.4	2.83	0.00	n/a	2546	900
DUNE05loHT012	1.38	0.165	3.4	2.83	0.00	n/a	2546	900
DUNE05loH_P07_wet _rep0_H2	1.38	–	–	–	–	–	–	–
DUNE05loHT013	1.38	0.165	3.4	2.83	0.00	n/a	2546	900
DUNE05loHT014	1.38	0.165	3.4	2.83	0.00	n/a	2546	900
DUNE05loHT015	1.38	0.165	3.4	2.83	0.00	n/a	2546	900
DUNE05loH_P08_dry_rep0_H1	0.00	–	–	–	–	–	–	–
DUNE05loH_P08_dry_rep0_H2	0.00	–	–	–	–	–	–	–

Table 23 - Test program for dune geometry DUNE05var.

Test or profile ID [-]	h_p [m]	$H_{m0,ss}$ [m]	$T_{p,ss}$ [s]	T_{m02} [s]	$H_{m0,fig}$ [m]	$T_{p,fig}$ [s]	Duration [s]	#waves [-]
DUNE05_P00_dry_rep0_H2	0.00	–	–	–	–	–	–	–
DUNE05var_P00_dry_rep1_H4	0.00	–	–	–	–	–	–	–
DUNE05var_P00_wet_rep0_H2	1.173	–	–	–	–	–	–	–
DUNE05varT001	1.172	0.291	2.99	2.49	0.00	n/a	1018	409
DUNE05varT002	1.223	0.296	3.04	2.54	0.00	n/a	1018	401
DUNE05varT003	1.225	0.301	3.09	2.58	0.00	n/a	1018	395
DUNE05varT004	1.188	0.306	3.14	2.62	0.00	n/a	1018	389
DUNE05var_P01_wet_rep0_H1	1.199	–	–	–	–	–	–	–
DUNE05varT005	1.199	0.34	3.39	2.83	0.00	n/a	1018	360

DUNE05varT006	1.342	0.34	3.39	2.83	0.00	n/a	1018	360
DUNE05var_P02_wet_rep0_H4	1.380	-	-	-	-	-	-	-
DUNE05varT007	1.380	0.34	3.39	2.83	0.00	n/a	1018	360
DUNE05var_P03_wet_rep0_H2	1.362	-	-	-	-	-	-	-
DUNE05varT008	1.362	0.34	3.39	2.83	0.00	n/a	1018	360
DUNE05varT009	1.311	0.34	3.39	2.83	0.00	n/a	1018	360
DUNE05varT010	1.237	0.34	3.39	2.83	0.00	n/a	1018	360
DUNE05varT011	1.147	0.34	3.39	2.83	0.00	n/a	607	215
DUNE05varT011_part2	1.147	0.34	3.39	2.83	0.00	n/a	411	145
DUNE05var_P04_wet_rep0_H2	1.265	-	-	-	-	-	-	-
DUNE05varT012	1.265	0.301	3.09	2.58	0.00	n/a	1018	395
DUNE05varT013	1.297	0.296	3.04	2.54	0.00	n/a	1018	401
DUNE05varT014	1.269	0.291	2.99	2.49	0.00	n/a	1018	409
DUNE05varT015	1.209	0.286	2.93	2.44	0.00	n/a	1018	416
DUNE05var_P05_wet_rep0_H2	1.166	-	-	-	-	-	-	-
DUNE05varT016	1.197	0.216	2.22	1.85	0.00	n/a	1018	550
DUNE05varT017	1.178	0.208	2.14	1.78	0.00	n/a	1018	570
DUNE05varT018	1.380	0.202	2.08	1.73	0.00	n/a	1018	589
DUNE05var_P06_wet _rep0_H2	1.380	-	-	-	-	-	-	-
DUNE05varT019	1.166	0.330	3.39	2.83	0.00	n/a	2546	900
DUNE05var_P07_dry_rep0_H2	0.00	-	-	-	-	-	-	-

Table 24 - Test program for dune geometry DUNE05fig.

Test or profile ID [-]	h_p [m]	$H_{m0,ss}$ [m]	$T_{p,ss}$ [s]	T_{m02} [s]	$H_{m0,fig}$ [m]	$T_{p,fig}$ [s]	Duration [s]	#waves [-]
DUNE05fig_P00_dry_rep0_H1	0.00	-	-	-	-	-	-	-
DUNE05fig_P00_dry_rep1_H5	0.00	-	-	-	-	-	-	-
DUNE05fig_P00_wet_rep0_H4	1.38	-	-	-	-	-	-	-
DUNE05figT001	1.38	0.34	3.4	2.83	0.06	18.7	283	100
DUNE05fig_P01_wet_rep0_H3	1.38	-	-	-	-	-	-	-
DUNE05figT002	1.38	0.34	3.4	2.83	0.06	18.7	519	183
DUNE05figT002_part2	1.38	0.34	3.4	2.83	0.06	18.7	81	29
DUNE05fig_P02_wet_rep0_H3	1.38	-	-	-	-	-	-	-
DUNE05figT003	1.38	0.34	3.4	2.83	0.06	18.7	1131	400
DUNE05fig_P03_wet_rep0_H3	1.38	-	-	-	-	-	-	-
DUNE05figT004	1.38	0.34	3.4	2.83	0.06	18.7	2546	900
DUNE05fig_P04_dry_rep0_H2	1.38	-	-	-	-	-	-	-

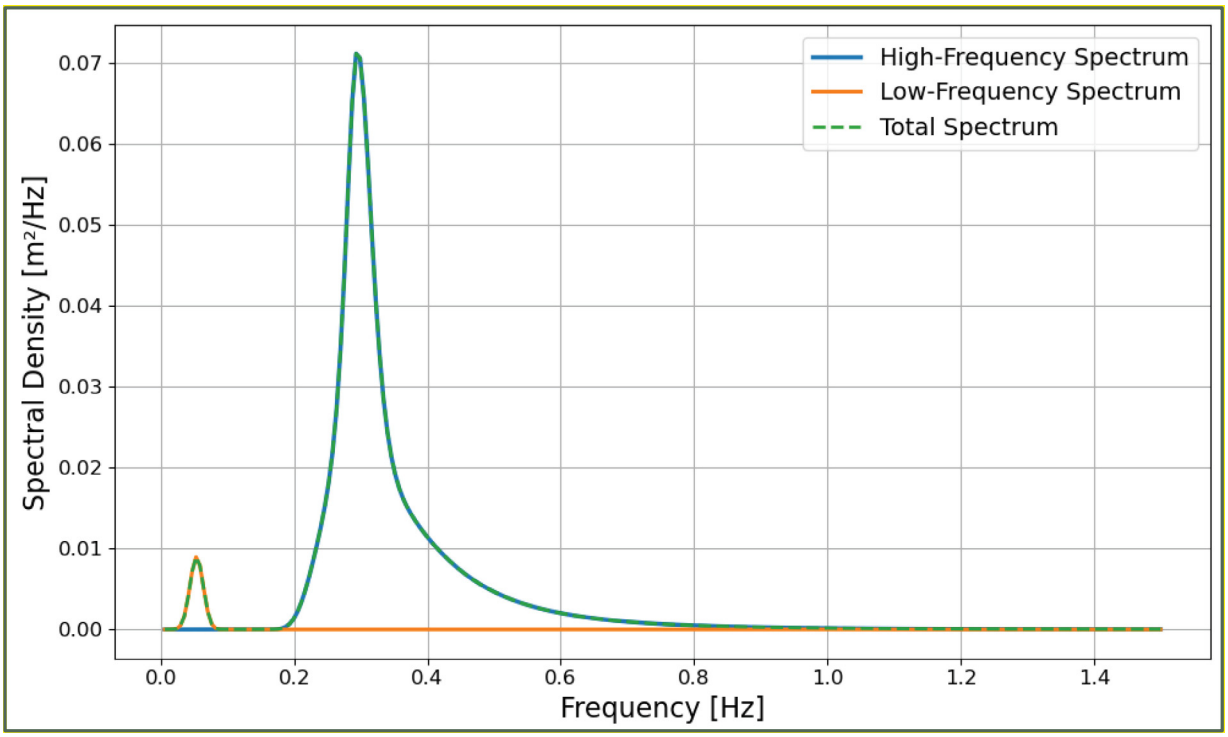


Figure 29 - Custom spectrum with added gaussian shape energy as FIG ($H_{m0,FIG}$=0.06m) for test DUNE05fig.

4.8 DUNE06

The DUNE06 case represents the dune geometry at Katwijk with shorter dune crest width. In this configuration, AWG 10 is co-located with PTG 02 at X= 71.378 m, while AWG 11 is co-located with PTG 04 at X= 73.922 m. The test program corresponding to the DUNE06

geometry is presented in Table 25.

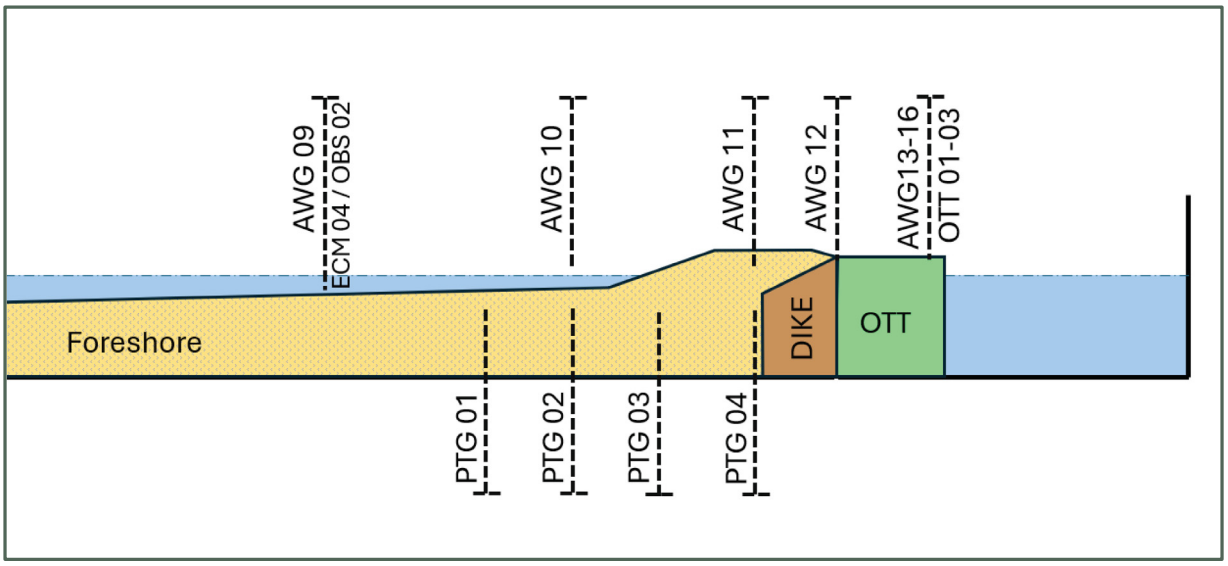


Figure 30 - Close-up view of the dune–dike geometry and instrumentation layout for test DUNE06. The PTGs were located in the sand (at the top end of the dashed lines).

Table 25 - Test program for dune geometry DUNE06.

Test or profile ID [-]	h_p [m]	$H_{m0,ss}$ [m]	$T_{p,ss}$ [s]	T_{m02} [s]	$H_{m0,fig}$ [m]	$T_{p,fig}$ [s]	Duration [s]	#waves [-]
DUNE06_P00_dry_rep0_H2	0.00	-	-	-	-	-	-	-
DUNE06_P00_wet_rep0_H4	1.38	-	-	-	-	-	-	-
DUNE06T001	1.38	0.34	3.4	2.83	0.00	n/a	283	100
DUNE06_P01_wet_rep0_H2	1.38	-	-	-	-	-	-	-
DUNE06T002	1.38	0.34	3.4	2.83	0.00	n/a	600	212
DUNE06_P02_wet_rep0_H2	1.38	-	-	-	-	-	-	-
DUNE06T003	1.38	0.34	3.4	2.83	0.00	n/a	1131	400
DUNE06_P03_wet_rep0_H1	1.38	-	-	-	-	-	-	-
DUNE06T004	1.38	0.34	3.4	2.83	0.00	n/a	2546	900
DUNE06_P04_wet_rep0_H2	1.38	-	-	-	-	-	-	-
DUNE06T005	1.38	0.34	3.4	2.83	0.00	n/a	2546	900
DUNE06T006	1.38	0.34	3.4	2.83	0.00	n/a	2546	900
DUNE06_P05_wet_rep0_H1	1.38	-	-	-	-	-	-	-
DUNE06T007	1.38	0.34	3.4	2.83	0.00	n/a	2546	900
DUNE06T008	1.38	0.34	3.4	2.83	0.00	n/a	2546	900
DUNE06T009	1.38	0.34	3.4	2.83	0.00	n/a	2546	900
DUNE06T010	1.38	0.34	3.4	2.83	0.00	n/a	2546	900
DUNE06_P06_dry_rep0_H1	1.38	-	-	-	-	-	-	-
DUNE06_P06_dry_rep0_H2	0.00	-	-	-	-	-	-	-

4.9 DUNE07

The DUNE07 case represents the dune geometry at Middelkerke (a connected dune - dike system) on a foreshore with 1:40 slope. In this configuration, AWG 10 is co-located with PTG 03 at X= 72.620 m, while AWG 11 is co-located with PTG 04 at X= 73.922 m. The close-up view of the dune–dike geometry and instrumentation layout for this test is shown in Figure 31. The test program corresponding to this test is presented in Table 26.

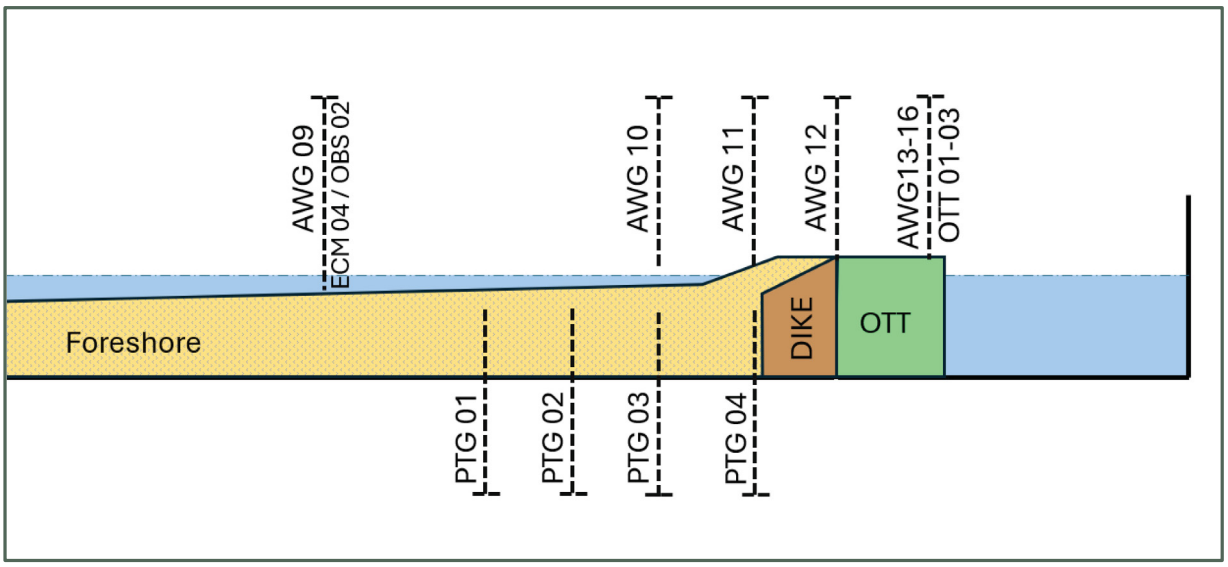


Figure 31 - Close-up view of the dune–dike geometry and instrumentation layout for test DUNE07.

Table 26 - Test program for dune geometry DUNE07.

Test or profile ID [-]	h_p [m]	$H_{m0,ss}$ [m]	$T_{p,ss}$ [s]	T_{m02} [s]	$H_{m0,fig}$ [m]	$T_{p,fig}$ [s]	Duration [s]	#waves [-]
DUNE07_P00_dry_rep0_H2	0.00	-	-	-	-	-	-	-
DUNE07_P00_dry_rep1_H5	0.00	-	-	-	-	-	-	-
DUNE07_P00_wet_rep0_H5	1.38	-	-	-	-	-	-	-
DUNE07T001	1.38	0.34	3.4	2.83	0.00	n/a	283	100
DUNE07_P01_wet_rep0_H3	1.38	-	-	-	-	-	-	-
DUNE07T002	1.38	0.34	3.4	2.83	0.00	n/a	600	212
DUNE07_P02_wet_rep0_H3	1.38	-	-	-	-	-	-	-
DUNE07T003	1.38	0.34	3.4	2.83	0.00	n/a	1131	400
DUNE07_P03_wet_rep0_H3	1.38	-	-	-	-	-	-	-
DUNE07T004	1.38	0.34	3.4	2.83	0.00	n/a	2546	900
DUNE07_P04_dry_rep0_H2	0.00	-	-	-	-	-	-	-

4.10 DUNE12

The DUNE12 case represents the Hybrid Dune (field case) geometry at the Sand Engine in the Netherlands as previously described in Section 2.4 . In this configuration, AWG 10 is at X= 71.978 m, while AWG 11 is co-located with PTG 04 at X= 73.922 m. The close-up view of the dune–dike geometry and instrumentation layout for this test is shown in Figure 32. The test program corresponding to this test is presented in Table 27. The target wave conditions were derived by de-shoaling the (Froude scaled) measured wave conditions near the dune foot in the field (Section 2.4). After test DUNE12T002, the dike slope was not exposed yet, after which it was decided to increase the water level and keep repeating the tests until full erosion of the dune on the dike slope.

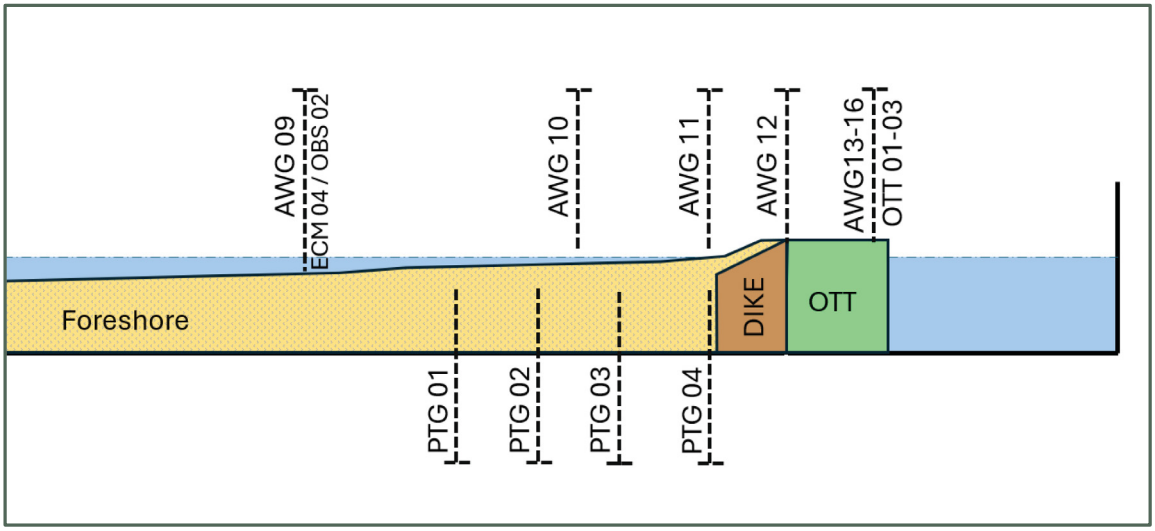


Figure 32 - Close-up view of the dune–dike geometry and instrumentation layout for test DUNE12. The PTGs were located in the sand (at the top end of the dashed lines).

Table 27 - Test program for dune geometry DUNE12.

Test or profile ID [-]	h_p [m]	$H_{m0,ss}$ [m]	$T_{p,ss}$ [s]	T_{m02} [s]	$H_{m0,fig}$ [m]	$T_{p,fig}$ [s]	Duration [s]	#waves [-]
DUNE12_P00_dry_rep0_H3	0.00	-	-	-	-	-	-	-
DUNE12_P00_wet_rep0_H5	1.376	-	-	-	-	-	-	-
DUNE12T001	1.376	0.115	7.1	2.02	0.02	9.12	882	524
DUNE12_P01_wet_rep0_H3	1.382	-	-	-	-	-	-	-
DUNE12T002	1.382	0.120	8.0	2.26	0.02	9.12	882	468
DUNE12_P02_wet_rep0_H3	1.410	-	-	-	-	-	-	-
DUNE12T003	1.410	0.120	8.0	2.26	0.02	9.12	882	468
DUNE12T004	1.410	0.120	8.0	2.26	0.02	9.12	882	468
DUNE12_P03_wet_rep0_H2	1.410	-	-	-	-	-	-	-
DUNE12T005	1.410	0.120	8.0	2.26	0.02	9.12	882	468
DUNE12_P04_dry_rep0_H2	0.00	-	-	-	-	-	-	-

5. Data processing and first visualizations

All data processing and visualizations were done by using a python toolbox developed specifically for post-processing the raw data obtained from the LWF of FH. This chapter describes the post-processing steps that were taken for each instrument and includes first visualizations to demonstrate the quality of the data.

5.1 Overview

An overview of the data available for each tested dune geometry is provided in Table *28*. In general, the DUKEx campaign resulted in an extensive dataset covering the hydrodynamics, dune morphodynamics, sediment transport, and overtopping/overwash processes. For most dune configurations, measurements from the main instrumentation systems are available; however, some individual tests contain missing, incomplete, or faulty records due to instrument malfunction, data acquisition issues, or instruments not being operational at that stage of the campaign. These limitations are explicitly indicated in Table *28* and should be considered when selecting and interpreting the data for further analysis.

Table 28 - Overview of the available data for each tested DUNE geometry. Indication of missing, partial or faulty data for the instruments.

Order [-]	Dune ID [-]	AWG	RWG	PTG	OBS	ECM	OTT	TMP	2DL	3DL
15	DUNE00	all	no T001	no T001	no T001	no T001	no T001	no T001	all	all
1	DUNE01	all	all	all	n/a	all	all	n/a	all	all
2	DUNE02	all	all	all	all	all	all	n/a	No T003, T004, T005, T006, T007, T008	No T003, T004, T005, T006, T007, T008
10	DUNE02cor	all	all	all	all	all	all	n/a	all	all
9	DUNE02loH	split T005	faulty RWG_07 (T001, T002)	all	all	all	all	n/a	no T007, T008, T009	no T007, T008, T009
6	DUNE03	all	all	all	all	all	all	all	all	all
3	DUNE04	all	no T001, T002	no T001, T002	no T001, T002	no T001, T002	no T001, T002	n/a	partial T003, no T006, T007	no T006, T007
4	DUNE05	all	no T006	no T006	no T006	no T006	no T006	n/a	all	all
7	DUNE05rep	all	all	all	all	all	all	all	no T007, T008, T009	no T007, T008, T009
8	DUNE05loH	incomplete AWG_11 (T007)	all	all	all	all	all	all	No T012	No T012

11	DUNE05var	no AWG_09 (T001, T002, T003, T004, T005, T011, T015, T016, T017, T018)	all	all	all	faulty ECM_04	all	all	all	all
12	DUNE05fig	all	all	all	all	faulty ECM_04	overflow OTT (T004)	all	all	all
5	DUNE06	all	all	all	all	all	all	n/a	all	all
13	DUNE07	all	all	all	all	faulty ECM_04	all	all	all	all
14	DUNE12	all	all	all	all	faulty ECM_04	all	all	all	all

5.2 Bed profiles

5.2.1 Distance laser bed profiles

The data obtained from the mobile distance-laser bed-profile system require extensive post-processing, as described in steps below. Most of the post-processing steps are automated using a dedicated Python script developed for this purpose. Examples of the resulting bed profiles are presented in the following figures. The post-processing steps include:

- Reading from the raw data, the four lasers (distance in [mm], output laser 1, output laser 2, output laser 3, output laser 4, wheel distance [-], binary sensor [1 (or 0): sensor (not) above reference block];
- Outlier removal;
- Moving average filtering of the profile data to remove noise;
- Z-correction of bed level taking into account the laser refraction in the water (using a calibrated refractive index of light through the water of the flume n_w = 1.346398);
- X and Z-correction of bed level for taking the angled laser (3.2°) into account;
- Down-sampling to dx = 0.01 m (as user defined) and averaging LDM_02, LDM_03 and LDM_04 to the final mean bed profile.

Remark: The accuracy of the X-position measurement by the bed profile trolley was generally < 0.01 m (acceptable) checked at the dike crest location. However, during the first test series (DUNE01), starting from profile P07, the error in the measurement of the X-position increased incrementally and up to ~0.09 m (dike crest location, Table 29). After DUNE01 the trolley was serviced and updated, including extra reference blocks over the full profile length to allow for X-coordinate corrections between the start of the measurement and the dike crest. For all subsequent tested dune geometries, the absolute error at the dike crest remained < 0.01 m.

Table 29 – Absolute error by the bad profile trolley in the X-position at the dike crest relative to the first (dry) profile measurement P00.

Profile ID	abs(X_dike,Pxx – X_dike,P00) [m]
DUNE01_P01	0.0003
DUNE01_P02	-0.0021
DUNE01_P03	0.0009
DUNE01_P04	0.0045
DUNE01_P07	0.0107
DUNE01_P08	0.0145
DUNE01_P09	0.0230
DUNE01_P10	0.0145
DUNE01_P11	0.0257
DUNE01_P12	0.0382
DUNE01_P13	0.0882

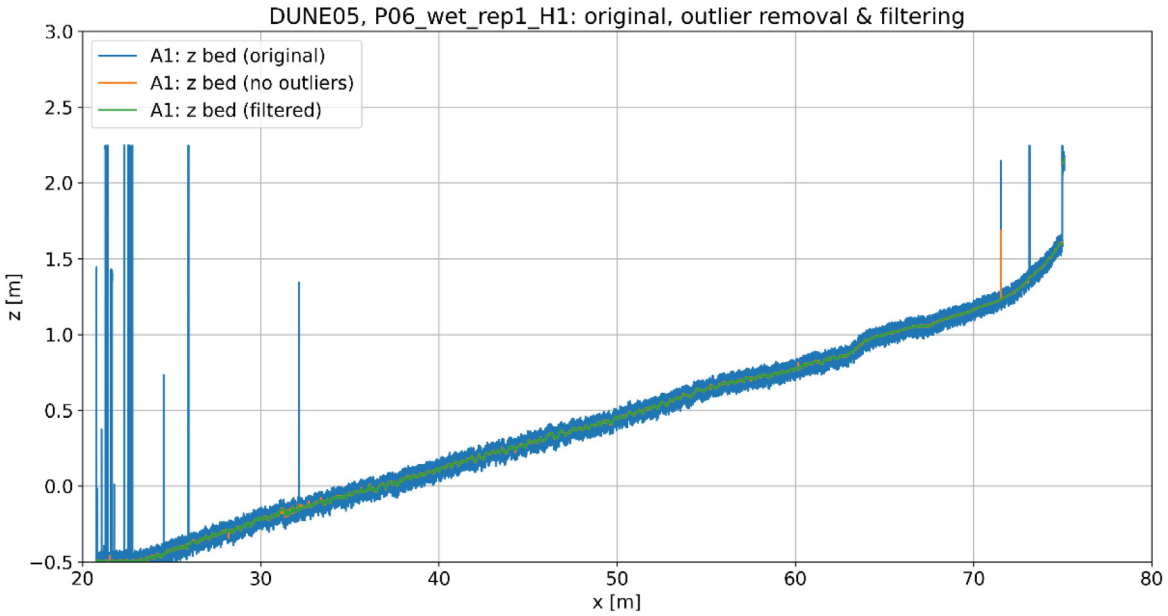


Figure 33 - Example of a measured bed profile before and after filtering outlier values.

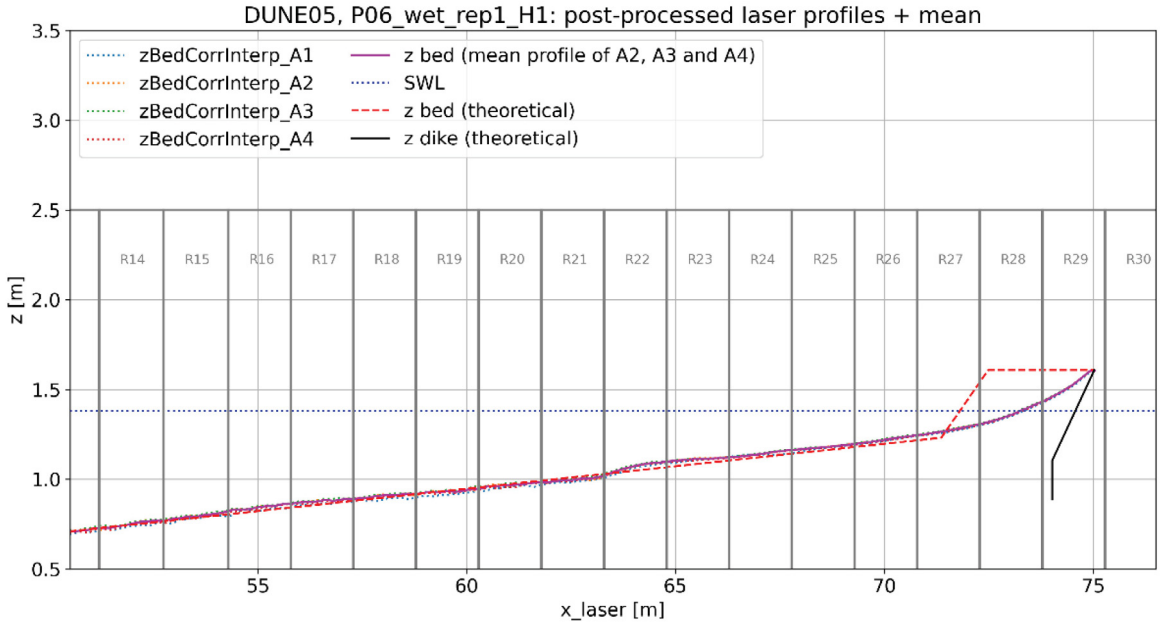


Figure 34 - Final cleaned bed profile for test DUNE05, Profile 06, showing the four individual laser measurements and the corresponding mean profile.

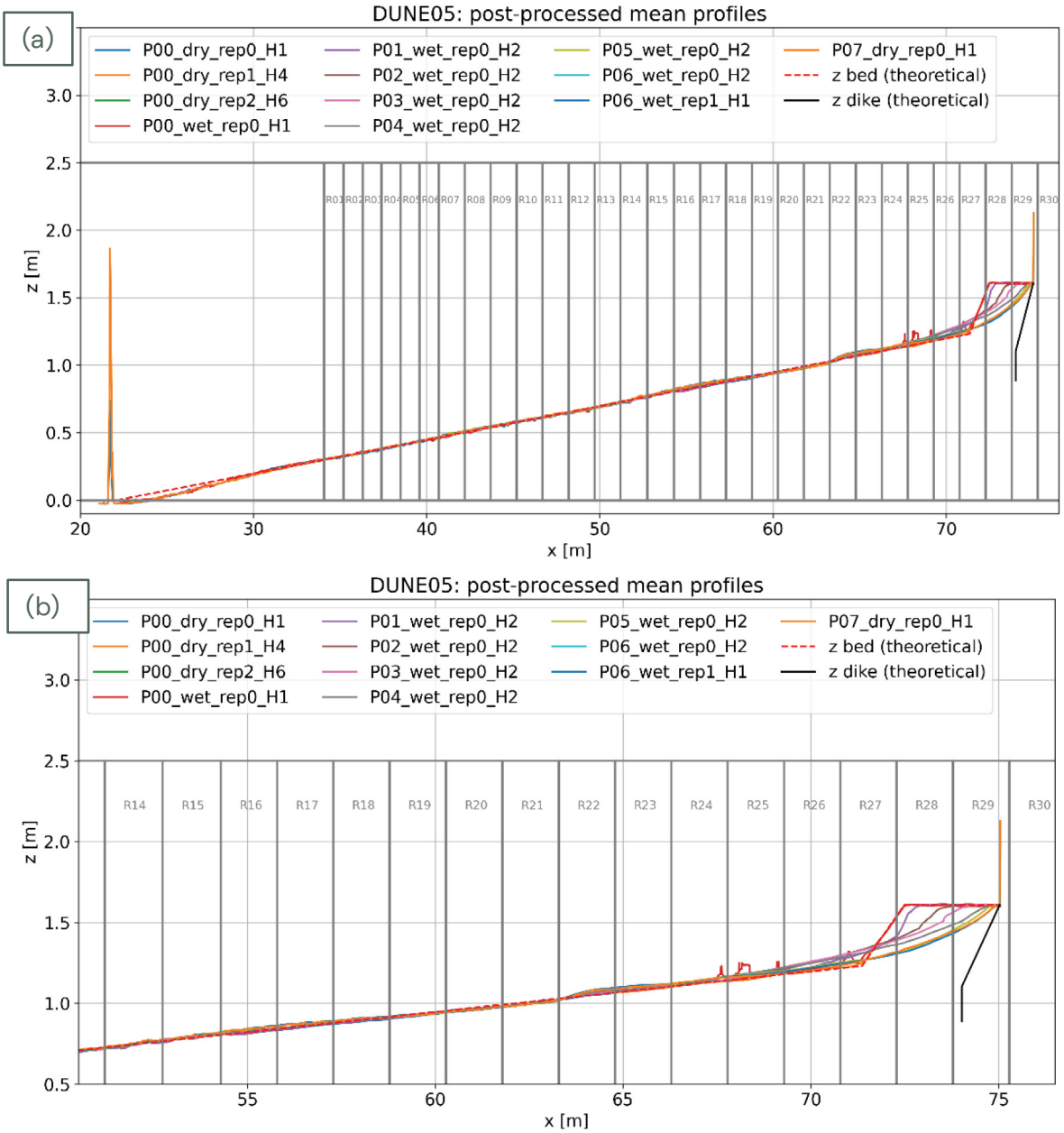


Figure 35 - Final cleaned mean bed profiles for test DUNE05, from Profile 00 to Profile 07: (a) full profiles and (b) zoomed-in view.

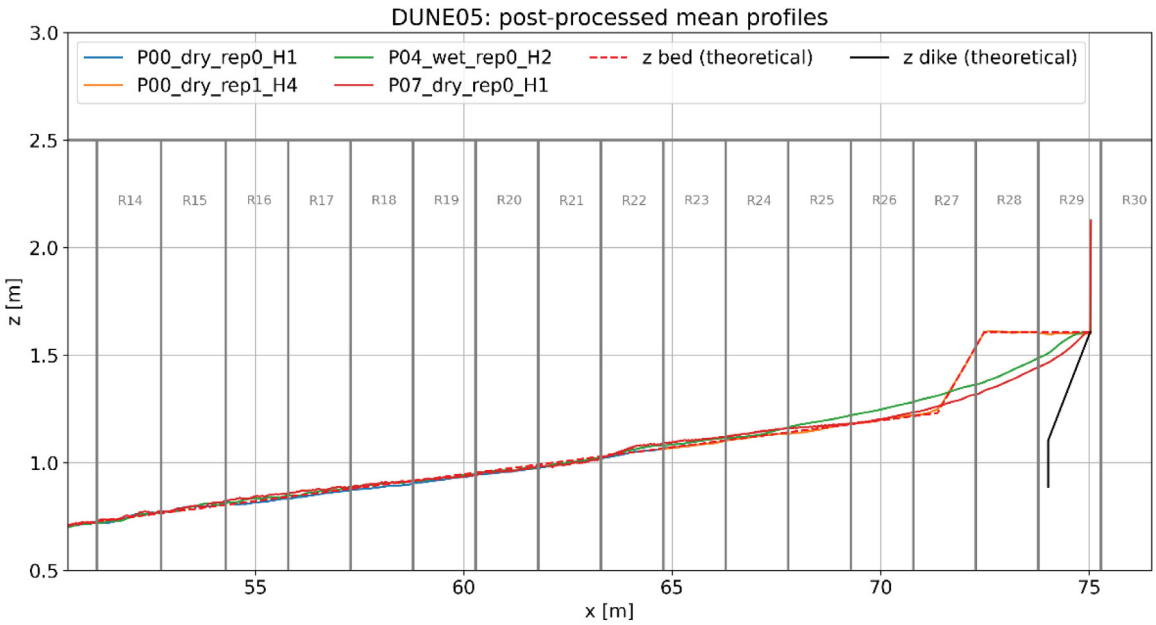


Figure 36 – Zoomed-in view of the final cleaned mean bed profiles for test DUNE05, showing Profile 00, Profile 04, and Profile 07.

5.2.1 LIDAR

2D LIDAR

The two-dimensional profiles acquired with the SICK LMS511-20100 PRO-HR LiDAR were post-processed using a dedicated Python workflow. Measurements were recorded in SOPAS ET and exported from the native data format to CSV for further analysis. Because the SOPAS export contains numerous unused data channels, the files were first cleaned by removing columns that were entirely empty. The processing routine then automatically identified the distance channels and associated metadata, including the initial scan angle, angular increment, scale factor, offset, and elapsed time. The recorded distances were corrected using the relevant scale and offset values, converted from millimeters to meters, and screened to remove invalid or out of range measurements.

For each scan, the polar distance measurements were transformed into Cartesian coordinates in a scanner-centered reference system. A prescribed rotation was subsequently applied to orient the measured profile consistently with the flume cross-section. The recorded timestamps were retained to reconstruct and visualize the temporal sequence at the actual measurement rate. Individual scans or the complete time series could therefore be examined to assess changes in the exposed dune crest and slopes during wave loading. Since the near-infrared LiDAR measurements do not reliably resolve the submerged bed and no correction for refraction through the water surface was applied,

the interpretation was restricted to portions of the dune represented by valid direct returns above the water level. An example snapshot of a resulting processed two-dimensional profile for Dune03 Test 001 is presented in Figure 37.

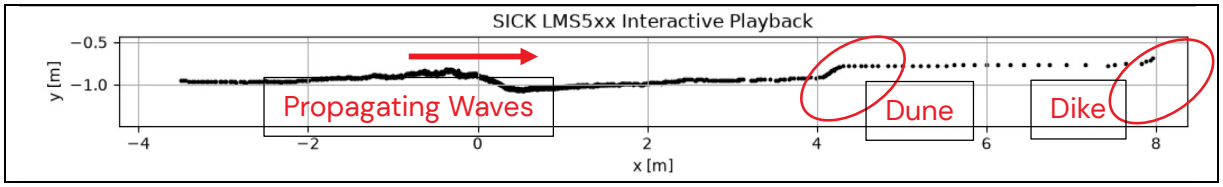


Figure 37 - Two-dimensional snapshot profile for Dune03 Test 001 measured with 2D LIDAR

3D LIDAR

The three-dimensional measurements acquired with the Ouster OS0 LiDAR were post-processed using a dedicated Python workflow. The raw PCAP recordings were decoded together with their corresponding JSON metadata using the Ouster SDK and converted into Cartesian point clouds. Invalid returns, points outside the predefined region of interest, and measurements below the selected reflectivity threshold were removed. The remaining point clouds were transformed from the sensor coordinate system to the flume-aligned longitudinal, transverse, and vertical axes. Three-dimensional visualizations and two-dimensional cross-sectional slices were subsequently used to verify the spatial coverage, alignment, and overall quality of the processed scans. Because reliable LiDAR returns could not be obtained through the water column, the analysis was restricted to the exposed portion of the dune.

For the quantitative analysis, selected reference frames were interpolated and averaged to construct a representative initial dune surface. The exposed dune face was represented on a fixed 2.5D grid, defined in the transverse and vertical directions, with each grid cell containing the corresponding longitudinal position of the dune surface. Each subsequent scan was interpolated onto the same grid using inverse-distance weighting, allowing direct cell-by-cell comparison at a consistent spatial resolution of 0.02 m. Erosion volumes were determined by integrating the positive surface retreat relative to the reference condition over the valid grid cell area. Cells containing no data and frames with insufficient or discontinuous coverage of the erosion zone were excluded to prevent occlusion or missing LiDAR returns from being interpreted as morphological change. The resulting processed surfaces and calculated morphological changes are presented in Figure 38.

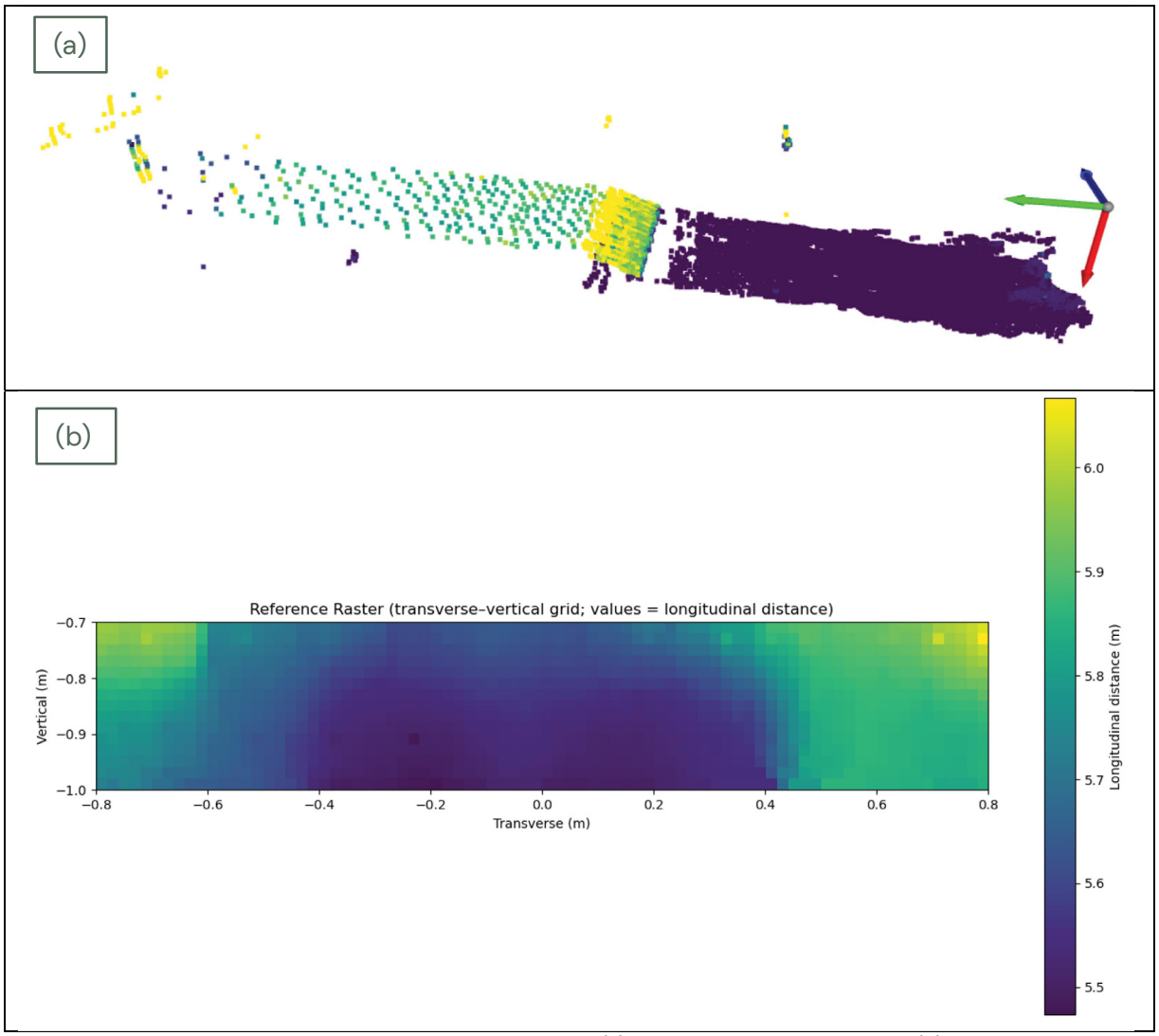


Figure 38 – Example of post-processed 3D LiDAR results: (a) processed point cloud and (b) calculated morphological changes of the dune face relative to the reference condition.

5.3 Hydrodynamics

5.3.1 Acoustic wave gauges (AWG_01-AWG_11)

The acoustic wave gauge (AWG) measurements generally do not require filtering prior to visualization and further analysis. However, occasional outliers may be present in some records. When necessary, these outliers should be detected and removed. This outlier-detection and correction procedure has not yet been applied systematically during the initial post-processing stage, as it can be performed automatically at a later stage when the data are used for specific analyses, such as reflection analysis in WaveLab software. An example of the processed AWG time series is shown in Figure 39.

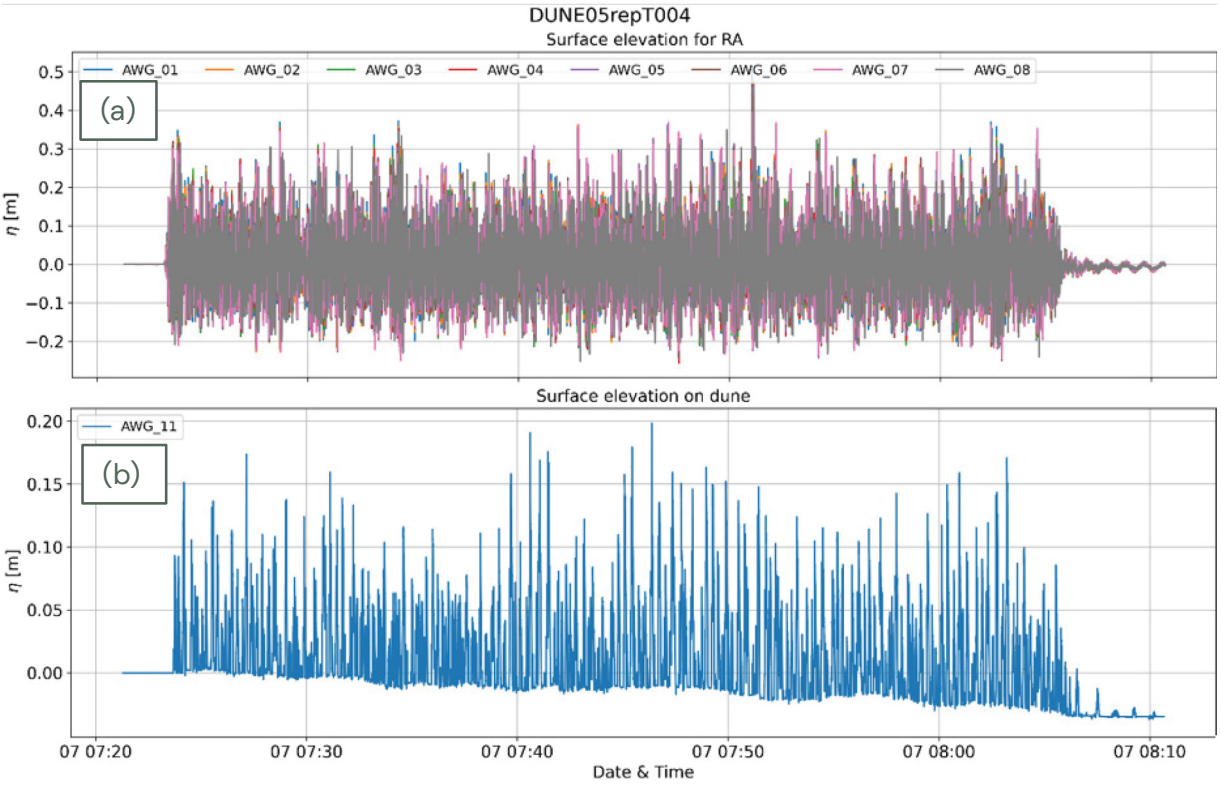


Figure 39 - Acoustic wave gauge (AWG) measurements for case DUNE05rep, Test 04: (a) AWG 01 to AWG 08 at offshore location and (b) AWG 11 located at the top of the dune.

5.3.2 Resistive wave gauges (RWG)

The resistive wave gauge (RWG) measurements are of good quality and generally do not require additional filtering or outlier removal prior to visualization and further analysis. The measured time series can therefore be used directly in the subsequent data-processing and analysis steps. An example of the RWG measurements is shown in Figure 40.

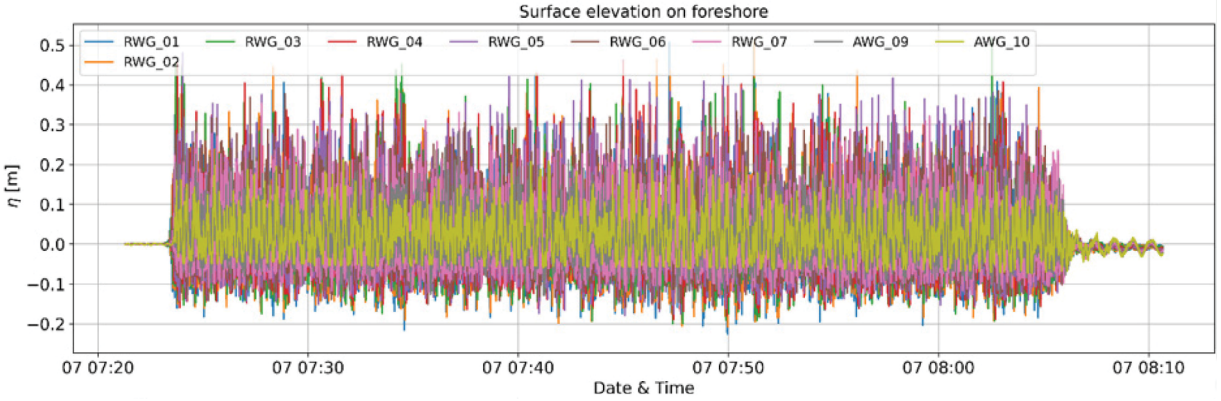


Figure 40 - Resistive wave gauges (RWG) measurements for case DUNE05rep, Test 04, from RWG 01 to RWG 10

5.3.3 Pressure transducer gauges (PTG)

The pore pressure data can be further processed to surface elevations (for MWL higher than the bed level) taking into account pressure attenuation over the water depth using, e.g., linear wave theory and the exponential decay of pressure into the sand bed following poro-elastic theory (Raubenheimer *et al.*, 1998). For MWL lower than the dune crest at the PTG locations, the ground water table levels (and variations due to wave action) can likely be derived similarly from poro-elastic theory. An example of the pressure transducer gauge (PTG) measurements, with and without the application of a Butterworth low-pass filter, is shown in Figure 41. Also, an example of wave hydrodynamics measurements at the dune for test T004 of DUNE05rep with pressure measurements under the dune/foreshore and measurements of collocated PTG and AWG sensors are shown in Figure 42.

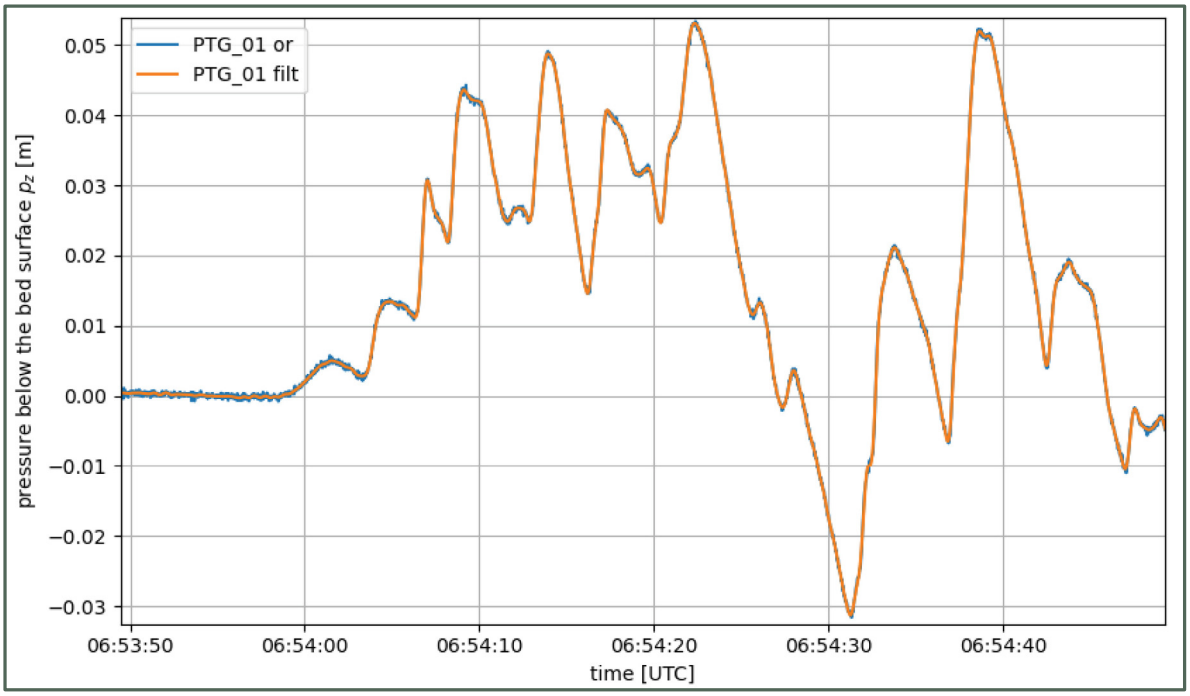


Figure 41 – Filtering of PTG_01 (signal noise) using a Butterworth lowpass filter (f_c = 2 Hz).

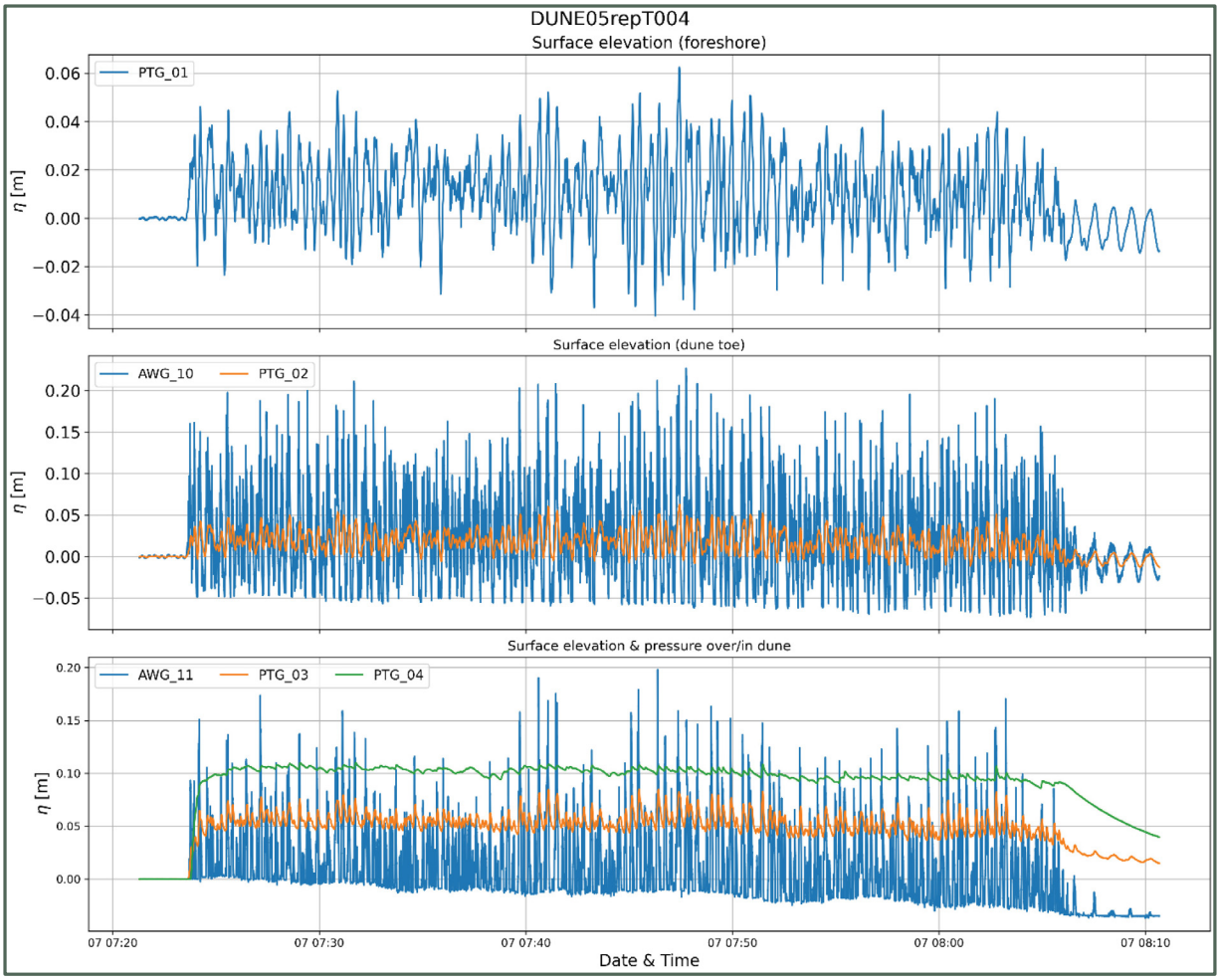


Figure 42 - Example of wave hydrodynamics measurements at the dune for test T004 of DUNE05rep. Pressure measurements under the dune/foreshore and measurements of collocated PTG and AWG sensors ((b) AWG_10 + PTG_02, (c) AWG_11 + PTG_03) under/at the dune.

5.3.4 Electromagnetic current meters (ECM)

The electromagnetic current meter (ECM) measurements provide time series of the horizontal flow velocity at several locations along the flume. Depending on the instrument and test conditions, some ECM signals contain high-frequency disturbances that require filtering before further analysis. These disturbances can originate, for example, from instrument vibration under wave action or from signal noise. Where required, a Butterworth low-pass filter with a cut-off frequency of (f_c = 2 Hz) is applied to remove these high-frequency components while retaining the relevant wave-induced velocity variations. Examples of the filtering procedure are shown in Figure 43 for (a) ECM_01, where the signal is affected by instrument vibration, and (b) ECM_03, where signal noise is present.

Following the required filtering, the ECM measurements are used to obtain horizontal flow-velocity time series. Several ECMs are collocated with wave gauges, allowing the combined water-level and velocity measurements to be used for wave-reflection analysis. Other ECMs are collocated with optical backscatter sensors (OBSs), providing simultaneous flow-velocity and suspended-sediment-concentration measurements for SSC analysis. Examples of the processed horizontal flow-velocity measurements for these collocated instrument configurations are presented in Figure 44.

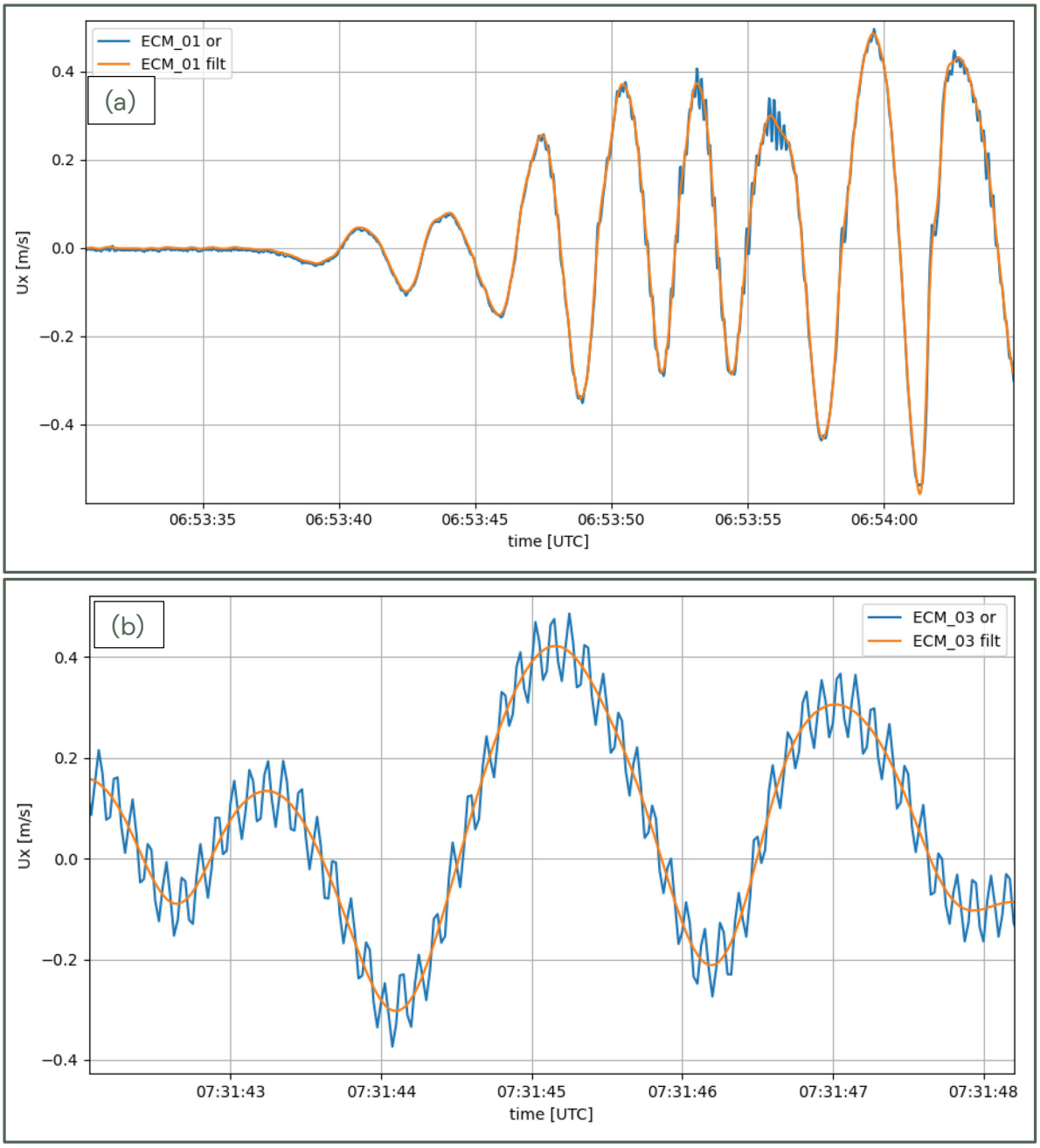


Figure 43 - Filtering of (a) ECM_01 (instrument vibration under wave action) and (b) ECM_03 (signal noise) using a Butterworth lowpass filter (fc = 2 Hz).

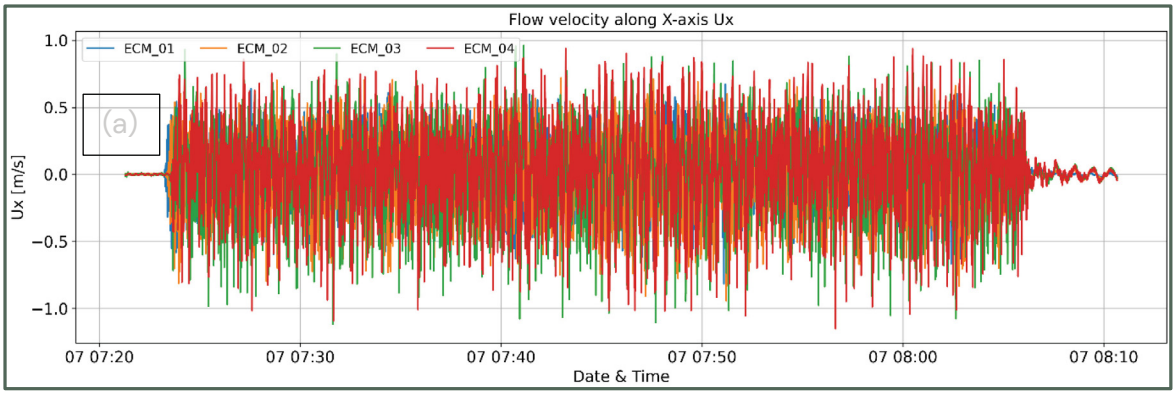


Figure 44 - Horizontal flow velocities measured by the ECMs for collocated wave gauge measurements (reflection analysis) and collocated OBS measurements (for SSC analysis).

5.4 Overtopping and -wash

5.4.1 Load cells

The overtopping box is supported by three load cells (OTT_01, OTT_02, and OTT_03), which continuously measure the load exerted by the box and the collected overtopping water. The raw load-cell signals contain some high-frequency noise and therefore require filtering before further analysis. A Butterworth low-pass filter with a cut-off frequency of (f_c = 3 Hz) is applied to reduce this signal noise while preserving the relevant variations in the measured load. An example of the filtering applied to the three overtopping-tank load-cell signals is shown in Figure 45.

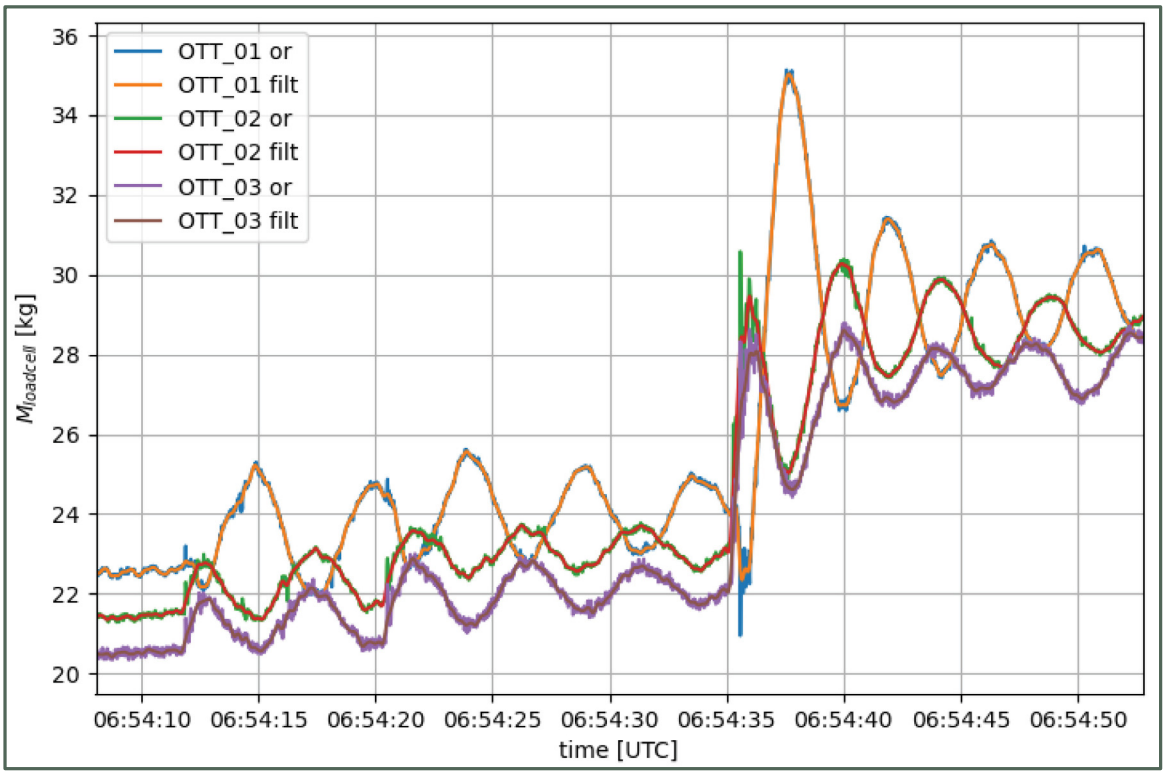


Figure 45 - Filtering of signal noise from the overtopping tank load cell signals (OTT_01, OTT_02 and OTT_03) using a Butterworth lowpass filter (f_c = 3 Hz).

5.4.2 Acoustic wave gauges (AWG_12-AWG_16)

As mentioned before, five acoustic wave gauges (AWG_12–AWG_16) are installed inside the overtopping tank to monitor overtopping events and the water-surface elevation in the OTT during overtopping. AWG_12 is located at the entrance of the chute and primarily used for overtopping event detection and requires outlier removal but no additional filtering. AWG_13

to AWG_16 are positioned at corners of the OTT tank and are used to measure the water level inside the tank. Their measurements are combined with the OTT load-cell data to determine the overtopped water volume and the amount of sediment transferred into the tank, following the methodology described in 5.4.3 Overtopping/-wash calculation.

The signals from AWG_13–AWG_16 can contain high-frequency fluctuations associated with signal noise and water sloshing inside the tank. These components are removed using a Butterworth low-pass filter with a cut-off frequency of (f_c = 0.60) Hz, as illustrated for AWG_13 in Figure 46. The filtered signals from AWG_13–AWG_16 are subsequently averaged to obtain a representative tank water-level signal. Residual oscillations in this averaged signal are further reduced using a Butterworth low-pass filter with (f_c = 0.20) Hz, as shown in Figure 47.

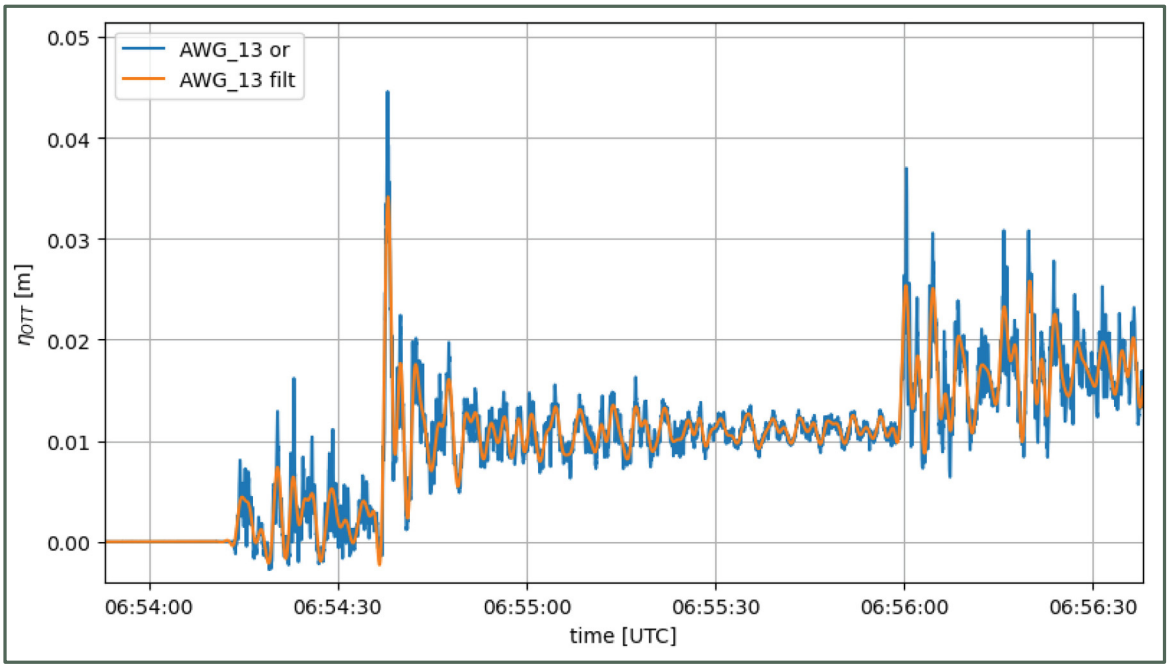


Figure 46 - Filtering of signal noise and high frequency sloshing from the overtopping tank AWG signals (here example for AWG_13) using a Butterworth lowpass filter (fc = 0.60 Hz).

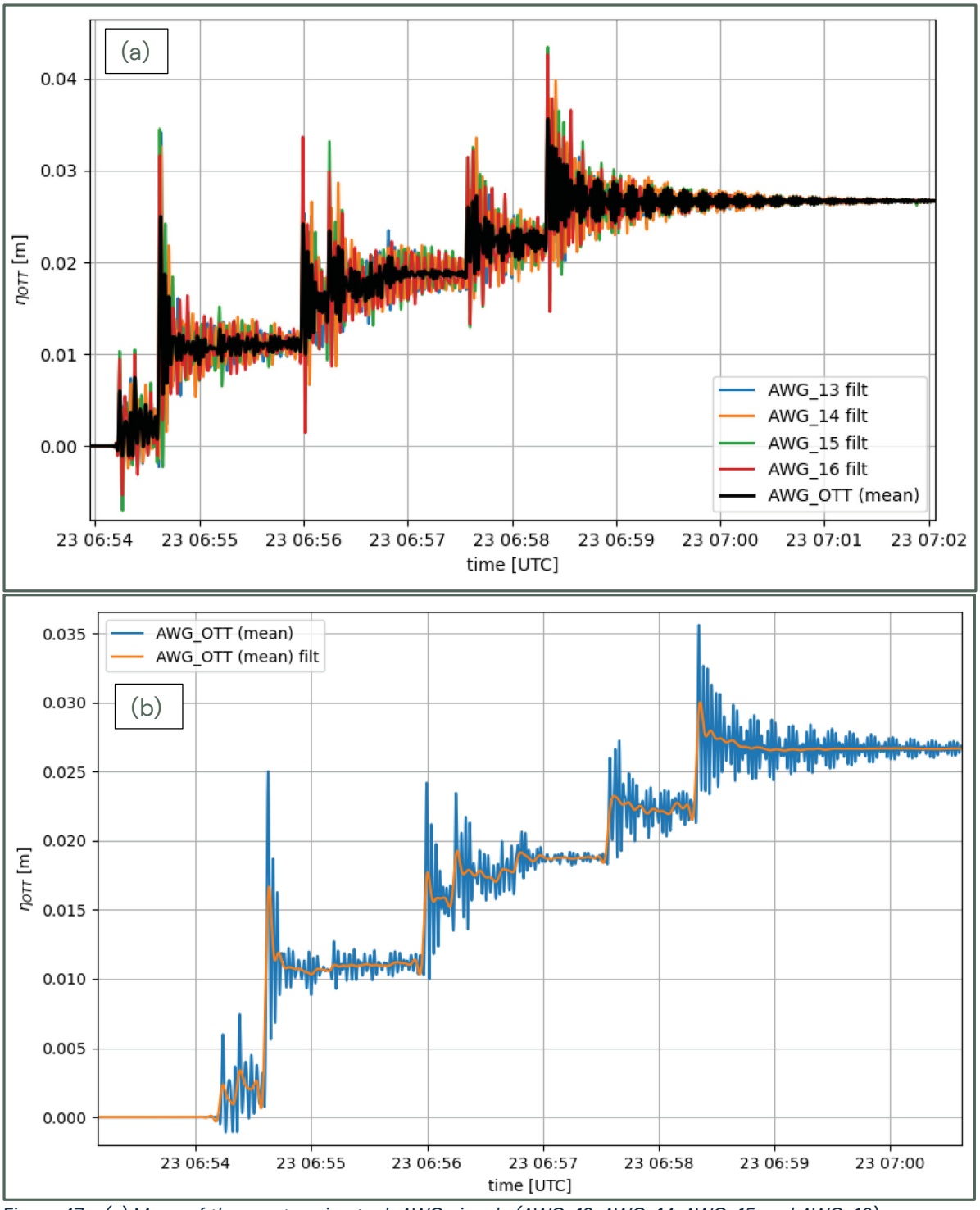


Figure 47 - (a) Mean of the overtopping tank AWG signals (AWG_13, AWG_14, AWG_15 and AWG_16), AWG_OTT. (b) Filtering of residual oscillations from AWG_OTT using a Butterworth lowpass filter (fc = 0.20 Hz).

To calculate the total mass of overtopped water and overwashed sediments inside the OTT, the measurements from the three overtopping-tank load cells (OTT_01, OTT_02, and OTT_03) are summed to obtain the total measured tank mass, (OTT_tot). An example of the resulting total-mass signal, including a detailed view of the first overtopping events, is presented in Figure 48. The combined AWG and load-cell measurements provide the basis for the subsequent overtopping and sediment-transfer calculations.

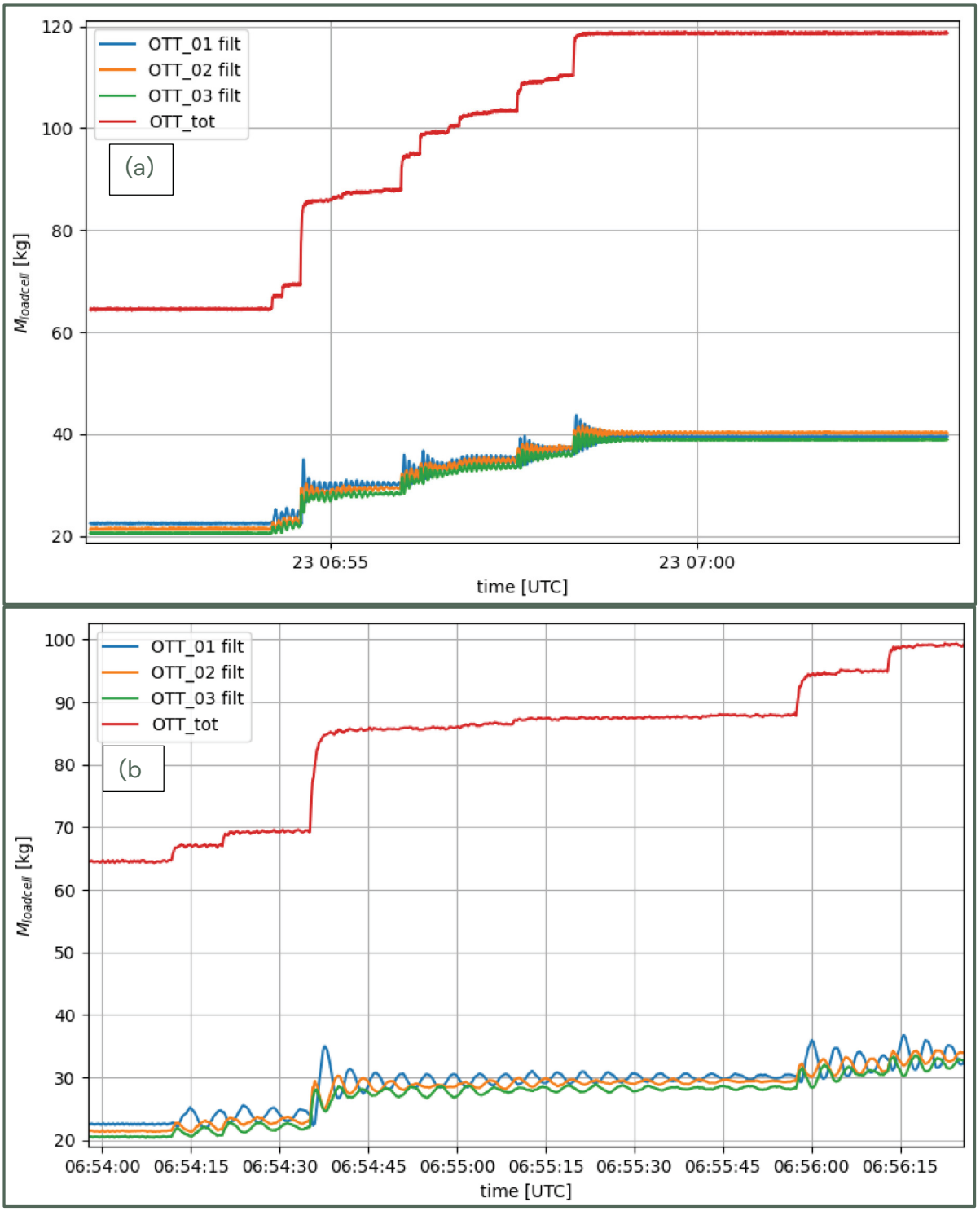


Figure 48 - Adding the masses measured by the three OTT load cells to obtain the total measured mass OTT_tot: (a) full measured signals of test DUNE07TO01; (b) zoom to first overtopping events.

5.4.3 Overtopping/-wash calculation

The measurements of the mass and water level in the OTT can be used to decompose into the volume of overtopped water V_w (=m_w/ρ_w , with ρ_w = 1000 kg/m³) and dry mass of the (fully submerged) overwashed sediment m_{sed} by using equation (7), derived in the following.

The water fills all the space in the OTT up to the water surface, including any pores in the settled sediment pile. However, the pores are part of the water volume, so the total measured volume V_{total} [m³] is:

$$V_{total} = V_w + V_{solid} \tag{1}$$

Where:

- V_{total} [m³] is the total volume occupied in the OTT (V_{total} = h_{ott} * A_{ott}). The depth h_{ott} is calculated from the start and end value of the averaged AWG water level measurement in the OTT. A_{ott} is the area of the OTT;
- V_w [m³] volume of (only) water in the OTT;
- V_{solid} [m³] is the volume displaced by the solid grains (excluding the pores).

Rearranging for water volume:

$$V_w = V_{total} - \frac{m_{sed}}{\rho_{sed}} \tag{2}$$

Where:

- m_{sed} [kg] is the dry mass of the sediment in the OTT;
- ρ_{sed} [kg/m³] is the density of the sediment grains (Table 2).

The total measured mass m_{total} [kg] is the sum of the water mass m_w [kg] and m_{sed}:

$$m_{total} = \rho_w V_w + m_{sed} \tag{3}$$

Substitute V_w from equation (2) and rework:

$$m_{total} = \rho_w \left(V_{total} - \frac{m_{sed}}{\rho_{sed}} \right) + m_{sed} \tag{4}$$

$$m_{total} = \rho_w V_{total} - \frac{\rho_w m_{sed}}{\rho_{sed}} + m_{sed} \tag{5}$$

$$m_{total} - \rho_w V_{total} = m_{sed}\left(\frac{\rho_{sed} - \rho_w}{\rho_{sed}}\right) \quad (6)$$

Until finally obtaining the formula for m_{sed} based on known parameters:

$$m_{sed} = \frac{\rho_{sed}(m_{total} - \rho_w V_{total})}{\rho_{sed} - \rho_w} \quad (7)$$

The resulting mean overtopping discharge q [m³/s/m] of a test is then calculated by:

$$q = \frac{V_w}{t_{total} B_{chute}} \quad (8)$$

Where:

- t_{total} [s] is the test duration [s] (from Table 13 to Table 27);

B_{chute} [m] is the width of the overtopping chute entrance (

- Table 11).

An example of the mass and water level measurements in the OTT, together with the resulting q and m_{sed} is provided in Figure 49. The prototype values are also provided by multiplying the model values by the Froude scaling factor $n_h^{3/2}$.

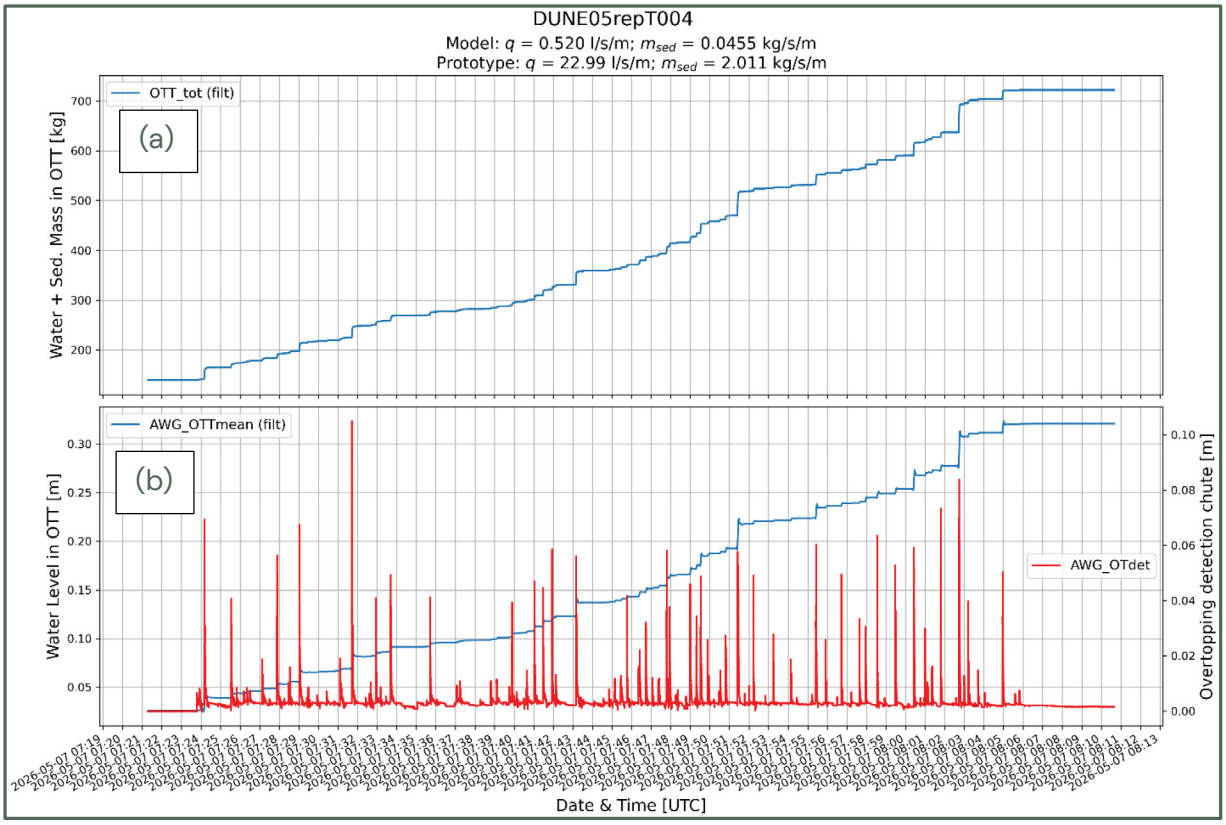


Figure 49 - Example of post-processed overtopping/-wash measurement (DUNE05rep test T004) and calculated mean overtopping discharge (q) and dry mass of overwashed sand (m_{sed}) (see title of figure). (a): total water and sediment mass measured by the load cells LCS

The same method can be applied to determine individual overtopping volumes $V_{w,i}$ and sediment masses $m_{sed,I}$, by identifying sudden mass and water level increases with the help of the overtopping event detection measurements using AWG_OTdet (=AWG_12).

5.5 Sediment transport

5.5.1 Optical backscatter sensors (OBS)

The optical backscatter sensor (OBS) measurements are used to characterize variations in suspended sediment concentration during the tests. The raw OBS signals may contain high-frequency signal noise and are therefore filtered using a Butterworth low-pass filter with a cut-off frequency of (f_c = 2) Hz. An example of the filtering applied to OBS_01 and OBS_02 is shown in Figure 50, including (a) an overview of the complete signals and (b) a zoomed-in view. The processed OBS measurements are subsequently evaluated together with the collocated electromagnetic current meter (ECM) measurements. OBS_01 is collocated with ECM_03, while OBS_02 is collocated with ECM_04, allowing simultaneous assessment of

suspended sediment concentration and horizontal flow velocity. An example of these measurements for DUNE05rep, Test 004, is presented in Figure 51.

Remark: the measured voltages by OBS_01 and OBS_02 still need to be converted to SSC [g/l] using the calibration results from Annex 2.

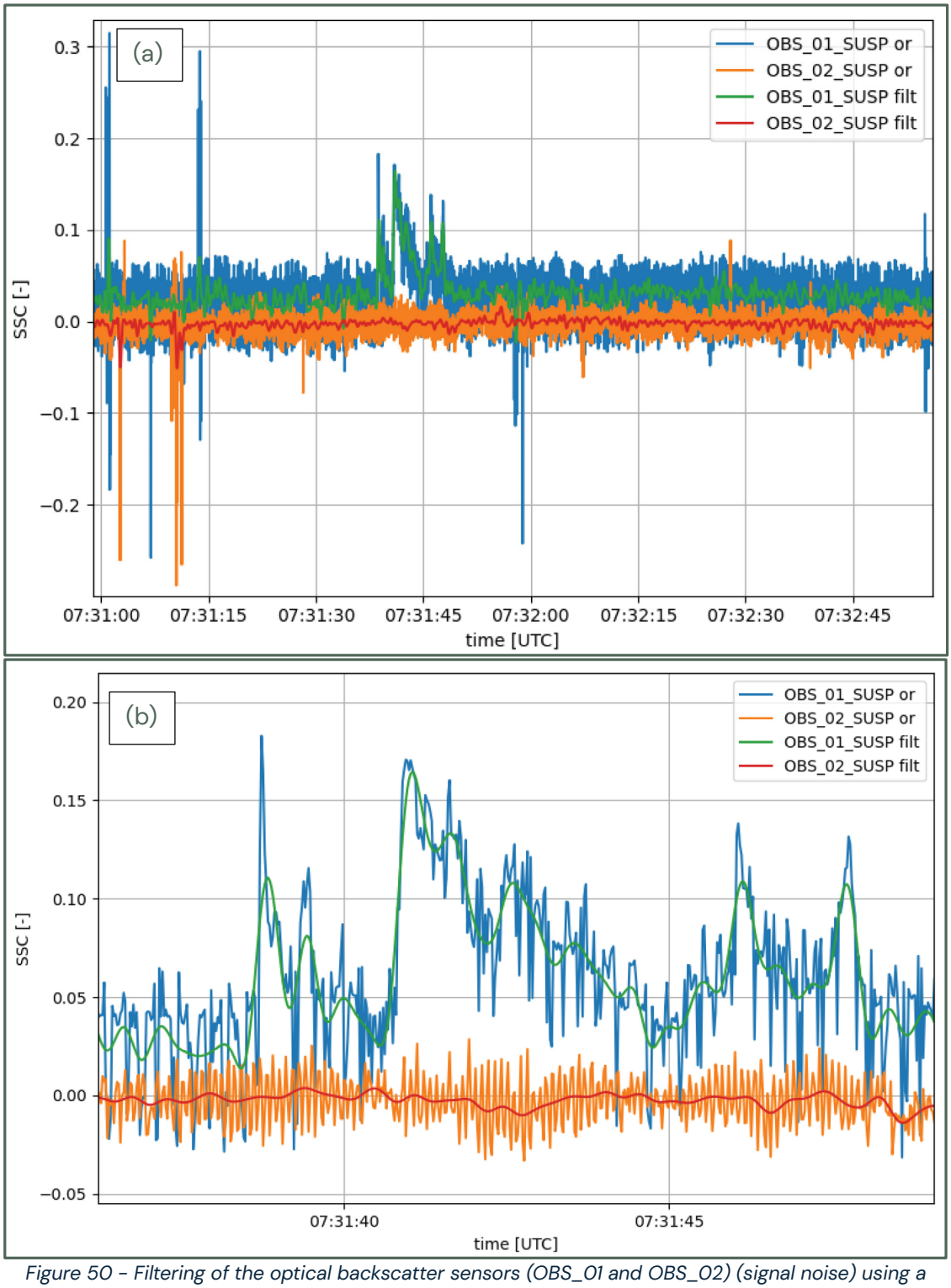


Figure 50 – Filtering of the optical backscatter sensors (OBS_01 and OBS_02) (signal noise) using a Butterworth lowpass filter (fc = 2 Hz): (a) overview; (b) zoom.

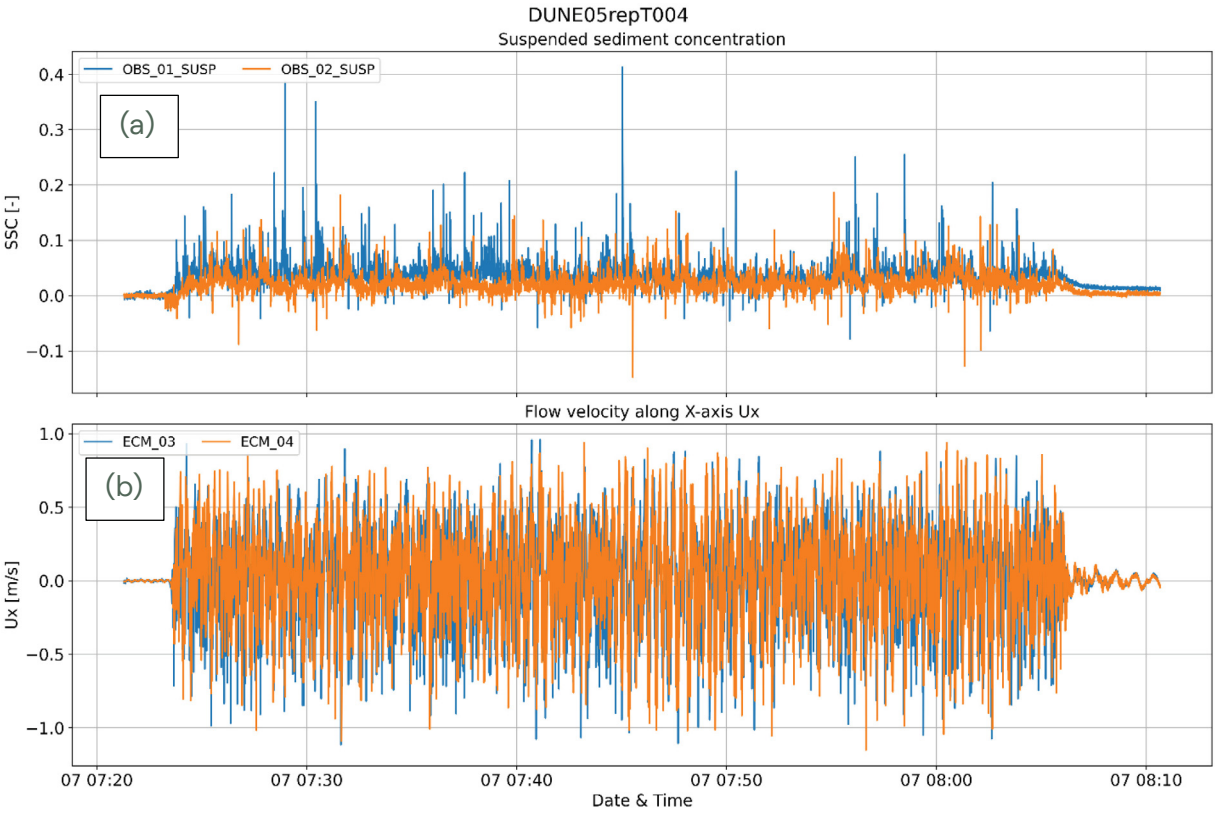


Figure 51 - Optical backscatter sensor (OBS) measurements for DUNE05rep, Test 004, showing (a) OBS_01 and OBS_02, (b) ECM 03 and ECM_04 collocated with OBS 01 and OBS 02 respectively.

6. The DUKEx-dataset structure, archiving and availability

All the gathered datasets, except 2D and 3D LIDAR measurements (data available upon request), were uploaded to ZENODO (https://zenodo.org/) as post-processed data (following Chapter 5). The dataset for this deliverable can be found from the following link: https://doi.org/10.5281/zenodo.23032964.

All post-processed data are organised into eight directories – one for each instrument or measurement setup – containing the measured data in ASCII format:

1. bedLDM: first row is header. First column is x-coordinate [m] (resolution 0.01 m) and second column is z-coordinate [m] of the bed profile.
2. etaAWG: first row contains the sampling frequency [Hz] of each column. The 11 columns are respectively the instruments AWG_01 until AWG_11 [m].
3. etaRWG: first row contains the sampling frequency [Hz] of each column. The seven columns are respectively the instruments RWG_01 until RWG_07 [m].
4. overtop-washOTT: contains two files per test:
    a. with suffix "ottAWG": first row is header. Second row contains the sampling frequency [Hz] of each column. The first four columns are respectively the instruments AWG_13 until AWG_16 [m]. The last two columns are the averaged AWG_13-16 [m] and the overtopping event detector AWG_12 [m].
    b. with suffix "ottLCS": first row is header. Second row contains the sampling frequency [Hz] of each column. The first three columns are respectively the load cell instruments OTT_01 until OTT_03 [kg]. The last column is the total measured mass OTT_tot [kg].
5. presPTG: first row contains the sampling frequency [Hz] of each column. The four columns are respectively the instruments PTG_01 until PTG_04 [m hydrostatic water column].
6. sscOBS: first row contains the sampling frequency [Hz] of each column. The two columns are respectively the instruments OBS_01 and OBS_02 [V] (to be converted to SSC [g/l] using the calibration from Annex 2).
7. temperature: first row contains the sampling frequency [Hz]. The column contains the water temperature in the flume [°C].
8. UxECM: first row contains the sampling frequency [Hz] of each column. The columns are respectively the instruments ECM_01 until ECM_04 [m/s].

Each test is identified by the dune geometry and chronological test number, e.g. for dune geometry DUNE05 and test 4, the test ID is: "DUNE05T004".

It is recommended to read the present report before using the DUKEx-dataset. The DUKEx-dataset will be under embargo until 01/10/2030.

7. Conclusion

This report documents the completion of the Belgian physical-modelling campaign undertaken within DuneFront Task 12.3. Its main objective was to establish a physical wave flume model dataset for dune-dike hybrid Nature-based Solutions under severe storm loading. The measurements cover the coupled evolution of dune and foreshore morphology, wave hydrodynamics, pore-water pressure, suspended-sediment transport, overwash and wave overtopping. The dune-dike experiments (DUKEx) were conducted from March to June 2026 in the Large Wave Flume at Flanders Hydraulics. A 1:12.5 Froude-scaled model with a mobile sandy foreshore and dune in front of a fixed dike was used.

The experimental matrix comprised 15 cases and 156 individual wave tests based on nine principal physical geometries. A common 1:40 foreshore and a smooth 1:2 dike were used, while dune volume, crest width, crest freeboard and distance from the dike were varied. The configurations were based mainly on Raversijde and Middelkerke, while also representing conditions derived from Katwijk and Dunkerque. A model-scale reproduction of the HybridDune field section at the Sand Engine was included to support the later assessment of scale effects. Most test series used the same design-storm hydrodynamic conditions, providing a consistent basis for comparing the effects of dune geometry. Complementary series addressed repeatability, reduced wave height, a variable tide and storm-surge level, and the addition of free infragravity-wave energy. Together, the experiments cover swash, collision, overwash and transition-to-inundation regimes.

The campaign combined several independent and collocated measurement systems. Acoustic and resistive wave gauges recorded free-surface elevation, while electromagnetic current meters measured horizontal velocity. Pressure transducers beneath the foreshore and dune recorded pore-water pressure and the wave-induced groundwater response. Mobile laser distance meters provided repeatable profiles of the subaerial and submerged bed between tests. Two-dimensional and three-dimensional LiDAR systems captured the time-dependent evolution of the exposed dune face. Optical backscatter sensors, collocated with velocity meters, recorded the suspended-sediment response. A dedicated overtopping tank was instrumented with three load cells and five acoustic gauges. The combined measurements provide a basis for determining the overtopped water volume and dry mass of overwashed sediment, subject to the stated assumption that the deposited sediment remains fully submerged.

Dedicated Python workflows were developed for quality control and initial post-processing. These workflows include outlier removal, signal filtering, coordinate transformations, laser-refraction and inclination corrections, profile averaging, LiDAR registration and interpolation, and the calculation of overtopping water and sediment quantities. The processed non-LiDAR data are organised into eight standardised directory groups with consistent test identifiers and sampling information. Table 27 records the availability and condition of each instrument dataset. The principal measurements are available for most configurations while also missing, incomplete, faulty or overflow-affected records that must be considered during subsequent analyses are presented in this table.

Several limitations define the appropriate use of the DUKEx-dataset. Long-crested flume waves do not reproduce the directional spreading in the field, leading to an overestimation of bound infragravity-wave energy. The foreshore slope was fixed at 1:40 and therefore does not reproduce every demonstrator profile. Furthermore, the measured fall velocity of the model sand gives a Dean-parameter difference of 57% relative to prototype conditions. This exceeds the approximately 30% difference adopted as the initial acceptability criterion. The influence of this distortion on morphodynamic scaling to prototype requires further investigation. LiDAR interpretation is restricted mainly to the exposed (above water) dune because reliable returns were not obtained through the water column.

This deliverable intentionally focuses on the experimental design, processing methods, data quality and first visualisations. It does not yet provide a complete comparative performance assessment or identify a preferred dune geometry. Such conclusions require systematic evaluation of cumulative dune erosion, the timing of dike exposure, hydrodynamic loading, overtopping discharge, overwashed sediment mass and experimental repeatability. Numerical-model validation should similarly consider several measured processes rather than relying on agreement with a single output variable.

Overall, the campaign provides a coherent and comprehensive benchmark dataset (https://doi.org/10.5281/zenodo.23032964) for investigating storm-driven dune-dike interactions. It supports the subsequent stages of DuneFront, including numerical-model validation, extension to a wider parameter range and development of evidence-based design guidance. For application in coastal engineering and policy, the findings should be translated through validated, site-specific models and accompanied by explicit treatment of scale effects and measurement uncertainty. Used in this manner, the DUKEx-dataset can help coastal authorities compare hybrid protection strategies before implementation and develop systems that combine a reliable hard safety line with the adaptive and ecological functions of dunes.

8. Acknowledgements

The authors acknowledge the support and hard work of the Flanders Hydraulics Engineering & Operations staff (Cleen, C.; Das, S.; Spiesschaert T.; Verlent, J.; Tijsmans; J.; Brouwers, B.; Henne, J.; van den Broeck, B.; Burke, W.; Latte; J.; Hassan; Bryan) with their contributions to the model and instrumentation design/setup, and conducting the experiments in the Large Wave Flume. Ghent University master thesis students Jonas Depoortere and Lukas Mergaert are also acknowledged for their support in conducting the experiments.

9. References

Adeli, A.; Gruwez, V.; Troch, P.; Hofland, B.; Tissier, M.; Bonte, D. (2024). Comprehensive investigation of existing designs of the DuneFront Demonstrators: DuneFront Project Deliverable 7.1. Available at: https://marineinfo.org/doc/publication/396141 [date of retrieval: 04/08/2026]

Ahrens, J.P. (2000). A Fall-Velocity Equation. *Journal of Waterway, Port, Coastal, and Ocean Engineering 126*(*2*): 99–102. doi:10.1061/(ASCE)0733-950X(2000)126:2(99)

Akrish, G.; Reniers, A.; Rijnsdorp, D.; Zijlema, M.; Rutten, J.; Tissier, M. (2025). The importance of free infragravity waves in the North Sea: Insights from field observations and unstructured SWAN modelling. *Ocean Modelling* 102619. doi:10.1016/j.ocemod.2025.102619

Atkinson, A.; Baldock, T.E. (2016). A high-resolution sub-aerial and sub-aqueous laser based laboratory beach profile measurement system. *Coastal Engineering 107*: 28–33. doi:10.1016/j.coastaleng.2015.10.005

Buckley, M.L.; Lowe, R.J.; Hansen, J.E.; Dongeren, A.R.V. (2015). Dynamics of Wave Setup over a Steeply Sloping Fringing Reef. *Journal of Physical Oceanography 45*(*12*): 3005–3023. doi:10.1175/JPO-D-15-0067.1

Chen, S.; Wu, Y.; Liu, S.; Yang, Y.; Wan, X.; Yang, X.; Zhang, K.; Wang, B.; Yan, X. (2023). Development of Electromagnetic Current Meter for Marine Environment. *Journal of Marine Science and Engineering 11*(*1*): 206. doi:10.3390/jmse11010206

Downing, J. (2006). Twenty-five years with OBS sensors: The good, the bad, and the ugly. *Continental Shelf Research 26*(*17*): 2299–2318. doi:10.1016/j.csr.2006.07.018

Gruwez, V.; Willems, M. (2026). Research on mobile bed modelling in the Large Wave Flume of Flanders Hydraulics: verification tests of the moveable bed modelling methodology: model design, test matrix and results. Flanders Hydraulics: Antwerp, Belgium

Guza, R.T.; Thornton, E.B.; Holman, R.A. (1984). SWASH ON STEEP AND SHALLOW BEACHES. *Coastal Engineering Proceedings 1*(*19*). doi:10.9753/icce.v19.%p

HR Wallingford. (2024). HR Merlin wave generation program - Software manual for v2.51. *Manual*

Mehrtens, B.; Vinkelau, L.; Bölker, T.; Lojek, O.; Ahrenbeck, L.; Schweiger, C.; Kosmalla, V.; Schürenkamp, D.; Goseberg, N. (2025). Benchmarking Overview on Methods for Spatiotemporal Detection of Dune Erosion in Physical Modeling. *Journal of Waterway, Port, Coastal, and Ocean Engineering 151*(*4*): 04025012. doi:10.1061/JWPED5.WWENG-2138

Poppema, D.W.; Rosman, R.G.C.; de Vries, S.; Mol, J.-W.; Antonini, A. (2026). Field measurements of dune erosion and hydrodynamics during the Hybrid Dune experiment. *Sci Data*. doi:10.1038/s41597-026-07985-8

Raubenheimer, B.; Elgar, S.; Guza, R. (1998). Estimating Wave Heights from Pressure Measured in Sand Bed. *J. Waterway, Port, Coastal, Ocean Eng. 124*(*3*): 151–154. doi:10.1061/(ASCE)0733-950X(1998)124:3(151)

Reniers, A.J.H.M.; Naporowski, R.; Tissier, M.F.S.; de Schipper, M.A.; Akrish, G.; Rijnsdorp, D.P. (2021). North Sea Infragravity Wave Observations. *Journal of Marine Science and Engineering 9*(*2*): 141. doi:10.3390/jmse9020141

Rijnsdorp, D.P.; Reniers, A.J.H.M.; Zijlema, M. (2021). Free Infragravity Waves in the North Sea. *Journal of Geophysical Research: Oceans 126*(*8*): e2021JC017368. doi:10.1029/2021JC017368

Sallenger, Jr.A.H. (2000). Storm Impact Scale for Barrier Islands. *Journal of Coastal Research 16*(*3*): 890–895

Sener, M.Z.; Yoon, H.K.; Nguyen, T.T.D.; Park, J.; Kose, E. (2023). An experimental study on capacitive and ultrasonic measurement principles and uncertainty assessment in laboratory wave measurements. *Ocean Engineering 285*: 115320. doi:10.1016/j.oceaneng.2023.115320

Sevindik, C.; Adeli, A.; Tissier, D.M.; Gruwez, V.; Hofland, B.; Troch, P.; Lojek, O. (2025). DuneFront: Deliverable 12.1 - Dutch physical model of the demonstrator(s) focus: Wave-dike interactions. *DuneFront report*. TU Delft. 58 pp. Available at: https://marineinfo.org/doc/publication/409918 [date of retrieval: 21/04/2026]

Sevindik, C.; Hofland, B.; Tissier, M.; Adeli Soleimandarabi, A.; Troch, P.; Gruwez, V.; Lojek, O. (2024). Boundary conditions for the physical modelling of dike-dune Demonstrators under extreme storms. *DuneFront report*

van Gent, M.R.A.; van Thiel de Vries, J.S.M.; Coeveld, E.M.; de Vroeg, J.H.; van de Graaff, J. (2008). Large-scale dune erosion tests to study the influence of wave periods. *Coastal Engineering 55*(*12*): 1041–1051. doi:10.1016/j.coastaleng.2008.04.003

Vellinga, P. (1986). Beach and Dune Erosion during Storm Surges (Doctoral thesis). Civil Engineering and Geosciences (CEG) (TU Delft): Delft, The Netherlands. Available at: https://repository.tudelft.nl/record/uuid:eb7a4d20-86d2-469a-932a-dec0518274bb

Annex 1: Sallenger storm impact regimes

The dune storm impact regimes as defined by Sallenger (2000) are provided in Table 30 based on the parameter definitions in Figure 52 and provided below:

$$R_{HIGH} = R_{2\%} + \eta_{mean}$$, with $$R_{2\%} = H_o(0.83\xi_o + 0.2)$$

$$R_{LOW} = R_{HIGH} - S_{2\%}$$, with $$S_{2\%} = H_o(0.85\xi_o + 0.06)$$

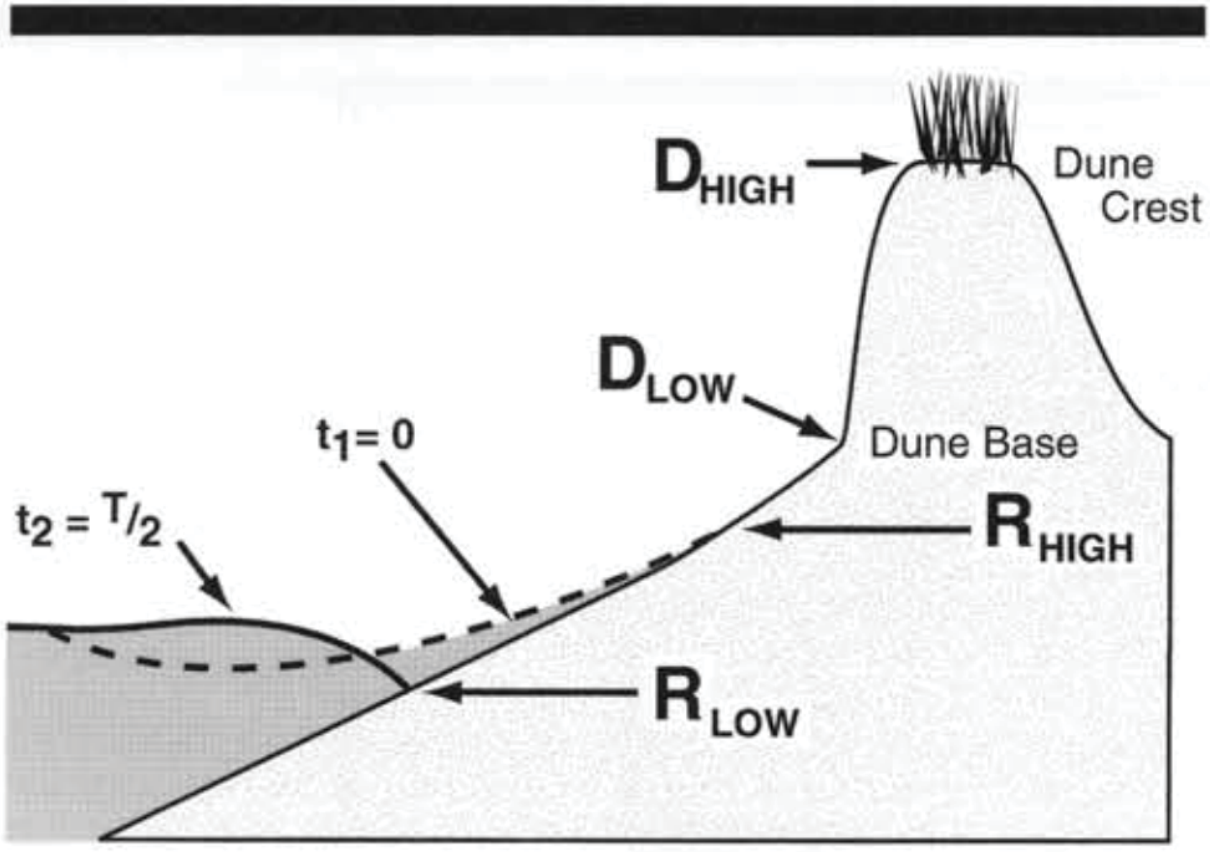


Figure 3. Definition sketch describing variables used in scaling the impact of storms on barrier islands.

Figure 52 – Definition sketch describing variables used in scaling the impact of storms on barrier islands (Sallenger, 2000).

Table 30 – The dune storm impact regimes as defined by Sallenger (2000).

Table 2. *Storm Impact Scale for Barrier Islands.*

Impact Level	Range of R_{HIGH}/D_{HIGH} and R_{LOW}/D_{HIGH}	Regimes and Predictions of Beach Changes
1	$R_{HIGH}/D_{HIGH} = 0$ to D_{LOW}/D_{HIGH}	SWASH REGIME: • Runup is confined to the foreshore of the beach. • During storms, the foreshore typically erodes and sand is transported offshore. • Following the storm, sand is transported onshore gradually, over weeks to months. Hence, the eroded sand is replaced and there is little net change to the beach.
2*	$R_{HIGH}/D_{HIGH} = D_{LOW}/D_{HIGH}$ to 1	COLLISION REGIME: • Runup collides with the base of the foredune ridge (if no foredune is present see note, *, below). • The collision forces sand to be eroded from the dune and transported offshore (&/or longshore). • Eroded dune sand is not readily returned to the dune, hence there is net erosion (relative to Impact Level 1).
3	$R_{HIGH}/D_{HIGH} > 1$ and $R_{LOW}/D_{HIGH} < 1$	OVERWASH REGIME: • Runup exceeds the elevation of the 'first line of defense', either dune ridge or, if dune is not present, the berm crest. • Sand is transported landward (tens to hundreds of meters) contributing to the net migration of the barrier beach landward (i.e. there is net erosion of the beach foreshore & net deposition landward of dune).
4	$R_{HIGH}/D_{HIGH} > 1$ and $R_{LOW}/D_{HIGH} > 1$	INUNDATION REGIME: • Elevation of the base of swash motion, R_{LOW}, exceeds the elevation of the 'first line of defense', D_{HIGH}, hence the entire beach/foredune ridge system is continuously subaqueous; • Limited observations suggest that massive net onshore transport occurs with landward migration of sand bodies on the order of 1 km.

* If no dune ridge is present, $D_{LOW} = D_{HIGH}$, and there is no Impact Level 2. Hence, as R_{HIGH}/D_{HIGH} increases from zero, a beach with no dune ridge will first experience the 'swash regime' followed in sequence by the 'overwash' and 'inundation regimes'.

Annex 2: OBS sensor calibration

The calibration setup for the OBS instruments included a mixer in a mixing barrel (Figure 54a and (Figure 54b). Both OBS were mounted (facing downwards because of space constraints) in the barrel in the middle between the barrel wall and the center of the barrel where the mixer was (Figure 54c and Figure 54d). The water volume in the barrel was 55 l and the water temperature was 23.2°C during the calibration.

The SSC was incrementally and exponentially increased following Figure 53. The calibration results are provided in Figure 55. OBS_01 shows a linear relation, while OBE_02 shows initially an exponential relation followed by a linear relation for voltages higher than -0.2938 V.

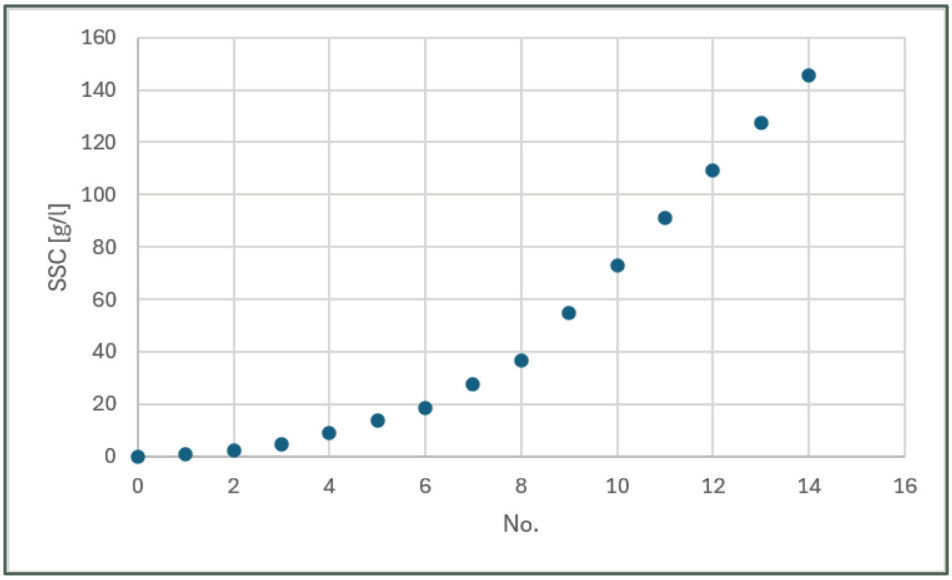


Figure 53 – Exponential SSC increment during calibration.

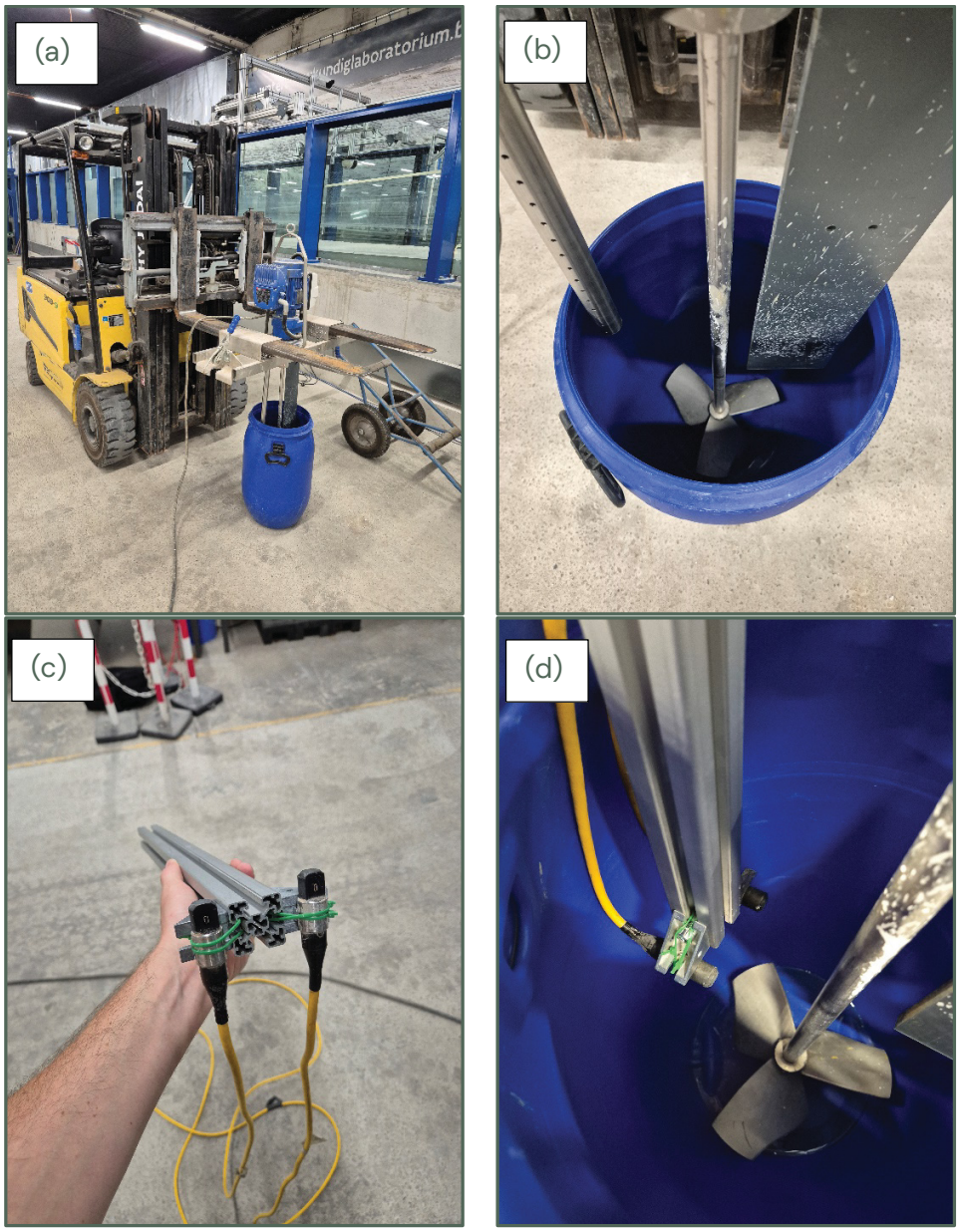
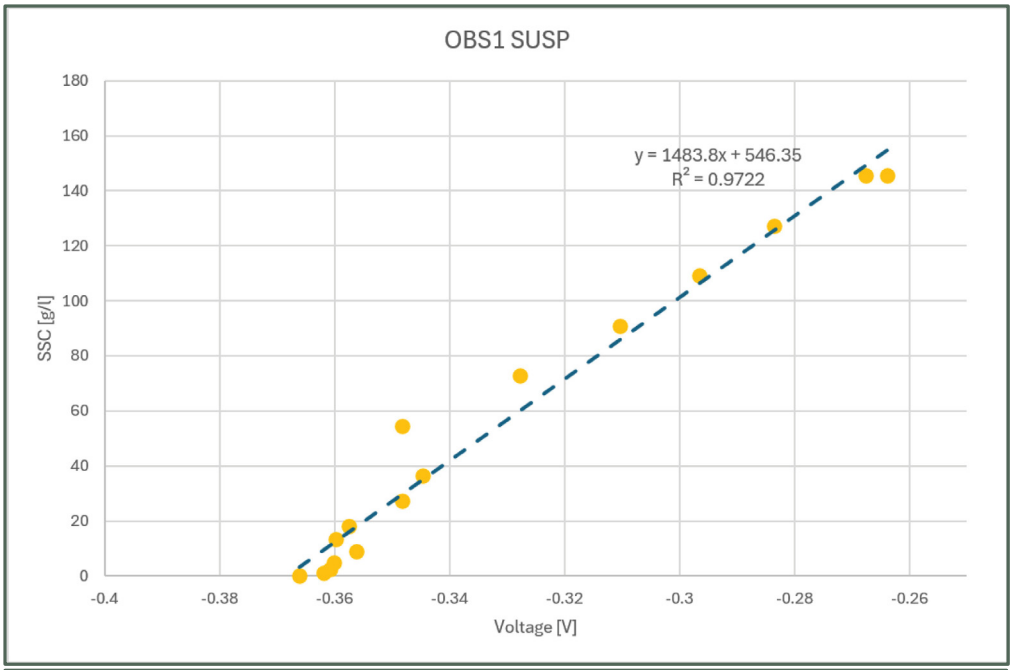


Figure 54 – OBS calibration setup. (a) General setup; (b) view into mixing barrel with mixer; (c) OBS_01 and OBS_02 with mount; (d) OBS mount fixed in mixing barrel.



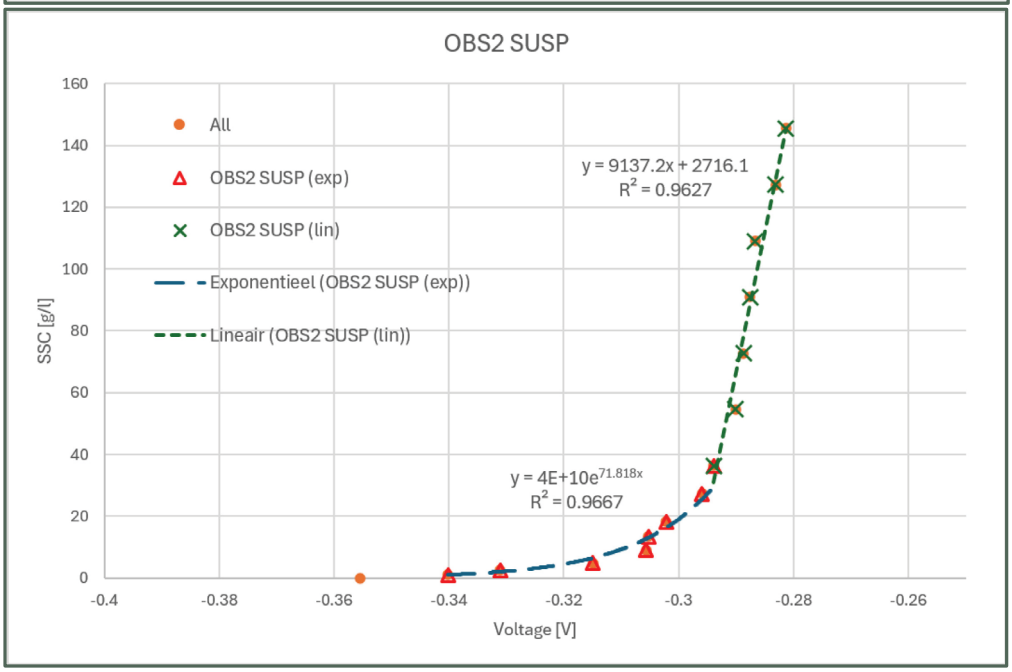


Figure 55 – OBS calibration results: (a) OBS_01, (b) OBS_02.